



## Review

## Emerging role of nanoclays in cancer research, diagnosis, and therapy

Diana Peixoto<sup>a</sup>, Irina Pereira<sup>a,b</sup>, Miguel Pereira-Silva<sup>a,b</sup>, Francisco Veiga<sup>a,b</sup>,  
Michael R. Hamblin<sup>c,\*</sup>, Yuri Lvov<sup>d</sup>, Mingxian Liu<sup>e,\*</sup>, Ana Cláudia Paiva-Santos<sup>a,b,\*</sup>



<sup>a</sup> Department of Pharmaceutical Technology, Faculty of Pharmacy of the University of Coimbra, University of Coimbra, Azinhaga Sta. Comba, 3000-548 Coimbra, Portugal

<sup>b</sup> LAQV, REQUIMTE, Department of Pharmaceutical Technology, Faculty of Pharmacy of the University of Coimbra, University of Coimbra, Azinhaga Sta. Comba, 3000-548 Coimbra, Portugal

<sup>c</sup> Laser Research Centre, Faculty of Health Science, University of Johannesburg, Doornfontein 2028, South Africa

<sup>d</sup> Institute for Micromanufacturing, Louisiana Tech University, P.O. Box 10137, Ruston 71272, LA, USA

<sup>e</sup> Department of Materials Science & Engineering, Jinan University, Guangzhou 510632, China

## ARTICLE INFO

## Article history:

Received 31 December 2020

Accepted 29 March 2021

## Keywords:

Nanoclays  
Cancer  
Chemotherapy  
Gene Delivery  
Phototherapy  
Co-delivery

## ABSTRACT

Cancer remains one of the deadliest diseases, and its effective diagnosis and treatment remains challenging; therefore, progress in earlier detection and improved therapeutics are urgently required. Conventional chemotherapy has only limited efficacy, suffers from non-specific toxicity and the induction of chemoresistance. Prospective templates for these are natural materials such as nanosized clay mineral structures of different shapes (platy, tubule, spherical, and fibrous) with tunable physicochemical, morphological, and structural properties. Their submicron size, individual morphology, high specific surface area, enhanced adsorption ability, cation exchange capacity, and multilayered organization of 0.7–1 nm thick single sheets have attracted considerable interest as multifunctional biocompatible nanocarriers with versatile applications in cancer research, diagnosis, and therapy.

The most common nanoclay minerals studied for oncology are kaolinite, halloysite, montmorillonite, laponite, bentonite, sepiolite, palygorskite, and allophane. These multilayered minerals can act as nanocarriers (with a typical drug load of 1–10 wt%) for improved dispersibility, stabilization, sustained controlled release, and the efficient transport of a wide range of anticancer drugs to the tumor site. Nanoclays having both positive and negative surfaces possess the potential to transport proteins and DNA/RNA. Nanoclays can serve as a platform for phototherapeutic agents. Several surface engineering strategies have been devised to develop clays with biofunctionality that could benefit cancer clinical practice. This review explores the potential of nanoclays as unique crystalline materials with applications in cancer research, diagnosis, and therapy.

© 2021 Elsevier B.V. All rights reserved.

\* Corresponding authors at: Department of Pharmaceutical Technology, Faculty of Pharmacy, University of Coimbra (FFUC); Pólo das Ciências da Saúde, Azinhaga de Santa Comba, 3000-548 Coimbra, Portugal; Tel.: (+351) 239 488 400. Fax.: (+351) 239 488 503 (A.C. Paiva-Santos); Department of Materials Science & Engineering, Jinan University; Guangzhou 510632, China (M. Liu); Laser Research Centre, Faculty of Health Science, University of Johannesburg; Doornfontein 2028, South Africa (M.R. Hamblin).

E-mail addresses: [hamblin@helix.mgh.harvard.edu](mailto:hamblin@helix.mgh.harvard.edu) (

## Contents

1. Introduction	2
2. Nanoclays chemistry	3
2.1. Kaolin group	5
2.2. Smectite group	6
2.3. Sepiolite and palygorskite group	7
2.4. Non-crystalline nanoclays	7
3. Nanoclays and cancer	8
3.1. Cancer research	8
3.2. Cancer diagnosis	8
3.2.1. Bioimaging	8
3.2.2. Biosensors	10
3.2.3. Detection of circulating tumor cells	11
3.3. Cancer therapy	13
3.3.1. Intrinsic anticancer bioactivity of pristine nanoclays	14
3.3.2. Anticancer drugs	14
3.3.3. Naturally-occurring compounds	24
3.3.4. Biopharmaceutical agents	26
3.3.5. Phototherapy	31
3.3.6. Co-delivery	34
3.3.7. Treatment of cancer-associated chronic pain	35
4. Nanoclays as theranostic nanoplatfoms	35
5. Nanoclays toxicological evaluation	36
5.1. <i>In vitro</i> toxicological assays	37
5.1.1. Cytotoxic analysis in healthy cells	37
5.1.2. Cytotoxic analysis in cancer cells	37
5.2. <i>In vivo</i> toxicological assays	38
6. Conclusions and future trends	39
Declaration of Competing Interest	40
Acknowledgments	40
Conflict of interest	40
References	40

## 1. Introduction

Although cancer ranks as the most studied human disease, it still continues to present a major challenge in the healthcare field,

affecting a sizable part of the population in all parts of the world [1]. Cancer arises from an accumulation of innate or acquired gene mutations, which result in alterations in gene expression, causing a loss of control of the cell cycle progression and an abnormal

**Abbreviations:** 5-FU, 5-Fluorouracil; 6-MP, 6-Mercaptopurine; ACN, Acrylonitrile; Ad, Adamantane; ADME, Absorption-Distribution-Metabolism-Excretion; ALP, Phosphatase Alkaline; APTES,  $\gamma$ -Aminopropyltrimethoxysilane; ASODN, Antisense Oligodeoxynucleotide; ATV, Atorvastatin; AUC, Area Under the Curve; BENT, Bentonite; BSA, Bovine Serum Albumin; CAM, Camptothecin; CD, Carbon Dots; CD, Cyclodextrin; CDDP, *cis*-Diamminedichloroplatinum; CdSe, Mercaptoacetic Acid Capped; CEC, Cation Exchange Capacity; CEL, Celecoxib; CIP, Ciprofloxacin; CLSM, Confocal Laser Scanning Microscopy;  $C_{max}$ , Plasma Concentration; CMC, Carboxymethyl Cellulose; CMCS, Carboxymethyl Chitosan; COS, Chitosan Oligosaccharide; CPT, Cisplatin; CRC, Colorectal Cancer; CS, Chitosan; CT, Computer Tomograph; CTAB, Cetyltrimethylammonium Bromide; CTC, Circulating Tumor Cell; CUR, Curcumin; DL, Drug Loading; DOX, Doxorubicin; DTAB, Decyltrimethylammonium Bromide; DX, Dextrin; DXS, Dextran Sulfate Sodium;  $EC_{50}$ , Half Maximal Effective Concentration; ECM, Extracellular Matrix; EE, Entrapment Efficiency; EOS, Triethoxy(octyl)silane; EpCAM, Epithelial Cellular Adhesion Molecule; ES, E-selectin; FA, Folic Acid; FAM, Fluorescein; FDA, Food and Drug Administration; FI, Fluorescein Isothiocyanate; FITC, Fluorescein Isothiocyanate Isomer I; FMOC-F, Fluoromethoxycarbonyl-L-Phenylalanine; FR, Folate Receptor; G2, Generation 2; GCE, Glassy Carbon Electrode; GEM, Gemcitabine; GFP, Green Fluorescence Protein; GNR, Gold Nanorod; GSH, Glutathione; GUV, Giant Unilamellar Vesicle; HAP, Hydroxyapatite; HDTMA, Hexadecyltrimethylammonium; HEC, Hydroxyethyl Cellulose; HNT, Halloysite Clay Nanotube; HPMACS, Hydroxypropyl Methylcellulose Acetate Succinate; HSA, Human Serum Albumin; IARC, International Agency for Research on Cancer;  $IC_{50}$ , Half Maximal Inhibitory Concentration; ICG, Indocyanine Green; ICPOES, Inductively Coupled Plasma Optical Emission Spectroscopy; IRN, Irinotecan; KI, Potassium Iodide; LAP, Laponite; LbL, Layer-by-layer; LIP, Soybean Phospholipid; LSPR, Localized Surface Plasmon Resonance; MDR, Multidrug Resistance; MHNT, Magnetic Halloysite Clay Nanotube; MMP-9, Matrix Metalloproteinase 9; MMT, Montmorillonite; MNP, Magnetic Nanoparticles; MRI, Magnetic Resonance Imaging; mRNA, Messenger RNA; MRT, Mean Residence Time; MSC, Mesenchymal Stem cell; MSC, Melanoma Skin Cancer; MTC, Mitomycin C; MTX, Methotrexate; NaL, Sodium Dodecanoate; NaMMT, Sodium Montmorillonite; NIR, Near-Infrared; NP, Nanoparticle; NSCLC, Non-Small Cell Lung Cancer; OMMT, Organically Modified Montmorillonite; OSA, Osteosarcoma; PAA, Poly (acrylic acid); PAH, Poly(allylamine hydrochloride); PAL, Palygorskite; PAMAM, Poly(amidoamine); PCL, Poly( $\epsilon$ -caprolactone); Pd, Palladium; PDADMAC, Poly (diallyldimethyl-ammonium); PDT, Photodynamic Therapy; PEG, Poly(ethylene Glycol); PEI, Poly(ethylenimine); PGE, Pencil Graphite Electrode; PHEMA, Poly(2-hydroxyethyl methacrylate); pI, Isoelectric Point; PLGA, Poly(*D,L*-lactide-co-glycolic acid); PMMM, Poly(methacrylic acid-co-methyl methacrylate); PMVEMA, Poly(methyl vinyl ether-co-maleic acid) polymer; PNEG, Pencil graphite electrodes; PPy, Polypyrrole; PRM, Protamine; PSA, Prostate-Specific Antigen; PSMA, Prostate-Specific Membrane Antigen; PSS, Poly(sodium-*p*-styrene sulfonate); PTT, Photothermal Therapy; PTX, Paclitaxel; PVP, Polyvinylpyrrolidone; QD, Quantum Dots; QUE, Quercetin; RIPK4, Receptor-Interacting Protein Kinase 4; ROS, Reactive Oxygen Species; RSV, Resveratrol; SAP, Saponins; SCLC, Small Cell Lung Cancer; SD, Sprague-Dawley; SH, Sodium Hyaluronate; siRNA, Small Interfering RNA; siVEGF, Vascular Endothelial Growth Factor siRNA; SPION, Superparamagnetic Iron Oxide Nanoparticle; SSA, Specific Surface Area;  $\beta$ -CD,  $\beta$ -Cyclodextrin; SWCNT, Single-Walled Carbon Nanotubes; T3, Triiodothyronine Hormone; T4, Thyroxine Hormone; TEM, Transmission Electron Microscopy; TGI, Gastrointestinal Tract; TME, Tumor Microenvironment; TMPS, Trimethoxy(propyl)silane; TMX, Tamoxifen; TPGS, *d*- $\alpha$ -Tocopheryl polyethylene glycol 1000 succinate; VEGF, Vascular Endothelial Growth Factor.

growth of a tumor. Every year, 18.1 million new cases of cancer are diagnosed, and 9.6 million deaths occur, of which the overwhelming majority are metastatic cancers [2]. Non-metastatic cancer treatments present a high chance of success. Surgery and radiotherapy are the most effective treatments for non-metastatic cancers but cannot be curative when the cancer has spread throughout the body [3–5]. The use of anticancer drugs such as cytotoxic chemotherapy, hormone antagonists, and biological therapies, is the current choice for the treatment of metastatic cancer [6]. However, the available treatments for metastatic cancer come with unresolved issues. The mechanism of action of anticancer drugs is characterized by the indiscriminate destruction of cells. Anticancer drugs inhibit the rapid proliferation of cancer cells, but they also affect some normal cells that also have rapid proliferation rates, such as hair follicles, bone marrow and gastrointestinal tract cells, accounting for the characteristic side effects of chemotherapy [3,7]. Prolonged administration of anticancer drugs generally leads to the development of tumor multidrug resistance (MDR), and significantly increases the cost of the treatment, which represents a waste of medical resources [7,8]. To avoid these problems, new targeted therapies with improved efficacy and safety are urgently needed.

The submicron particle size and high surface area of nanomaterials allow the selective targeting and eradication of cancer cells, increasing the precision of cancer therapy [9,10]. These nanostructures represent an opportunity to devise sophisticated targeting strategies and can enable multifunctional approaches. In the last three decades, notable progress in the development of advanced nanomaterials, (such as formation of stable nanocolloids of low water soluble drugs) have revolutionized cancer treatment [11]. The research focus led to the development of nanomaterials with desirable properties, such as longer circulation times, slower elimination, higher tumor accumulation, and the ability to provide controlled drug release. Subsequently, a second generation of nanomaterials emerged with additional capabilities, including allowing the co-administration of different drugs, specific targeting of tumor cells, and stimulus-triggered drug delivery. New functions were then added, paving the way for the third generation of nanomaterials, characterized by immune system modulation, penetration of biological barriers, and “self-recognition” properties [11]. Therefore, nanoformulations can now enhance the performance of anticancer drugs, with regard to bioavailability, specificity and safety [12]. The potential of nanomaterials in cancer treatment is due to their unique properties, such as nanoscale size, high surface area, and adjustable surface chemistry [9,10,13]. Nanosystems can be constructed from organic or inorganic materials, or a hybrid combination thereof. Among organic nanomaterials, are dendrimers, lipid-based particles (e.g., liposomes, solid-lipid systems), and polymer-based nanoparticles [9]. Inorganic nanomaterials comprise gold, silver, silica, magnetic nanoparticles, quantum dots, and carbon-based nanostructures [12,14].

Clay minerals are inorganic products obtained from the chemical weathering of sedimentary rocks [15]. Clay minerals have a nanometer-scale layering and are often named just nanoclays [16–19]. Due to the significant presence of clay minerals on earth, people have been collecting this material for thousand years using them in pottery and medical formulations [17,20–22]. Egyptians developed medicines from clay minerals many centuries ago: a wide range of healing clays have been documented on *Papyrus Ebers* [22]. Later, Galen, the famous Greek physician of ancient medicine, developed *terra sigillata*, which was a set of shaped and imprinted tablets of red earth (probably kaolinite or montmorillonite enriched with iron oxide). The *terra sigillata* remained popular in Europe until the sixteenth century [22]. In the beginning of the twentieth century, almost all Western pharmacopoeias listed clay minerals as a substance used in medicinal products [17]. Cur-

rently, materials involving clays have their own monographs in worldwide renowned Pharmacopoeias [21]. Furthermore, clay minerals have recently attracted attention in cancer research, diagnosis and therapy, due to the synergy between their biopharmaceutical and technological properties, such as biocompatibility, particle size, morphology, specific surface area (SSA), high density of charge [23,24].

Here, we summarize the literature describing the potential applications of nanoclays in cancer research, diagnosis, and therapy with a special attention to formulations using halloysite clay nanotubes (HNTs), which have a good prospective due to a favorable architecture, that includes a wide lumen, available wall interlayer space, and oppositely charged external/internal tubes' surfaces. Drugs may be selectively placed onto the tubes' surface, in the internal lumen or, in the gap between the wall layers. All these allow for the design of efficient and biocompatible core-shell systems for “torpedo-like” transmembrane delivery of single and dual drugs targeted to damaged tissues and providing a sustained drug delivery.

## 2. Nanoclays chemistry

Clay minerals are the end products that result from chemical weathering of various silicate minerals. These layered silicates belong to the phyllosilicate subclass (sheets), which is characterized by two main structural units: tetrahedral and octahedral sheets (Fig. 1) [25,26]. In the structure of clay minerals, each tetrahedron has a central cation, frequently silicon (IV) ( $\text{Si}^{4+}$ ), coordinated with four oxide anions ( $\text{O}^{2-}$ ), located at the vertices (Fig. 1A). As a result, each tetrahedron possesses three basal  $\text{O}^{2-}$  groups and an apical  $\text{O}^{2-}$  group (Fig. 1B). The three shared basal  $\text{O}^{2-}$  groups can interact with each other, and the tetrahedrons tend to polymerize to form a tetrahedral sheet with variable dimensions. The apical  $\text{O}^{2-}$  is the point of connection with an octahedral sheet [22,25,26]. Each octahedron contains a central metal cation ( $\text{M}^{n+}$ ), frequently the aluminum cation ( $\text{Al}^{3+}$ ) (Fig. 1C), coordinated with six  $\text{O}^{2-}$  groups located at the vertices (Fig. 1D). Adjacent octahedrons interact by sharing their edges (two  $\text{O}^{2-}$  or OH groups), forming an octahedral sheet [22,25,26]. Under some conditions, the central  $\text{Si}^{4+}$  of the tetrahedral sheet and the central  $\text{Al}^{3+}$  of the octahedral sheet may be replaced by lower valence ions with a similar atomic radius.  $\text{Si}^{4+}$  and  $\text{Al}^{3+}$  can be exchanged for  $\text{Al}^{3+}$  or magnesium cation ( $\text{Mg}^{2+}$ ), lithium cation ( $\text{Li}^+$ ), or ferrous cation ( $\text{Fe}^{2+}$ ), respectively [16]. Due to the symmetry and dimensional similarities between the tetrahedral and octahedral sheets, an octahedral sheet can establish a connection with one (1:1) or two (2:1) tetrahedral sheets thus forming crystalline structures through electrostatic interactions, Van der Waals forces, interlayer cations, or through hydrogen bonding [17,26]. These structures are approximately 1 nm thick, but have variable length and width, and can self-organize into multilayer stacks separated by a regular gap which may contain water and other molecules [17,22,23].

Clay minerals can be either electrically neutral or carry an overall negative charge (though may have a positive internal cavity, as HNTs) [22]. The 1:1 crystalline structure is electrically neutral because strong bonds are established between the octahedral sheet and the tetrahedral sheet, which leads to the absence of any counterbalancing cations in the interlayer space. Consequently, these type of clay minerals are not hydrated and are considered non-swelling in nature (Fig. 2A) [26]. On the other hand, the charge of the 2:1 crystalline structure is variable, because in this structure type weaker bonds are formed between the tetrahedral sheets of two layers. Given this variable nature, the interlayer space may contain counterbalancing cations if the structure has a negative charge; or may not contain any counterbalancing cations if the

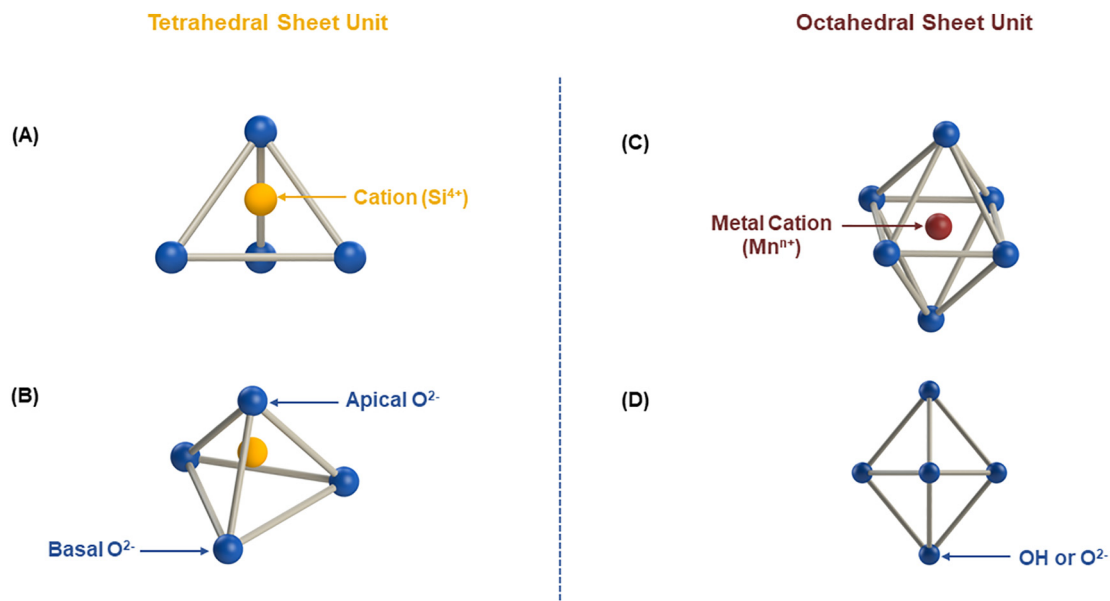


**Fig. 1.** Structural units of phyllosilicates. (A and B) Single tetrahedral sheet unit showing the central cation, usually  $\text{Si}^{4+}$ , surrounded by four oxide anions ( $\text{O}^{2-}$ ), three basal  $\text{O}^{2-}$  and one apical  $\text{O}^{2-}$ . (C and D) Single octahedral unit showing the central metal cation ( $\text{Mn}^{n+}$ ), surrounded by six  $\text{O}^{2-}$ .

structure is neutral. As a result, negatively charged structures can become hydrated, and therefore have the capability to swell (Fig. 2B) [16,22]. Considering that the cation exchange capacity (CEC) of clay minerals is directly related to the quantity and type of counterbalancing cations, it is possible to exchange counterbalancing cations for other molecules, such as metal cations, polymers, or therapeutic drugs. In this way, clay minerals can be chemically engineered to meet clinical requirements [22].

Natural nanoclays can be classified into two major subgroups: crystalline and non-crystalline (Fig. 3). Crystalline nanoclays can be either planar or non-planar hydrous phyllosilicates, which have a fibrous (ribbon-like) structure due to the periodic interleaving of the tetrahedral sheets with a discontinuous octahedral sheet [16].

There can be a different ratio between the tetrahedral and octahedral sheets, and the layer charge that may be located all over the structure. Planar hydrous phyllosilicates can be divided into three subtypes: 1:1, 2:1 and 2:1:1 phyllosilicates [22]. The 1:1-type phyllosilicates have one tetrahedral sheet stacked on top of another octahedral sheet. In the 2:1-type phyllosilicates, each layer consists of one octahedral sheet between two tetrahedral sheets [25]. Lastly, the 2:1:1-type phyllosilicates have an octahedral sheet contiguous to a 2:1 layer [22]. The non-crystalline minerals include minerals, such as allophane, imogolite and hisingerite [16]. Furthermore, nanoclays can be produced in the laboratory by chemical synthesis [27]. Synthetic nanoclays have the same structure and physicochemical properties as their natural counterparts.

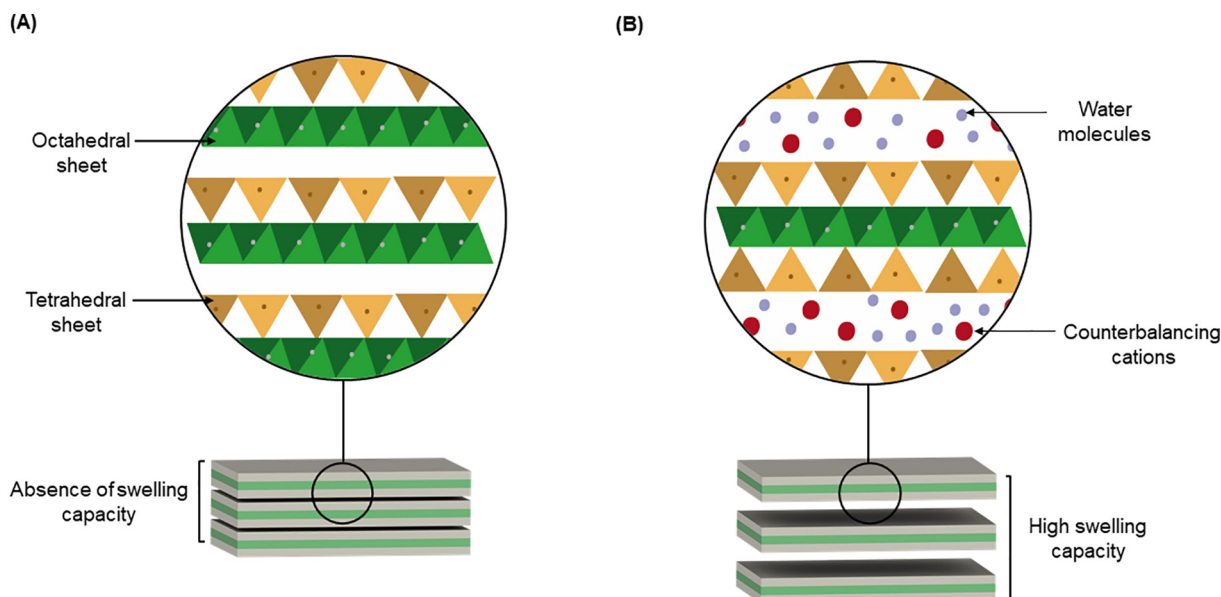


**Fig. 2.** The arrangement of phyllosilicate layers. (A) The 1:1 crystalline structure. (B) The 2:1 crystalline structure with red and blue circles representing exchangeable counterbalancing cations and water molecules, respectively. The continuous triangular and rectangular shapes illustrate tetrahedral and octahedral sheets, respectively.

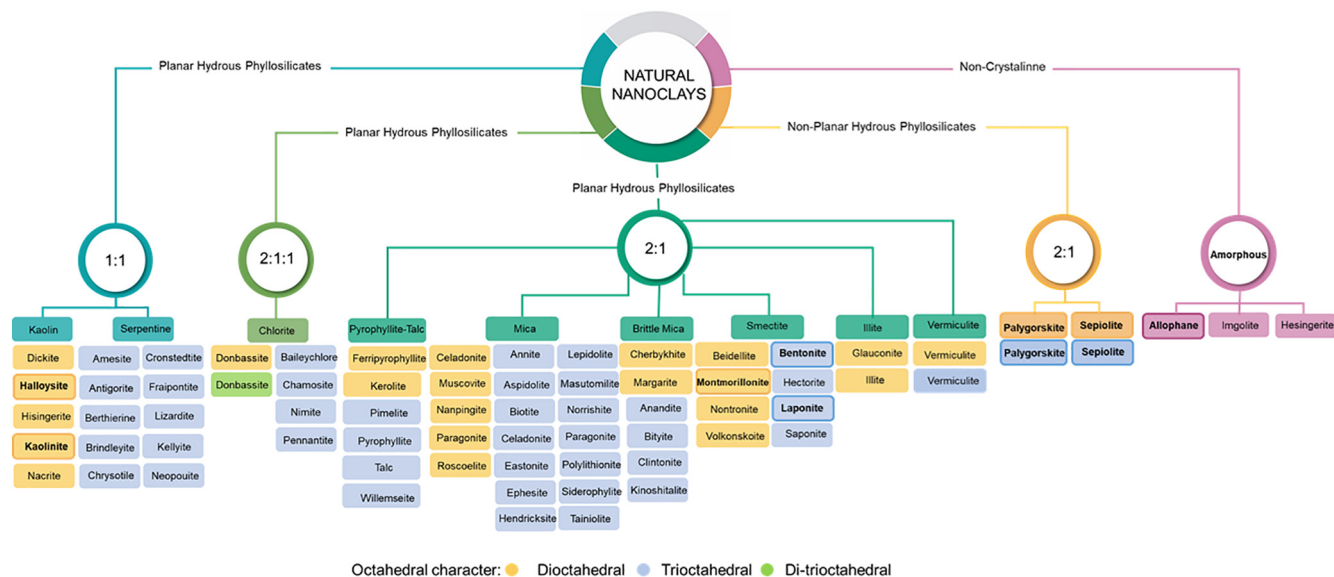


Fig. 3. Classification of natural nanoclays into crystalline (planar and non-planar hydrous phyllosilicates) and non-crystalline minerals.

Nonetheless, synthetic nanoclays have attracted more interest from companies, since they see an opportunity to produce nanoclays on a larger scale and with desired reproducibility [22].

### 2.1. Kaolin group

The kaolin group possesses a 1:1 type structure, thus, it does not display any swelling behavior (Fig. 4). Kaolinite is the most common nanoclay in the kaolin group. Usually, kaolinite takes the form of stacked pseudo-hexagonal platelets with a particle size

<2  $\mu\text{m}$  (Fig. 4A, B) [28]. Each platelet is an arrangement of two sheets, namely an aluminum octahedral sheet (aluminol surface) with a silicon tetrahedral sheet (siloxane surface) stacked one above the other. The negatively charged siloxane surface has a hydrophobic nature, while the positively charged aluminol surface is hydrophilic. Together, these sheets create a strong dipole structure, with the individual platelets of kaolinite strongly bound together by hydrogen bonds and ionic bonds. However, the edges of these platelets show a pH-dependent charge, due to the protonation or deprotonation of the OH groups [28]. Given that few or

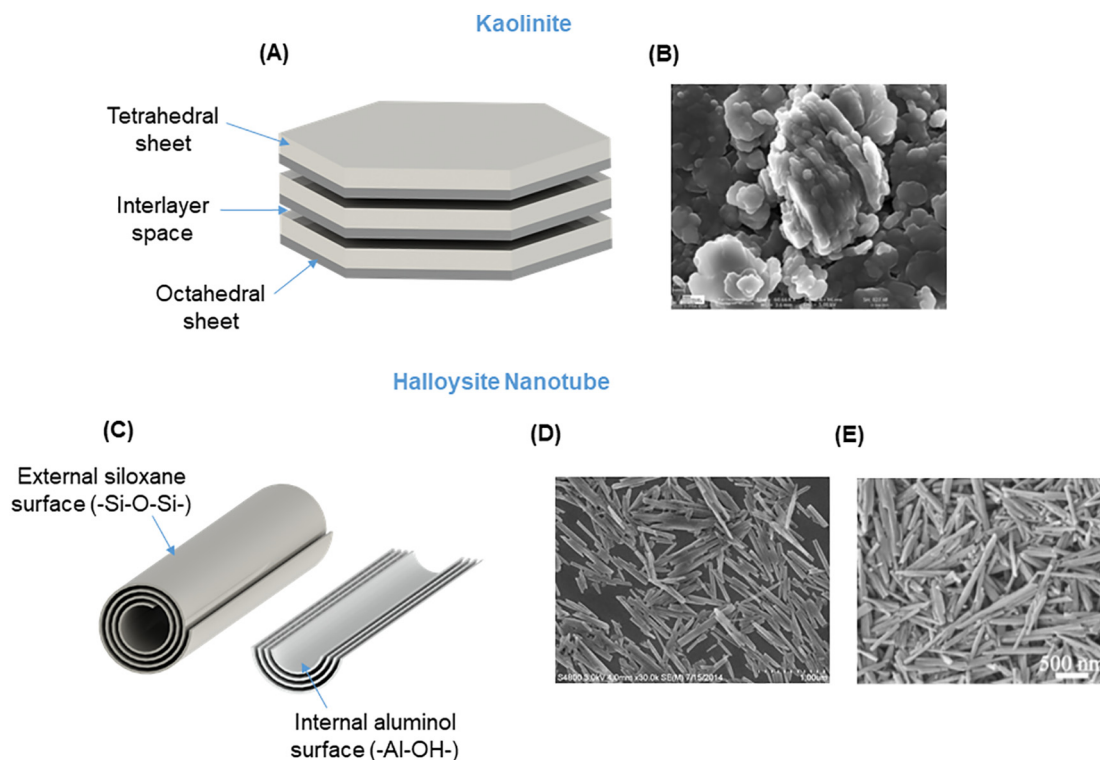
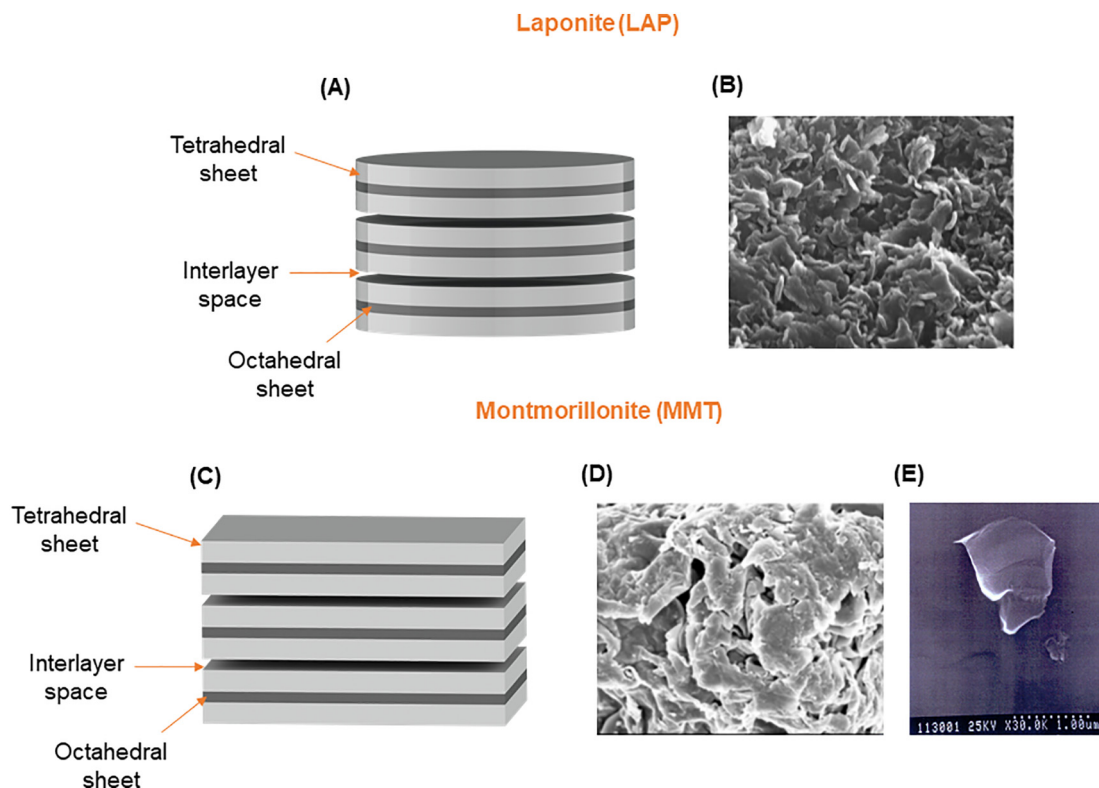


Fig. 4. The structure of nanoclays of the kaolin group. (A) Schematic illustration of kaolinite structure showing the tetrahedral sheet, the octahedral sheet, and the interlayer space. (B) Scanning electron microscopy (SEM) image of kaolinite (adapted from [28]). (C) Schematic illustration of a halloysite clay nanotube structure showing the external siloxane surface and the internal aluminol surface. (D) SEM image of halloysite clay nanotubes (HNTs) (adapted from [119]). (E) SEM image of HNTs.



**Fig. 5.** The structure of nanoclays of the smectite group. (A) Schematic illustration of the laponite (LAP) structure showing the tetrahedral sheet, the octahedral sheet, and the interlayer space. (B) Scanning electron microscopy (SEM) image of LAP (adapted from [38]). (C) Schematic illustration of montmorillonite (MMT) structure showing the tetrahedral sheet, the octahedral sheet, and the interlayer space. (D) SEM image of MMT (adapted from [44]). (E) SEM image of a single MMT layer.

no ionic substitutions are present within the kaolinite structure, this nanoclay shows two different types of charge, the permanent charge on its surface, and pH-dependent charges. The total layer charge is determined by the latter. Consequently, the CEC of kaolinite is typically low, ranging from 3 to 5 meq/100 g. The low adsorption capacity of kaolinite is a result of the low charge and also its low SSA, which is between 8 m<sup>2</sup>/g and 15 m<sup>2</sup>/g [25,26,29].

Another clay mineral in the kaolin group is called halloysite, which is often described as rolled kaolinite sheets. Halloysite is a hydrated polymorph of kaolinite, *i.e.*, it contains intercalated water molecules within the interlayer space. Halloysite is deposited in soil with different morphologies (including cabbage-like spheres), however, the hollow tubular morphology is the most common and well-studied (Fig. 4C, D, E). HNTs can result from the rolling of kaolinite sheets 15 to 20 times. HNTs have a lumen diameter that ranges from 10 nm to 30 nm, an outer diameter that varies from 40 nm to 90 nm, and a length between 0.2 μm and 2.0 μm (taken from one deposit, the nanotube sizes are similar; for example, Applied Minerals Inc. HNTs have 50 nm external, 15 nm lumen diameters and 700 nm length with parameters' distribution of ±10%) [30–32]. The large lumen (10–20 vol%) exhibits a loading capacity of 10–30 wt% and enables the encapsulation of large-sized molecules, including proteins. A notable feature of HNTs is the different chemical groups on their inner and outer surfaces: the inner surface (lumen) is composed of an aluminum octahedral sheet, while the outer one is composed of a silicon tetrahedral sheet. This arrangement confers a negatively charge on the outer surface and a positively charged inner lumen at pH 4–9, which allows the selective immobilization of charged drugs, proteins, or DNA. Another interesting feature is the presence of two different types of OH groups: those that are located between the layers

and lumen surfaces, inner OH groups (aluminols), and those that are located on the surface, outer OH groups (silanol). These hydroxyl groups endow functionalization of the tubes by various chemicals. In addition, the outer surface OH groups are at a low density, which makes HNTs relatively hydrophobic. The unique one-dimensional porous elongated structure, and the tunable external and internal surfaces make HNTs a promising material for the encapsulation and release of drugs and other compounds [31,33–36]. HNTs may be easily exfoliated in water by short sonication and stirring, resulting in stable water colloids contrary to many smectite group clays, where this process is difficult and energy costly.

## 2.2. Smectite group

The smectite group due to its 2:1 structure, is known for its swelling behavior in the presence of water. The surface of the smectite group nanoclays possesses negative charges resulting from isomorphous substitutions, and their edges show pH-dependent charges, which are created by the dangling OH end-groups. The smectite group is characterized by a high CEC, a large SSA and an increased adsorption capacity. All these characteristics result in an extensive range of possible interactions with other molecules, such as drugs or polymers. The most common nanoclays of the smectite group are, trioctahedral laponite (LAP) and dioctahedral montmorillonite (MMT) (Fig. 5) [25,26,37,38].

LAP occurs in thin strips with a lath-like shape, and it is notable for its small particle size (Fig. 5A, B). Considering that the optimal particle size for cellular internalization is between 25 nm and 30 nm, this clay, which has a diameter of 25 nm and thickness of approximately 1 nm, can readily be internalized by cells via

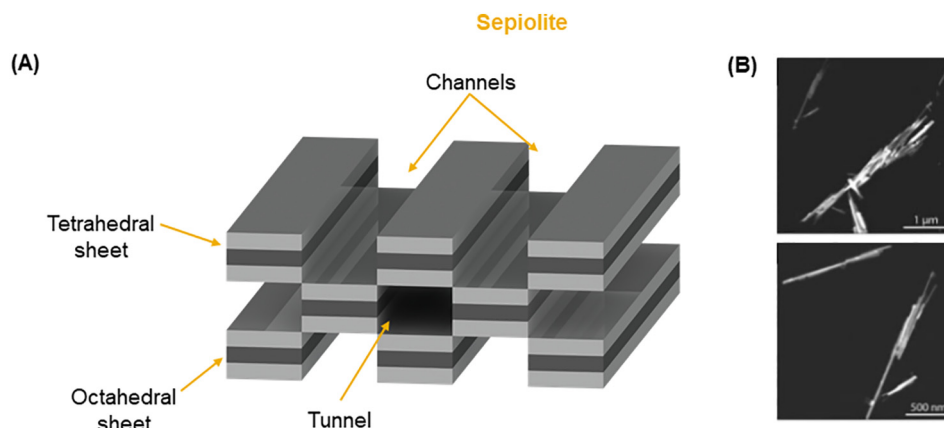


**Fig. 6.** The structure of sepiolite. (A) Schematic illustration of sepiolite structure. (B) Atomic force microscopy (AFM) image of sepiolite fibers (adapted from [15]).

endocytosis [39]. Additionally, the small particle size is responsible for its high SSA, which is equal to  $370 \text{ m}^2/\text{g}$  [37,39–41].

MMT is 1 nm thick but has a much larger diameter (300–500 nm) and is distinguished by its superb absorption capability due to its high SSA ( $756 \text{ m}^2/\text{g}$ ) (Fig. 5C, D, E) [42]. This nanoclay is a powerful detoxification material, with mucoadhesive properties, and can intercalate several types of molecules within its adjustable interlayer space. Firstly, its antioxidant properties contribute to the reduction of the gastrointestinal side effects of anticancer drugs, such as nausea, vomiting and diarrhea [43]. Secondly, the mucoadhesive properties of MMT are useful for drug delivery via non-parenteral routes of administration. MMT interacts with mucous membrane and binds to the oligosaccharide chains of mucins. These bioadhesive properties promote drug transport across the gastrointestinal (GI) tract mucous membrane, increasing drug bioavailability [44]. It should be noted that the mucoadhesive properties of MMT can increase the membrane thickness of epithelial cells, reinforcing the protective function of the mucous membrane. As a result, MMT can provide active protection to improve the GI transport of anticancer drugs [45]. Additionally, the characteristic bioadhesiveness of MMT enables the enhanced cellular uptake of some drugs. MMT attach to cells via London-Van der Waals forces and hydrogen bonds. For example, hydrogen bonds can be formed between the hydrated cations of MMT and the cellular glycoproteins. The formation of these bridges increases the cellular interactions with MMT, consequently increasing drug internalization by cellular uptake, which is a crucial factor for effective drug delivery [42].

The core component of the commercial bentonite (BENT) clay is MMT, thus the properties of BENT are determined by the amount and the CEC of the MMT core [46]. BENT is distinguished by its good absorption capability, high CEC, and swelling behavior. There are only a few types of BENT known by the main exchangeable cation type present in MMT. Therefore, some well-known types of BENT are calcium BENT and sodium BENT [47]. The lamellar structure of BENT is irregular, and it shows small dimensions associated with a high SSA. Frequently, this type of nanoclay tends to form thick and large agglomerates. Moreover, the structure of BENT can be modified by chemical reactions (including alkaline or acid activation) or the addition of organic molecules, which are known as active BENT and organic BENT, respectively. Acid activation of BENT with HCl or  $\text{H}_2\text{SO}_4$  results in an enhanced absorption capability. With this type of treatment it is possible to increase the net negative charge in BENT, because the charges at its edges are pH-dependent, as also occurs in MMT. The overall effects of all these properties is that BENT can interact with biomolecules and polymers [46,47].

### 2.3. Sepiolite and palygorskite group

Sepiolite and palygorskite (PAL) have fibrous morphology with typical cross-section of 30–50 nm with regular narrow channels of few nanometers diameter. Many centuries ago, ancient Maya prepared extremely stable blue color formulations with indigo, loading this dye into PAL nano-channels. Sepiolite and PAL present a 2:1 structure where the apical  $\text{O}^{2-}$  groups in the tetrahedral sheets are inverted, which leads to interruptions in the structure of the octahedral sheet, forming rectangular channels that are fully or partially available to encapsulate several molecules (Fig. 6A) [15]. In addition, the discontinuous octahedral sheet has regularly arranged silanol groups (Si-OH) on the external surface of the structure. The Si-OH groups have an important role in the functionalization of sepiolite and PAL [15]. Given their unique structural arrangement, sepiolite and PAL occur as crystals in the shape of flexible elongated needles (Fig. 6B), with a high SSA, a significant absorption capability, and are stable under different pH conditions [25]. However, when compared to the smectite group, sepiolite and PAL have a lower CEC [25].

### 2.4. Non-crystalline nanoclays

In nature, it is possible to find nanoclays with a non-crystalline structure, such as allophane. Allophane is an amorphous nanoclay with a hollow spherical shape. Allophane has a diameter that ranges from 3.5 nm to 5 nm, and it is composed of a shell-like wall with a thickness varying between 0.6 nm and 1.0 nm (Fig. 7). The wall of the hollow sphere is composed of two sheets, an external aluminum octahedral sheet and an internal silicon sheet. Nevertheless, allophane does not have a fixed composition, and the Si/Al ratio can range from 1 to 2. When the Si/Al ratio is close to 1 the spherical structure has a higher proportion of Al (Al-rich allophane). On the other hand, when the Si/Al is near to 2, there is a higher proportion of Si sheets (Si-rich allophane) [48]. The CEC and surface charge of allophane change according to the pH conditions. The charge variations in the surface of allophane are produced by the  $(\text{OH})\text{Al}(\text{H}_2\text{O})$  groups exposed within the channels, which are present throughout the wall of the hollow sphere. Moreover, due to its lower particle size, allophane has a high SSA ( $1000 \text{ m}^2/\text{g}$ ), which is the sum of the internal (intrasphere) and external (intersphere) areas depending on the particle size and density. However, when the SSA was calculated by measuring the loading capacity of ethylene glycol and ethylene glycol monoethyl ether, it ranged from  $700 \text{ m}^2/\text{g}$  to  $900 \text{ m}^2/\text{g}$  [16]. The reduced particle size and high SSA of allophane explain its high adsorption capacity.

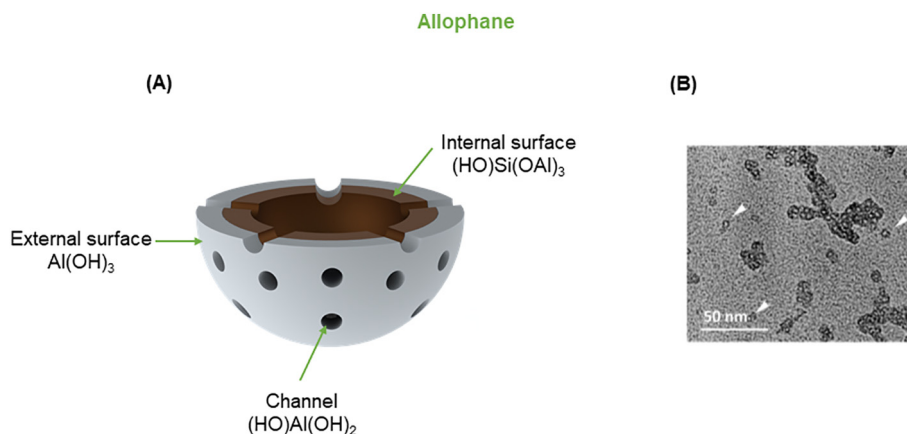


**Fig. 7.** The structure of allophane. (A) Schematic of the allophane structure showing a hollow sphere with channels. (B) Transmission electron microscopy (TEM) image of allophane (adapted from [48]).

### 3. Nanoclays and cancer

#### 3.1. Cancer research

The use of conventional two-dimensional (2D) cell cultures has been found to have many limitations and cannot accurately reproduce the *in vivo* situation of cancer cells and the tumor microenvironment (TME). In order to overcome these limitations, three-dimensional (3D) cancer models are being developed *in vitro* to more accurately mimic the biological and biochemical diversity of the TME [49,50]. Cellular spheroids are the most often-used type of 3D tissue model. Spheroids are important in preclinical drug development studies, particularly in cancer research, given that they can mimic the TME more precisely [51,52]. Spheroids can be produced using either scaffold-based or scaffold-free techniques. 3D scaffold-based models are produced by assembling cell multiple layers, by seeding individual or aggregated cells onto a scaffold. In the case of 3D scaffold-free models, cells are allowed to proliferate and aggregate spontaneously without using any exogenous structure [49,52]. Recent studies have suggested that nanoclays can be used to produce spheroids either by scaffold-based or scaffold-free methods.

Scaffolds based on poly-( $\epsilon$ -caprolactone) (PCL) and MMT were prepared to mimic the microenvironment of prostate cancer bone metastasis. The MMT was first modified with 5-aminovaleric acid, and later hydroxyapatite (HAP) was biomineralized on the modified MMT (*in situ* HAP clay). The resulting *in situ* HAP clay-PCL scaffold allowed the differentiation of mesenchymal stem cells (MSC) into osteoblasts in the absence of any osteogenic supplement. To study the interaction between the MSCs and prostate cancer cells, both cell lines were sequentially cultured on the HAP clay-PCL scaffold. Prostate cancer cells underwent the mesenchymal-epithelial transition and developed into multicellular spheroids with tight cellular junctions surrounding a hypoxic core region that mimicked the early stage of prostate cancer bone metastasis [49].

Furthermore, two different types of breast cancer cells, MDA-MB-231 and MCF-7, were co-cultured with MSCs in a HAP clay-PCL scaffold to mimic the late stage of breast cancer bone metastasis. The levels of the osteogenic marker, alkaline phosphatase (ALP), and matrix metalloproteinase 9 (MMP-9) activity showed that the 3D model could reproduce the cell-to-cell and cell-to-matrix interactions seen *in vivo* and preserve the different behavior of highly metastatic MDA-MB-231 and low metastatic MCF-7 cells. Moreover, gene expression and immunostaining studies showed the formation of multicellular spheroids with tight intercellular

junctions, which expressed markers of migration and invasiveness in MDA-MB-231 cells [50].

A classic example of a scaffold-free technique is the hanging drop method. This technique takes advantage of the ability of certain types of cells to form spheroids spontaneously when grown in hanging drops. Healthy MSC cells, adipose-derived stem cells (ADSC), human alveolar adenocarcinoma cells (A549), human cervical carcinoma cells (HeLa), and human hepatoma cells (Hep3B) have all been shown to form spheroids using this method. Because HNTs do not interfere with cell-to-cell and cell-to-matrix interactions, they allow cells to spontaneously form multicellular conglomerates that can either be from similar or different cell types. When different types of cells were grown in the presence of HNTs, the ability of the cells to form spheroids was not compromised and the organization of the cytoskeleton remained the same [52].

In conclusion, nanoclays could be useful to produce 3D *in vitro* cancer models, which might reduce the number of animals used, and allow easier high throughput screening of new drugs.

#### 3.2. Cancer diagnosis

The early diagnosis of cancer is fundamental to reduce cancer mortality. Thus, advanced methods are being developed to detect the early signs of the disease, through using biomarkers (nucleic acids, proteins, small metabolites) as well as detecting the presence of circulating cancer cells (CTCs) in the bloodstream or the lymphatic system. All these biomarkers can be employed for cancer diagnosis, prognosis, and for the monitoring of therapeutic outcomes. This section provides an overview of recent advances in the use of nanoclays in cancer diagnosis.

##### 3.2.1. Bioimaging

Magnetic resonance imaging (MRI) is an effective technique used for the diagnosis of many diseases, including cancer. Images obtained with MRI are produced by signals, which result from the interaction between a strong magnetic field and the water protons in human tissues. However, the resolution of the image is rarely satisfactory due to the variable water composition of different tissues, and water mobility. For this reason, the use of contrast agents is necessary. Contrast agents for MRI, as the name suggests, improve the contrast of the images by decreasing the relaxation time of the water protons. The contrast agents are classified as T1-shortening agents and T2-shortening agents, and their use results in a lighter or darker final image, respectively. Superparamagnetic iron oxide nanoparticles (SPIONs) are a well-known

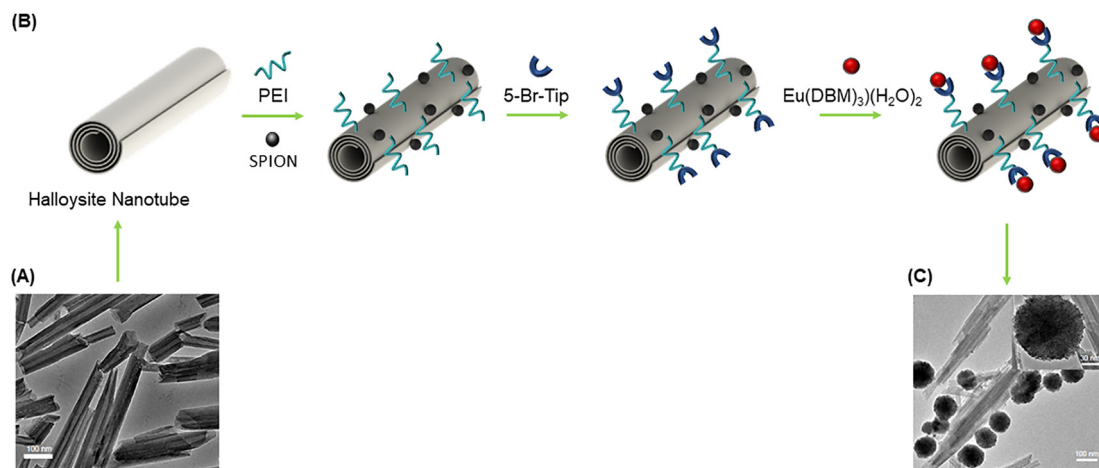


**Fig. 8.** Halloysite clay nanotubes-based nanocomposites. (A) Transmission electron microscopy (TEM) image of the halloysite clay nanotubes (HNTs) (adapted from [53]). (B) Schematic representation of the synthesis process of HNTs-based nanocomposites with photoluminescent and magnetic properties. (C) TEM image of HNTs-based nanocomposites, where superparamagnetic iron oxide nanoparticles (SPIOs) are aggregated on the surface of the HNTs rather than in the lumen (adapted from [53]).

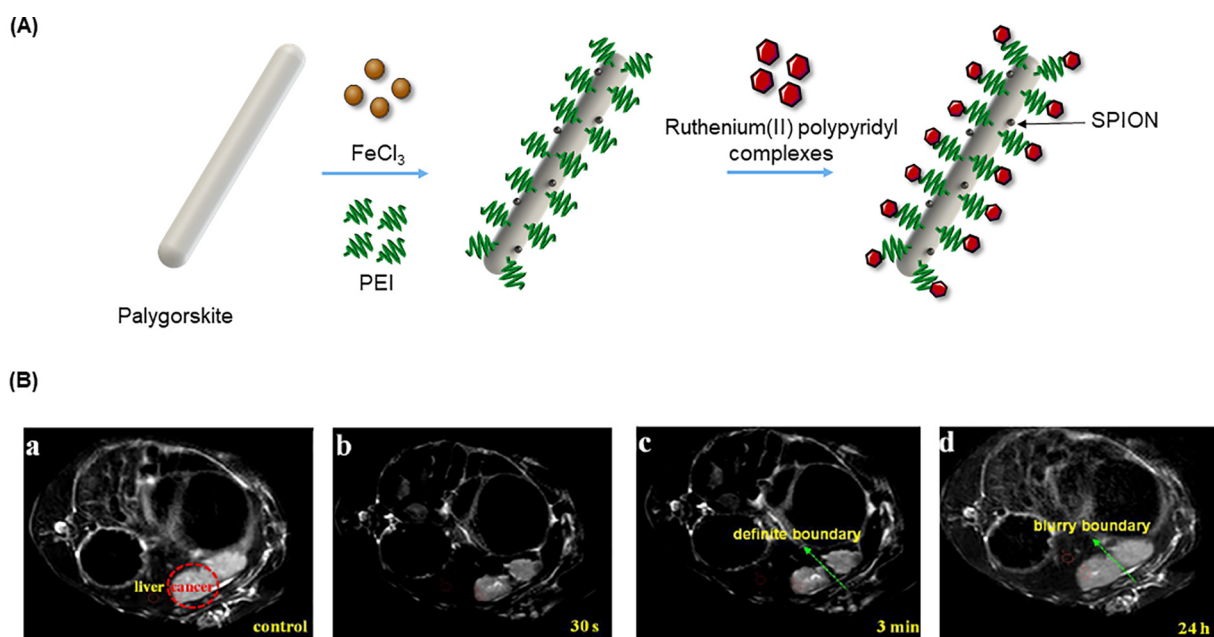


**Fig. 9.** Nanocomposite composed of palygorskite (PAL) and superparamagnetic iron oxide nanoparticles (SPIOs). (A) Schematic representation of the preparation (B) Magnetic resonance imaging (MRI) of rabbit liver showing healthy and tumor tissue before and after the administration of a nanocomposite of PAL and SPIOs (adapted from [54]).

example of T2-shortening agents. However, SPIOs naturally tend to form large aggregates, which, when coupled directly with photoluminescent labels, cause a drop in the photoluminescence intensity [53,54]. To overcome this limitation of SPIOs, an HNT-based nanocomposite with both photoluminescent and magnetic properties was prepared and functionalized with hydrophilic branched poly(ethyleneimine) (PEI). Europium-(dibenzoylmethane) $_3(\text{H}_2\text{O})_2$  ( $\text{Eu}(\text{DBM})_3(\text{H}_2\text{O})_2$ ) photoluminescent complexes were attached via ligand exchange with (2-(5-bromothiophen-2-yl)imidazo[4,5-f][1,10]phenanthroline (5-Br-Tip)) to the nanocomposite (Fig. 8A, B). The nanocomposite was stable, showed low cytotoxicity, and good photophysical properties. In contrast to free  $\text{Eu}(\text{DBM})_3(\text{H}_2\text{O})_2$  complexes, the nanocomposite showed a longer average luminescence lifetime and no obvious loss of luminescence. The photoluminescent label was effectively protected against quenching when attached to the surface of the nanocomposite. The

nanocomposite could detect human liver cancer cells (HepG2 cells) via a photoluminescent signal. Also, the nanocomposite showed a reduction in the T2-signal intensity in normal tissue, thus discriminating between normal and cancer cells [53].

A similar multifunctional nanoclay-based nanocomposite was reported by Zhu *et al.* [54]. SPIOs were attached to the surface of PAL and then functionalized with PEI. Afterwards, a ruthenium complex was coupled to the surface of the nanocomposite, resulting in a nanocomposite that displayed excellent water dispersibility, good photophysical and superparamagnetic properties (Fig. 9A). Cellular toxicity experiments showed that the nanocomposite evidenced was cytocompatible. The use of Z-Scan fluorescence imaging revealed that the nanocomposite penetrated the cellular membrane of HepG2 cells, enabling intracellular imaging. The *in vivo* experiments performed in an animal model of hepatic carcinoma confirmed that the nanocomposite could function as a

contrast agent, distinguishing between tumor and normal tissue (Fig. 9B) [54].

These studies proved that the nanocomposites could be effectively metabolized without leaving any residual accumulation within the organism. Furthermore, transmission electron microscopy (TEM) images showed that SPIONs, with an average size of 100 nm, accumulated on the surface of both HNTs and PAL without forming any aggregates (Fig. 8C). This assembly occurred due to the high density of negative charges on the nanoclays (HNTs and PAL), which enabled their modification by positive metal cations, which were subsequently reduced into SPIONs [53,54].

Fluorescent biolabels are useful tools in cancer diagnosis due to their high sensitivity and selectivity for cancer cells. Several nanoclay-based nanocomposites have been proposed as cancer bioimaging platforms.

Amino-functionalized HNTs were coated with the positively charged poly(allylamine hydrochloride) (PAH) and the negatively charged poly(sodium-*p*-styrene sulfonate) (PSS) via a layer-by-layer (LbL) assembly process. After the deposition of five polyelectrolyte layers, HNTs were finally functionalized with a PAH layer labeled with fluorescein isothiocyanate isomer I (FITC), allowing the visualization of HNT uptake by cancer cells using confocal laser scanning microscopy (CLSM) [55].

Hydrogen peroxide ( $\text{H}_2\text{O}_2$ ), hydroxyl radicals ( $\cdot\text{OH}$ ), singlet oxygen ( $^1\text{O}_2$ ), and superoxide radical anions ( $\text{O}_2^{\cdot-}$ ) are examples of reactive oxygen species (ROS), which are by-products of normal biological metabolism. High concentrations of  $\text{H}_2\text{O}_2$  contribute to oxidative stress inside cells. The excessive accumulation of  $\text{H}_2\text{O}_2$  in the human body may lead to diseases, including cancer [56]. Thus,  $\text{H}_2\text{O}_2$ -sensitive fluorescent probes are useful to detect  $\text{H}_2\text{O}_2$  at low levels to diagnose ROS-related diseases [57].  $\text{H}_2\text{O}_2$  fluorescent probes usually consist of a fluorophore, a linker, and an  $\text{H}_2\text{O}_2$ -sensing moiety, known as the responsive group. The bond between  $\text{H}_2\text{O}_2$  and the responsive group results in either the enhancement (turn-on), quenching (turn-off), or a ratiometric change in the fluorescence intensity [56]. The most frequently used responsive group for  $\text{H}_2\text{O}_2$  detection is arylboronate [56]. Recently, the inner surface of HNTs was modified with an organic fluorescein derivative bearing arylboronate acid. The formation of a B-C linkage gave the nanocomposite the ability to display a highly specific "turn on" fluorescence response to  $\text{H}_2\text{O}_2$ . The nanocomposite had good dispersion in aqueous media and showed a high fluorescence response in the presence of 100 nM  $\text{H}_2\text{O}_2$ . Experiments using A549 cells showed that the nanocomposite was able to detect the  $\text{H}_2\text{O}_2$  produced by cells under physiological conditions. A549 cells were successfully labeled, and the fluorescence intensity increased with time due to the accumulation of  $\text{H}_2\text{O}_2$  in cancer cells. The proposed HNT-based nanocomposite may be a promising tool for cancer diagnosis [57].

Quantum dots (QDs) are semiconductor nanoparticles (NPs) that have been extensively used for cellular labeling due to their high brightness, good photostability, and multicolor emissions. Although QDs have good intrinsic optical properties, several studies have pointed out that their use in living organisms might lead to toxicity issues. The immobilization of QDs onto the surface of HNTs has been found to reduce the toxicity of QDs. Cadmium-zinc sulfide ( $\text{Cd}_{0.7}\text{Zn}_{0.3}\text{S}$ ) QDs were attached to the surface of HNTs via linkage through a Schiff base (azine) bond, thus producing a core-shell nanoarchitecture. The HNTs were covered with  $\text{Cd}_{0.7}\text{Zn}_{0.3}\text{S}$  QDs with a diameter from 5 nm to 10 nm, corresponding to strong light absorption in the blue spectral range. CLSM images *in vitro* showed that the nanocomposites were concentrated at the periphery of the nucleus in prostate cancer cells (PC-3 cell line). The nanocomposite showed low cytotoxicity and moderate resistance to photobleaching and could therefore be a promising cancer bioimaging strategy [58].

Sepiolite has a perfectly stable intrinsic fluorescence and can be used for fluorescence imaging and microscopy for intracellular tracking. Castro-Smirnov *et al.* [59] observed the natural fluorescence of sepiolite fibers inside fibroblasts (V79 cell line). Whilst the sepiolite fluorescence quantum yield was low, it was sufficient to image the sepiolite fibers inside the V79 cells [59].

### 3.2.2. Biosensors

Chemical sensors have two key components: a receptor and a transducer. The receptor, so-called recognition element, must be specific for the targeted analyte. On the other hand, the transducer, also known as the functional element, converts the molecular binding into a measurable signal. Chemical sensors are called biosensors when the receptor is a biological molecule. The biological recognition element acts as an intermediary between the analyte and the transducer, recognizing the presence, activity, or concentration of a specific analyte via a binding process or a biocatalytic reaction.

There has been a growing interest in the application of electrochemical biosensors in cancer diagnosis, as an alternative or a complement to optical biosensors. Electrochemical biosensors offer several advantages, namely a rapid response, highly-sensitive recognition, the need for only small amounts of sample, and often these biosensors are relatively cost-effective [60–63]. Mitomycin C (MTC) is an anticancer drug that interacts with DNA. Erdem *et al.* [60] developed a biosensor that could detect DNA and MTC-DNA interactions by measuring the electrochemical oxidation signals from MTC with guanine and adenine. The biosensor was based on pencil graphite electrodes (PGEs) modified with sepiolite and single-walled carbon nanotubes (SWCNTs). Sepiolite provided a high surface area for nucleic acid hybridization, whereas the SWCNTs enhanced the biosensor response [60].

Polyamines, such as spermine and spermidine, have been used as cancer biomarkers due to their roles in cell proliferation. Ikeda *et al.* [64] developed a fluorocolorimetric biosensor for the rapid detection of spermine and spermidine within biological fluids. The fluorocolorimetric biosensor was based on the combination of a supramolecular hydrogel with a MMT preparation containing an adsorbed cationic coumarin dye (G-coum). G-coum was released from the MMT via a selective cation exchange process with spermine or spermidine, resulting in fluorescence spectral changes. G-coum had a weak greenish excimer emission, which changed to a more intense blue monomer emission after its release from the MMT, and translocation to the supramolecular hydrogel fibers (Fig. 10). This hybrid biosensor could detect spermine at 20  $\mu\text{M}$  and spermidine at 100  $\mu\text{M}$ . The analyte concentrations inducing 50% of the maximum signal change were  $29 \pm 1.4 \mu\text{M}$  and  $55 \pm 4.8 \mu\text{M}$  for spermine and spermidine, respectively [64]. Prostate-specific antigen (PSA) is a cancer biomarker often used in the diagnosis and monitoring of prostate cancer. Li *et al.* [62] used polypyrrole (PPy)-coated HNTs in order to stabilize palladium (Pd) NPs, to provide an electrochemical biosensor for the amperometric detection of PSA in human serum samples. PPy is an electrically conducting polymer material, which was absorbed on the surface of the HNTs by *in situ* oxidative polymerization of the pyrrole monomers. The PPy shell promoted the absorption of Pd NPs and improved the conductivity of the nanocomposite, as well as the electrocatalytic activity. Subsequently, the nanocomposite was deposited onto the surface of glassy carbon electrodes (GCEs), followed by immobilization of antibodies to increase the specificity of the biosensor. The biosensor showed a wide detection range for PSA, and a low detection limit of 0.03 pg/mL [62].

Recently, Yaman *et al.* [63] described an innovative electrochemical sensor for diagnosis of breast cancer. The authors modified PGEs with an MMT-human serum albumin (HSA) complex to produce a biosensor for living cells. The cytosensor was able to

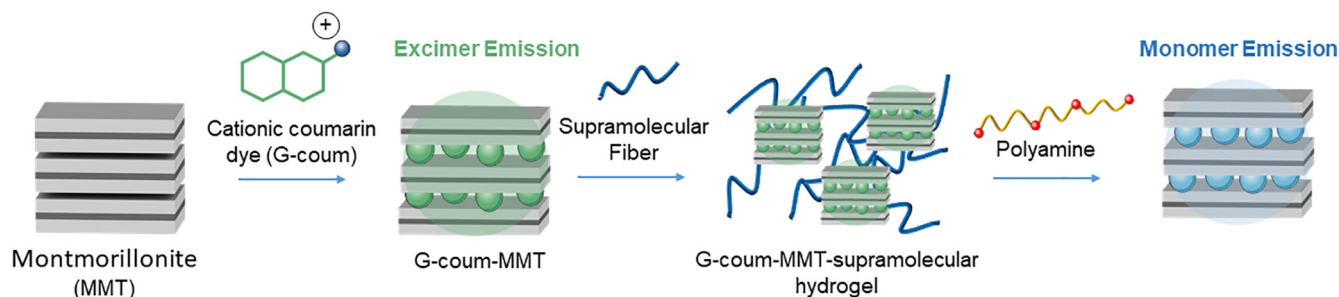


Fig. 10. Schematic diagram of the production and mechanism of action of a fluorocolorimetric sensor for the detection of polyamines.

detect MCF-7 breast cancer cells, with a limit of detection of 148 cells/mL. The same principles could be replicated for the detection of other types of cancer cells, encouraging further research in cancer diagnosis [63].

### 3.2.3. Detection of circulating tumor cells

CTCs are malignant cells that have become dislodged from a primary tumor and can then circulate around the body *via* the bloodstream or lymphatic vessels. CTCs can act as seeds for the formation of secondary tumors at distant locations, a process known as metastasis [65]. During their migration, CTCs display similar behavior as that seen in the adhesion cascade of leukocytes, a hallmark of inflammation [66]. Initially, the adhesion of CTCs to the endothelial surface of the blood vessel wall is mediated by sialylated carbohydrate ligands expressed on the surface of CTCs. The sialylated carbohydrate ligands interact with selectin receptors expressed on the endothelium with a low-affinity binding. The selectin-mediated rolling of the cells along the endothelial surface is followed by a tighter adhesion, resulting in the *trans*-endothelial migration of only a few CTCs into the tissue [4,67].

CTCs are important indicators of the presence or progression of cancer, given that CTC-mediated interactions are the major cause of cancer metastasis, which is responsible for ~90% of cancer deaths [4,66]. Considering this, numerous approaches are being studied to detect and capture viable CTCs from the blood, to prevent or detect metastasis, and to develop personalized cancer therapy [67]. However, it should be noted that CTCs are technically difficult to detect due to their extremely rare occurrence within the bloodstream (only 1 to 100 cells in 1 mL of blood) [67].

Currently, there is one CTC isolation system approved by the FDA, called CellSearch<sup>®</sup>. This system was developed to detect CTCs in blood samples by distinguishing them using immunological parameters. In CellSearch<sup>®</sup>, ferrofluid-coupled antibodies, specific

to the epithelial cellular adhesion molecule (EpCAM) that is expressed by CTCs, are used to bind and separate CTCs from other blood cells when exposed to a magnetic field. Next, the CTCs are stained using fluorochrome-coupled antibodies against specific intracellular epithelial cell markers, known as cytokeratins [66,67]. However, CTCs do not generally remain viable after CellSearch<sup>®</sup> isolation, thereby making these CTCs unsuitable for individualized disease prognosis and *in vitro* experiments to select personalized cancer therapies [67]. Therefore, innovative techniques are needed to isolate CTCs at high purity without inducing any cellular damage. To achieve this, nanostructures conjugated to antibodies specific for cellular adhesion markers have been studied to capture and isolate CTCs [68]. Nevertheless, these nanostructures fail to detect 30.0% of the adhesion markers expressed by CTCs. Hence, surfaces without antibodies but equipped with “nanoroughness” have also been used to isolate CTCs, *via* unique interactions between the CTCs and the nanomaterial surface [69].

In the last decade, HNTs with or without conjugated antibodies have been investigated as CTC isolation systems, taking advantage of a selective interaction between the sialylated carbohydrate ligands on CTCs and the selectin proteins (P-selectin or E-selectin) expressed on epithelial cells [69].

Polyurethane microtubes coated with recombinant human P-selectin-functionalized HNTs were tested to capture acute myeloid leukemia CTCs (Fig. 11). A positively charged poly-L-lysine monolayer was employed to attach the negatively charged HNTs to the inner surface of the microtubes, and to create a nanoscale roughness. The HNTs attached to the poly-L-lysine-coated microtubes significantly reduced the CTC rolling speed and increased the number of captured cells. The use of HNTs also increased the total surface area and promoted more interactions between the P-selectin molecules and the acute myeloid leukemia CTCs, contributing to the successful capture of the cells [66].

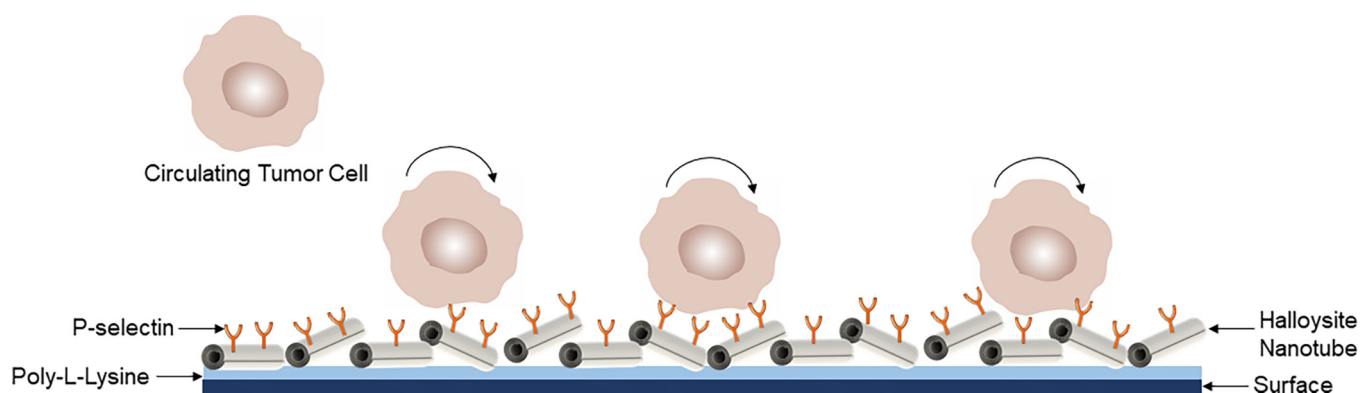
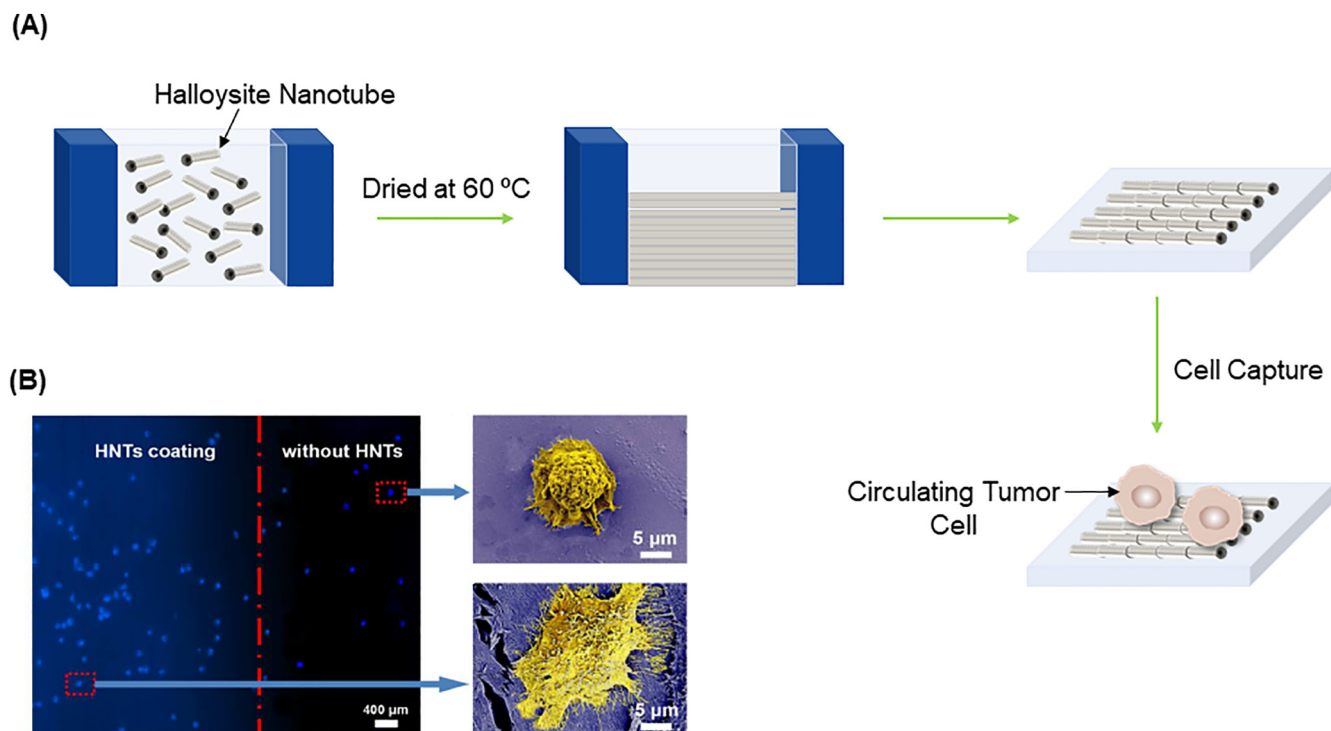


Fig. 11. Schematic illustration of the selective capture of circulating tumor cells (CTCs) by recombinant human P-selectin-functionalized hallosite clay nanotubes (HNTs) on the inner surface of poly-L-lysine-coated microtubes.



**Fig. 12.** Capture of circulating tumor cells (CTCs) on a glass surface covered with patterned halloysite clay nanotubes (HNTs). (A) Schematic representation of the preparation. (B) Scanning electron microscopy (SEM) images of the conformation of cancer cells on a smooth surface and HNTs-coated surface (adapted from [69]).

In a different study, polyurethane microtubes were coated with HNTs that had been functionalized with E-selectin (ES) protein and antibodies specific for epithelial markers (CTC-specific antibodies). This microtube system mimicked the natural process by which CTCs adhere to the endothelial surface. ES triggers the initial rolling adhesion of cancer cells, and enabled a faster capture of CTCs, which was an advantage compared to alternative microfluidic devices that required more time for CTCs to interact with the endothelial mimicking surface. The microtube device could separate viable CTCs from the blood of metastatic cancer patients, with high purity and without causing any cellular damage. Around 50% of the CTCs were captured from samples with a purity >50%. It should be noted that the HNT coating was essential to obtain these results, because the use of HNTs increased the surface area for protein adsorption and reduced the leukocyte spreading [65,68].

Rough nanosurfaces have shown the ability to improve cell adhesion, proliferation and migration. Therefore patterned HNTs with a surface coating with the appropriate roughness can be used to capture CTCs. Recently a dispersion of PSS-modified HNTs was introduced into a slit-like confined space between two glass slides and two gaskets, which formed a uniform coating on the surface of one glass slide after drying (Fig. 12A). To increase the HNTs coating stability on glass substrates, a surface treatment was performed by immersing the HNTs pattern in a solution containing  $\gamma$ -aminopropyltrimethoxysilane (APTES) before capture of cancer cells. When compared to a smooth glass surface, the resulting HNT coating showed an enhanced ability to capture different cancer cells, such as MCF-7, Hep-G2, Neuro-2A, A549, or B16F10. Additionally, significant differences were observed between the smooth surface and the HNT coated surface regarding the microstructure of the cancer cells. For example, the captured cells formed large protuberances on the HNT-coated surface, while the on the smooth surface the cells showed a more rounded configuration (Fig. 12B). The cancer cells adhered rapidly to the HNT-coated surface since this nanorough structure mimicked the extracellular matrix (ECM). To fur-

ther improve the capture efficacy of the HNT coating, anti-EpCAM antibodies could be attached to the surface of the HNTs, bestowing a superior capture ability compared to an unmodified HNT coating, and to smooth surfaces covered with anti-EpCAM antibodies. The anti-EpCAM antibody-covered HNT coating showed a capture efficacy of 92% towards MCF-7 cells after 3 h of incubation, while the unmodified HNT coating and the smooth glass surface with anti-EpCAM antibodies showed a capture efficacy of only 9.4% and 34.3%, respectively. These results underline the efficiency of HNTs in creating nanorough surfaces that encourage the adhesion of CTCs [69].

A simple, rapid, and low-cost thermal spraying technique is another strategy to produce uniform HNT coatings with a large surface area. The HNTs were uniformly dispersed in anhydrous ethanol, and the dispersion was sprayed onto a hot glass slide. The HNTs bound to the glass slide through Van der Waals forces and hydrogen bonds, creating a uniform rough coating (Fig. 13A). The HNT coating formed by the thermal spraying technique showed a capture efficacy of 90% for MCF-7 cells, due to the suitable roughness as well as the grafted anti-EpCAM antibodies. The capture efficacy could be further improved by providing a suitable dynamic shear condition within a fluid-circulating device using a peristaltic pump (Fig. 13B). The dynamic shear process using an appropriate flow rate increased the interaction between the MCF-7 cells and the HNT coating, thereby increasing the number of captured cells. Furthermore, HNTs could be loaded with doxorubicin (DOX) before the preparation of the HNT coating to create a nanocarrier that could efficiently kill the captured CTCs, thus lessening metastasis. In fact, MCF-7 cells captured on DOX-loaded HNT coatings showed significant membrane damage and only 3% of the cells remained viable after 16 h [70].

ES and PEG-functionalized liposomes that had been loaded with DOX were immobilized onto the HNT-coated microtube surface to simultaneously target and kill CTCs within the bloodstream. This microtube device increased the capture efficiency and the

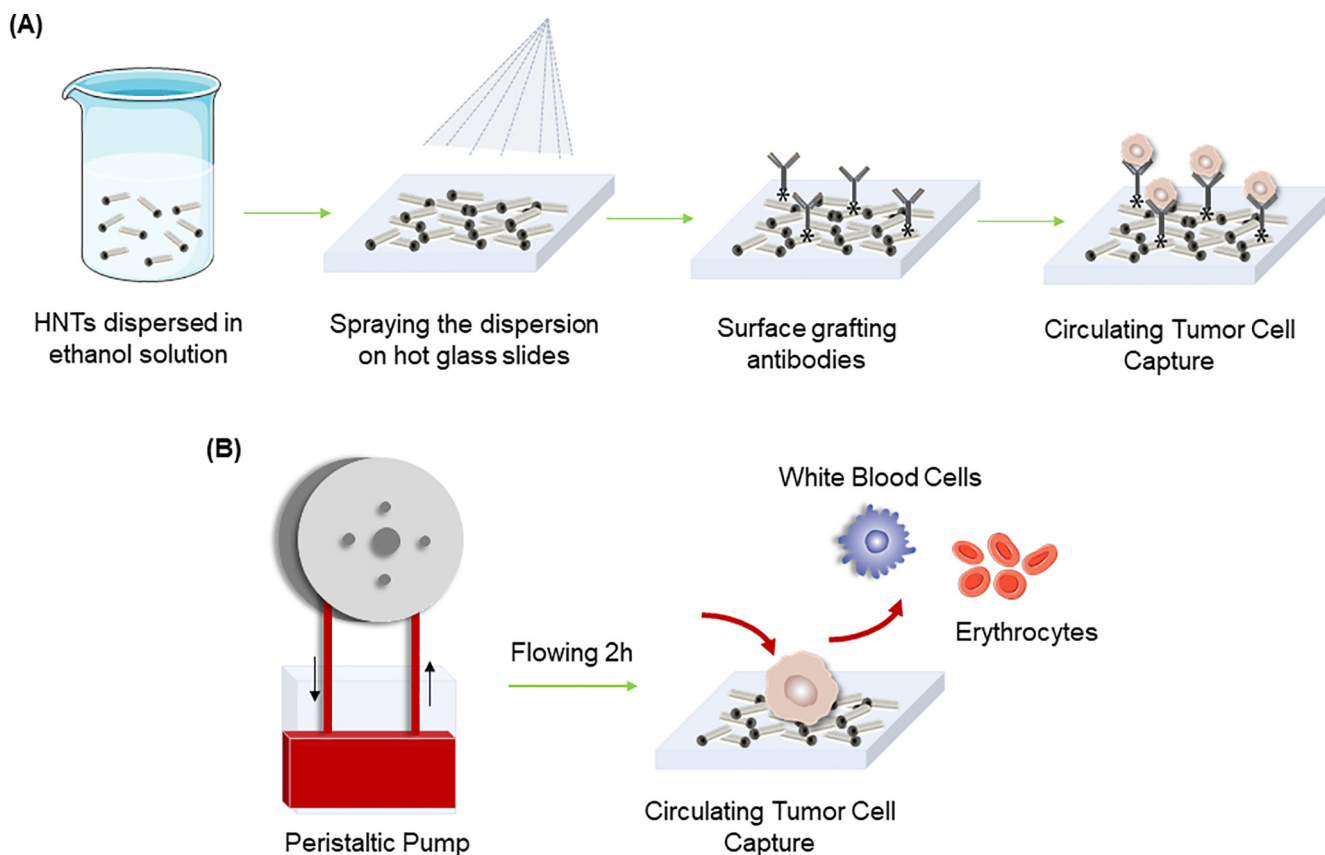


**Fig. 13.** Halloysite clay nanotubes (HNTs) coating grafted with antibodies to capture circulating tumor cells (CTCs). (A) Schematic illustration of the thermal spraying technique used for preparation. (B) Cell capture from blood samples using a peristaltic pump.

anticancer activity against CTCs under both static and dynamic conditions. This microtube device did not damage red blood cells, because they do not express ES ligands, however, it did slightly decrease the viability of leukocytes. Although leukocytes do express ES ligands, the CTCs formed better connections to the liposomes than the leukocytes. Moreover, the use of this microtube device required a lower dose of DOX than that administered to patients, since the biodistribution of the liposomal DOX in normal tissue was avoided [4].

HNTs combined with cationic and anionic surfactants have been used to capture CTCs and leukocytes under flow conditions. Sodium dodecanoate (NaL) and decyltrimethylammonium bromide (DTAB) were used to neutralize the positively charged internal surface and the negatively charged external surface of the HNTs, respectively. Leukocytes possess a negative charge on the membrane; therefore, these cells were captured by surfaces bearing positively charged HNTs functionalized with DTAB (HNTs-DTAB), whereas surfaces containing negatively charged HNTs functionalized with NaL (HNTs-NaL) repelled the leukocytes. In this way, any interaction between the leukocytes and adhesion receptors can be avoided using surfaces containing negatively charged HNTs. In contrast, the capture of CTCs was increased by surfaces containing negatively charged HNTs-NaL. There is a sugar-rich coating on the surface of CTCs, known as the glycocalyx, which interacts with HNTs-NaL via electrostatic interactions [5]. Therefore, HNTs with anionic surfaces are a viable option to facilitate the capture of CTCs. *In vitro* experiments using cells that over-expressed EpCAM molecules (COLO 205 and MCF-7 cell lines) demonstrated that surfaces containing HNTs-NaL modified with ES induced strong adhesion of cancer cells under flow conditions. A549 and Hs 578T cancer cells, which display a low to negligible

surface expression of EpCAM, were also efficiently captured on surfaces covered with ES-coated HNTs-NaL. These results showed that surfaces coated with HNTs-NaL do not necessarily require the use of CTCs-specific biomarkers [67].

The folate receptor (FR) is a membrane glycoprotein used for folic acid (FA) uptake by cells, is frequently over-expressed on the surface of many types of cancer cells. This biomarker may be used for the detection of CTCs, since it can be targeted by FA with high affinity. Hence, FA may be used as a targeting ligand. Magnetic HNTs (MHNTs) coated with  $\beta$ -cyclodextrin ( $\beta$ -CD) were coupled to FA through a PEG-adamantane (Ad) linker in order to capture CTCs, which over-expressed the FR. The capture efficiency values of FA-functionalized MHNTs for human ovarian cancer (Skov3), HeLa and A549 cancer cells were 96.3%, 97.0%, and 95.6%, respectively. Captured cells remained viable and exhibited a normal growth pattern *in vitro*, which enabled subsequent analyses. FA-functionalized HNTs could be recycled since the capture efficiency remained above 90% for the three cancer cell lines (Skov3, HeLa and A549) after three successive regeneration cycles [71].

All the studies discussed above suggest that the ability to capture CTCs from the blood of cancer patients could be used in the diagnosis and treatment of cancer.

### 3.3. Cancer therapy

The hallmarks of cancer were originally described by Hanahan and Weinberg in 2011 to encompass the entire complexity of cancer [72]. Cancer biology can only be fully explained by understanding the individual specialized cell types inside the tumor, as well as the surrounding TME that contributes to the hallmark traits. The TME results from an interaction between cancer cells, multiple

stromal cell types, and also non-cellular proteins (Fig. 14) [73]. The complexity of cancer biology is the main reason behind the lack of effectiveness ascribed to conventional anticancer therapies. Understanding the TME provides a valuable opportunity to create smart nanocarriers that could more efficiently deliver anticancer drugs to the tumor site [72,74].

The application of nanoclays in cancer therapy is not restricted to their use as carriers for the delivery of anticancer agents. Actually, certain types of nanoclays have an intrinsic anticancer bioactivity. The following sections will cover in-depth the anticancer therapeutic use of nanoclays *per se* and as delivery carriers of a myriad of bioactive molecules.

### 3.3.1. Intrinsic anticancer bioactivity of pristine nanoclays

Recent *in vitro* and *in vivo* experiments have suggested that nanoclays evidence intrinsic bioactivity against cancer [75–78].

Pristine BENT affected the proliferation of glioblastoma cells while enhancing the cellular growth of lung adenocarcinoma cells, depicting cell-specific effects that arguably result from the interaction of this type of nanoclay with cancer-related proteins [75]. In mice inoculated with Lewis lung carcinoma cells (LLC cell line), pristine kaolinite reduced the generation of superoxide radicals and the size of the tumor mass, preventing metastases [76].

Pristine nanoclays, due to their high SSA and the surface charge, modulate the adhesion between cancer cells and the surrounding ECM, preventing cancer cell metastasis [77]. Abduljawad *et al.* [77] have investigated the use of Na-MMT, PAL, and hectorite to control cancer cell-ECM adhesions. Na-MMT promoted cell–cell adhesions, whereas PAL and hectorite increased cell-ECM adhesions in a lymphoma cell line (Raji cells). The combination of Na-MMT with PAL (75:25) exhibited the highest increase in cell–cell-ECM adhesions. In a wound-healing assay using MCF-7 cells, the nanoclays controlled cell migration, causing a delay in the gap closure, which indicates that the tested nanoclays reduced the migration of cancer cells, preventing the formation of metastasis [77].

Also, recently, the combination of Na-MMT and PAL (75:25) reported above [77] was tested to control melanoma metastasis [78]. In human malignant melanoma cells (SK-Mel-28 cell line), the treatment with the nanoclay mixture induced changes in the membrane potential and significantly reduced cell viability and proliferation in a dose-dependent manner. In contrast, no significant changes in the viability were detected in normal melanocytes,

indicating that this nanoclay mixture has selective cytotoxicity against melanoma cells. These results were corroborated by *in vivo* studies. The injection of the nanoclay mixture reduced the tumor volume and weight in an SK-Mel-28-xenografted mice model. The histological analysis revealed that the treatment with the combination of Na-MMT and PAL (75:25) inhibited cancer cell mitosis, leading to necrosis. The intrinsic anticancer bioactivity of nanoclays is essentially related to the formation of nanoclay-cancer cell adhesions [78].

### 3.3.2. Anticancer drugs

It is widely known that the anticancer drugs used in conventional cancer chemotherapy, have a narrow therapeutic index, low bioavailability, lack specificity, and require multiple dosing at high concentrations. In this way, the targeted delivery of conventional anticancer drugs using nanoclays as drug nanocarriers could reduce the side effects of the drugs and improve their overall therapeutic efficacy [10,79]. Anticancer drugs can be immobilized inside nanoclays, producing a novel drug nanodelivery system. In comparison with conventional dosage protocols, this nanodelivery strategy specifically targets cancer cells, improving the bioavailability of the drugs, and can reduce their side effects by modifying the drug release rate. Moreover, this nanodelivery strategy can be used to enhance the stability of drugs, and protect the anticancer drugs from degradation within the body [17,22].

To be able to effectively use nanoclays in drug delivery, it may be necessary to improve some of their properties, such as SSA, type of exchangeable cations, zeta potential, porosity, and surface chemistry. In this regard, nanoclays can be subjected to several modifications, for instance being combined with polymers or magnetic nanoparticles, (Fig. 14) [1,12].

In the next section, the use of nanoclay-based delivery systems against several types of cancers is discussed, with an emphasis on the functionalization strategy carried out in each delivery system.

**3.3.2.1. Lung cancer.** In global cancer statistics, lung cancer remains at the top of the incidence and mortality rates. There are two main types of lung cancer, non-small cell lung cancer (NSCLC), and small cell lung cancer (SCLC), which are each treated with different therapies. NSCLC is the most common lung cancer, and the anticancer drugs most used for its treatment include gemcitabine (GEM) and cisplatin (CPT) [80]. GEM is a pyrimidine analog, acting specifically in the S phase of the cell cycle, when the replication of DNA occurs.

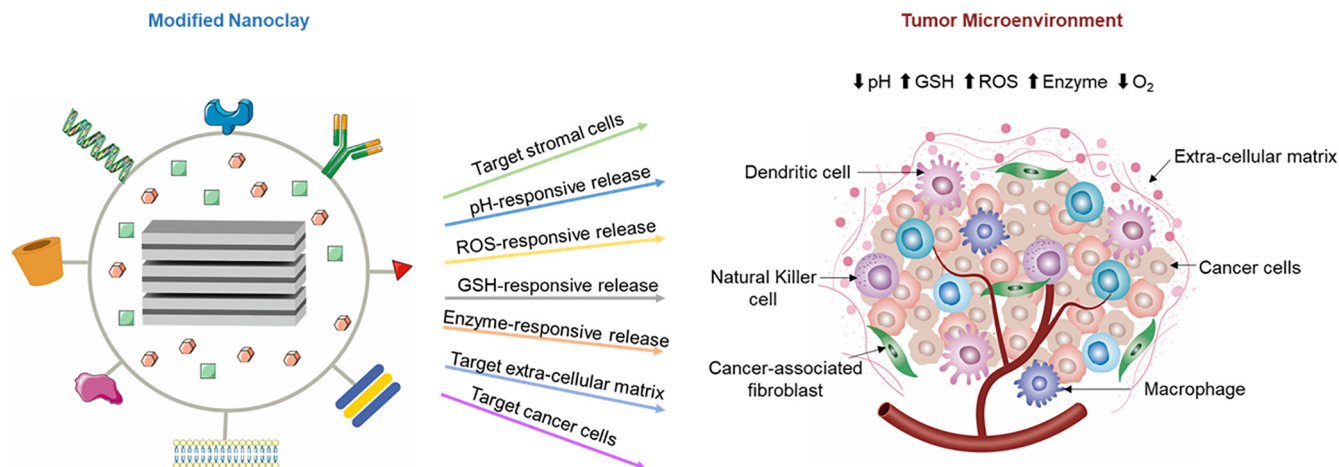


**Fig. 14.** Schematic illustration of strategies used to expand the functions of nanoclays. The modified-nanoclays target the tumor microenvironment (TME), increasing the efficacy of cancer therapy. TME has been shown to have different characteristics from normal tissues, which can be vascular defects, higher expression of given enzymes, elevated glutathione (GSH), hydrogen ion and reactive oxygen species (ROS) concentrations.

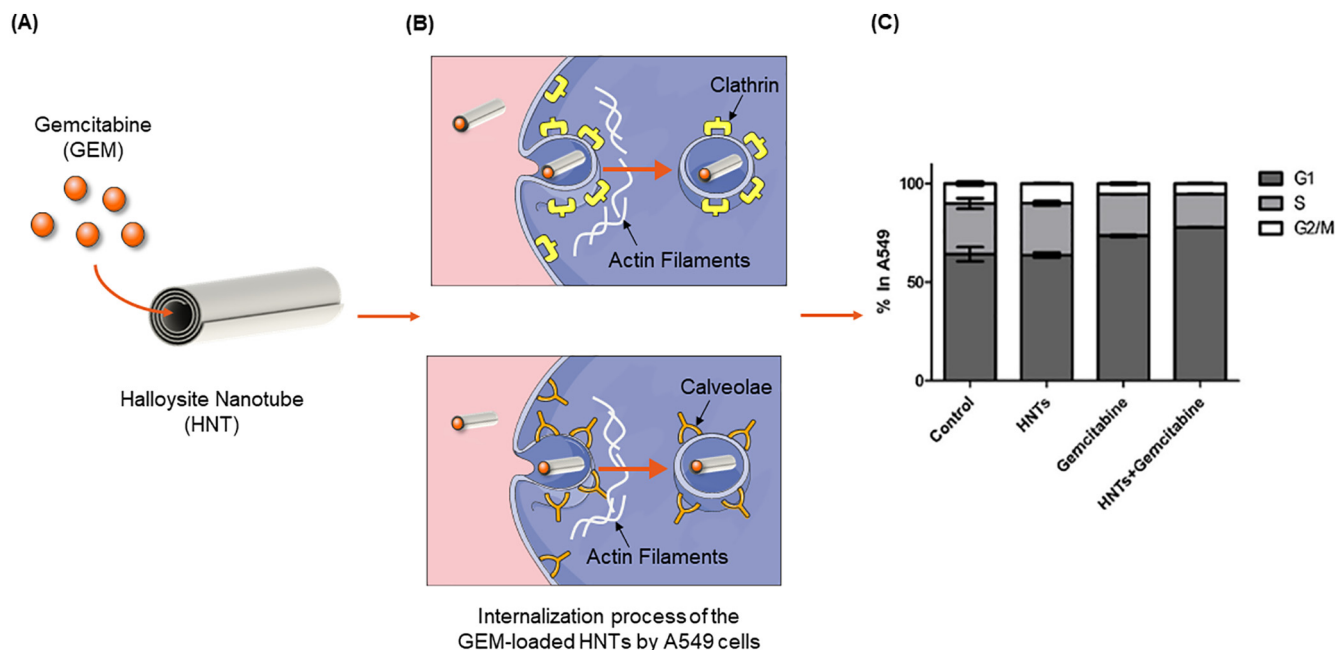


**Fig. 15.** Halloysite clay nanotubes (HNTs) for gemcitabine (GEM) delivery to cancer cells. (A) Schematic illustration of GEM-loaded HNTs. (B) The internalization process of GEM-loaded HNTs into A549 cell via clathrin-dependent or caveolae-dependent pathways. (C) Percentage of A549 cell in each phase of the cell cycle after exposition to pristine HNTs, free GEM, and GEM-loaded HNTs (adapted from [81]).

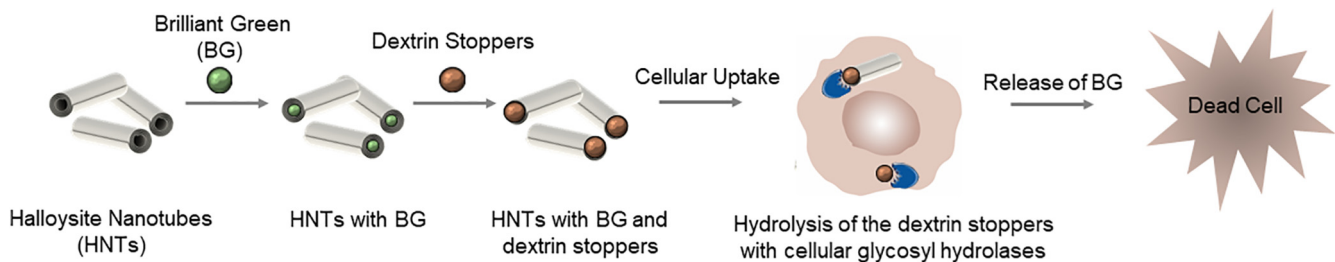


**Fig. 16.** Brilliant green-loaded halloysite clay nanotubes (HNTs) capped with dextrin tube-end stoppers for enzyme-activated brilliant green release.

In certain conditions, GEM also blocks the progression of cells in the G1 and S phases. Typically, GEM is administered intravenously, but it has a non-specific action and inefficient biodistribution. HNTs could be a possible solution to overcome these problems, since these nanoclays can transport GEM through cell membranes via several pathways (Fig. 15A, B). Liu *et al.* [81] showed that GEM-loaded HNTs could inhibit the cell cycle in A549 cells and reduce the fraction of cells in the S phase (Fig. 15C). Consequently, GEM-loaded HNTs inhibited the cell division and growth of A549 cells [81].

In another study, water-dispersed DOX-loaded HNTs damaged the cellular organization of A549 cells and allowed the sustained release of DOX over 2 weeks without any initial burst release [82].

Furthermore, HNTs were loaded with an off-label anticancer drug (brilliant green) and capped with dextrin (DX) tube-end stoppers. This system exhibited an enzyme-activated drug release pattern and accumulated only in highly-proliferating A549 cells (Fig. 16) [83].

Only approximately 10–15% of all lung cancers are SCLCs, which tend to grow and spread faster than NSCLCs. Since SCLCs have a very high proliferation rate, this type of lung cancer generally responds well to chemotherapy and radiotherapy. SCLCs are treated with anticancer drug regimens that often include CPT [80]. CPT is a platinum-based anticancer drug that interacts with DNA,

forming cross-links. The main side effect of CPT is bone marrow suppression. However, CPT can also cause nephrotoxicity, neurotoxicity, nausea, and severe vomiting. Allophane was used as a CPT nanocarrier to reduce its side effects. Toyota *et al.* [84] investigated the complex formation of allophane NPs with CPT against A549 cells (Fig. 17A). CPT-allophane NPs were released at acidic and neutral pH conditions. The release was higher in acidic media, where approximately 60% of CPT was released in the first 50 h, whereas, at pH 7.4, around 44% of CPT was released in 70 h, showing a sustained release profile (Fig. 17B). Using fluorescent microscopy, it was possible to demonstrate that the CPT-allophane NPs were internalized by A549 cells (Fig. 17C). Moreover, the CPT-allophane NPs were less cytotoxic than free CPT at comparable doses (Fig. 17D, E) [84].

**3.3.2.2. Colorectal cancer.** Colorectal cancer (CRC) is the third most frequent cancer in the world, accounting for 10.2% of the estimated 18.1 million new cancer cases diagnosed in 2018 [2]. The colon and rectum have different embryological origins, anatomy, and functions. Thus, primary colon and rectal cancers require individualized treatments and different surgical approaches. However, in general, metastatic colon and rectal cancers are considered to be a single entity and treated in the same manner [85]. Oral administration is the preferred administration route for delivering anticancer

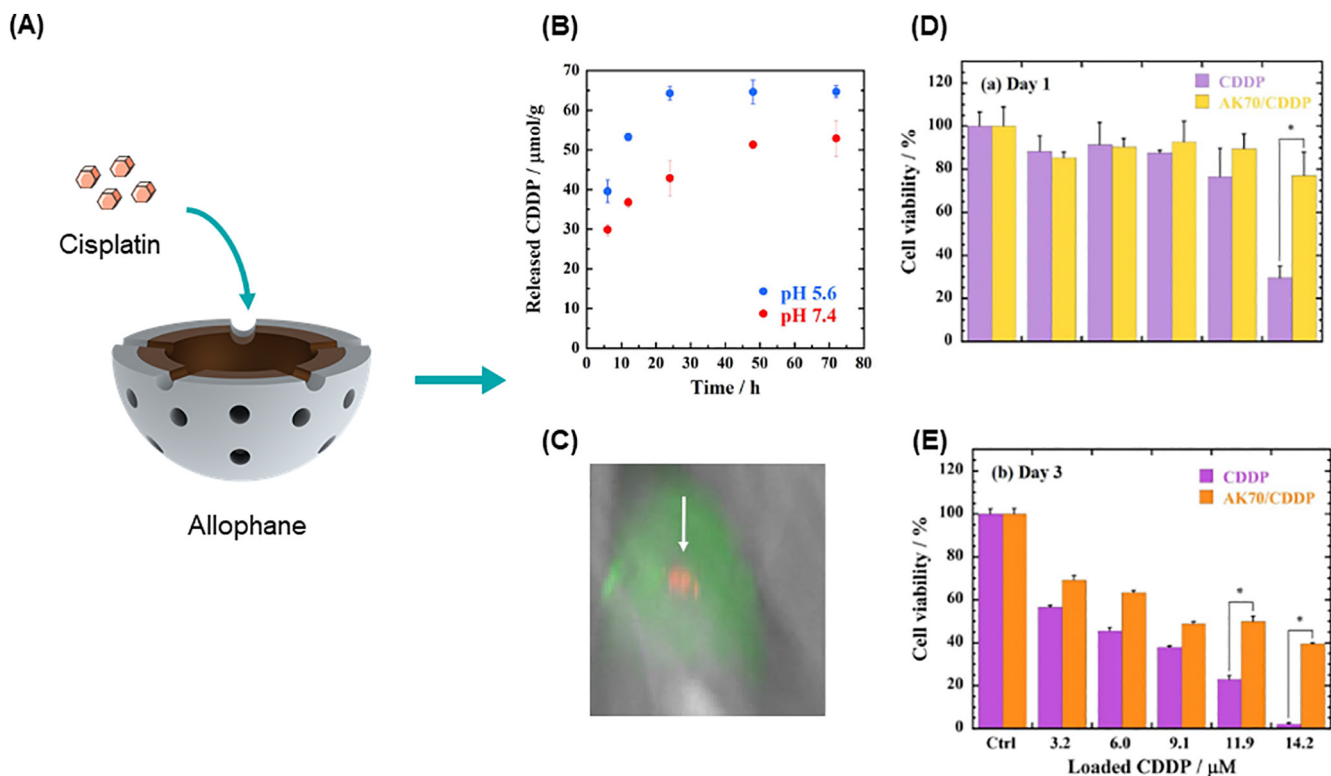


**Fig. 17.** Complex formation between cisplatin (CPT) and allophane nanoparticles (NPs). (A) Schematic representation of the preparation. (B) Release profile of CPT-allophane NPs in acid (pH 5.6) and physiological conditions (pH 7.4) (adapted from [84]). (C) Accumulation of CPT-allophane NPs in the periphery of the nuclear region after cellular internalization (adapted from [84]). (D) A549 cells viability after 1 day of incubation with CPT-allophane NPs (adapted from [84]). (E) A549 cells viability after 3 days of incubation with CPT-allophane NPs (adapted from [84]).

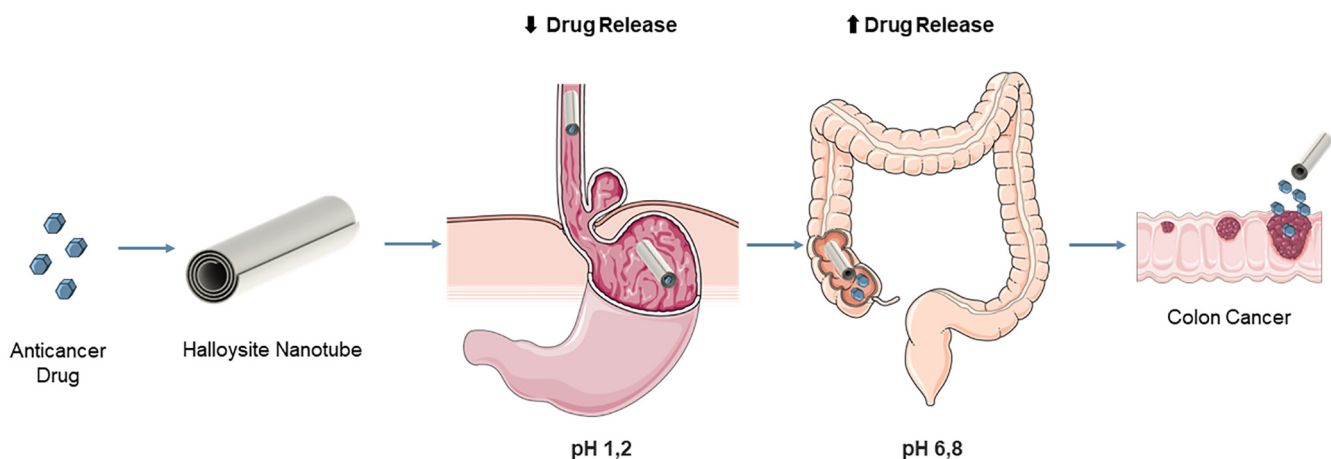


**Fig. 18.** Schematic illustration of a pH-responsive nanoclay for anticancer drug delivery to the intestines, avoiding early release in the stomach.

drugs for colon and rectal cancers [86]. Thereby, pH-responsive and time-dependent nanocarriers could be desirable for the oral delivery of anticancer drugs, since these nanotechnology-based strategies maximize drug release in the intestinal tract and minimize the early drug release in the stomach (Fig. 18) [45]. 5-fluorouracil (5-FU), camptothecin (CAM), and paclitaxel (PTX) are examples of anticancer drugs that are frequently used in therapeutic regimens for colon and rectal cancer [2,87–89].

5-FU is an antimetabolite drug prescribed for metastatic CRC and is also used in neo-adjuvant regimens. The main route of administration is oral tablets; however, 5-FU shows incomplete and unpredictable absorption due to its degradation within the

gastrointestinal tract. However the intravenous administration of 5-FU leads to severe collateral damage to normal organs [87,90]. Lin *et al.* [87] suggested that MMT could be used as a nanocarrier to overcome the problems of 5-FU administration. In this study, 5-FU was embedded into the interlayer space of MMT by free surface adsorption or by sodium and OH substitution [87]. MMT was found to be a suitable nanocarrier for 5-FU delivery, however, its loading capacity was only *ca.* 2 wt%. Amino-modified MMT was functionalized with  $\beta$ -CD *via* a nucleophilic substitution reaction to increase the MMT loading capacity (Fig. 19A). The nanocomposite underwent self-assembly into supramolecular dendrimer-like structures, that could be loaded with 5-FU with a high loading

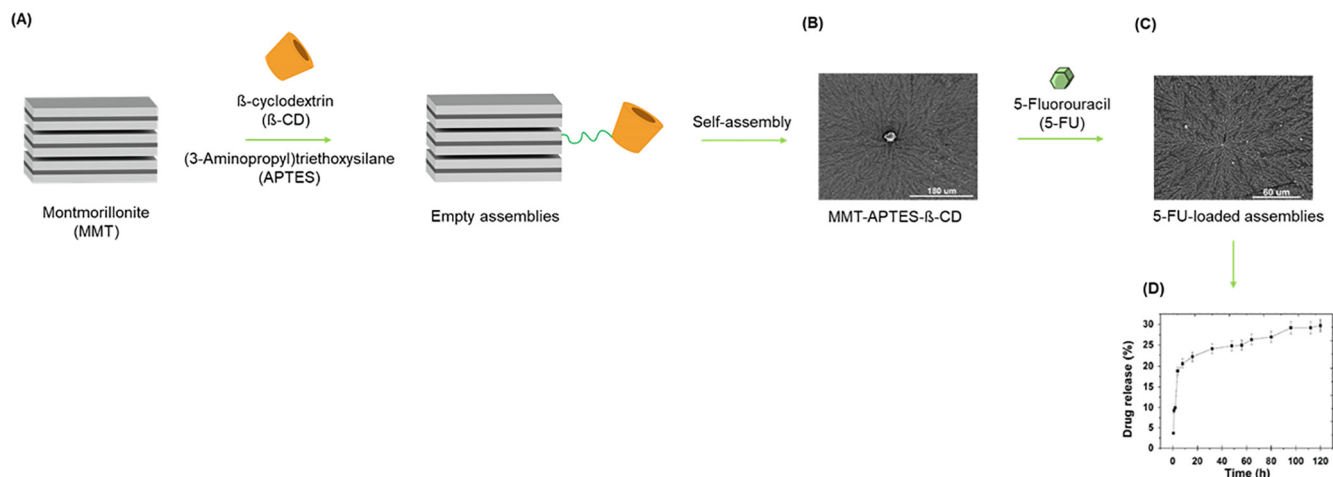


**Fig. 19.** Aminopropyltrimethoxysilane (APTES)-modified montmorillonite (MMT) decorated with β-Cyclodextrin (β-CDs) (MMT-APTES-β-CDs). (A) Schematic representation of the preparation. (B) Scanning electron microscopy (SEM) image of an empty supramolecular dendrimer-like structure obtained by self-assembly of MMT-APTES-β-CDs (adapted from [91]). (C) SEM image of the 5-Fluorouracil (5-FU)-loaded supramolecular dendrimer-like structure (adapted from [91]) (D) Sustained 5-FU release from the supramolecular dendrimer-like structure for over 120 h (adapted from [91]).

capacity (Fig. 19B, C). The *in vitro* drug release studies showed that this 5-FU-loaded supramolecular dendrimer-like structure provided sustained drug release over 120 h (Fig. 19D) [91]. In an alternative approach, Rao *et al.* [90] prepared an HNT-based nanocomposite hydrogel that also proved to be suitable for 5-FU delivery. First, hydrogels were prepared using sodium hyaluronate (SH) plus poly(2-hydroxyethyl methacrylate) (PHEMA). Then, 5-FU was loaded both inside the lumen of the HNTs and in the hydrogel network. The resulting HNT-based nanocomposite hydrogel showed a pH-responsive activity. The *in vitro* studies revealed that in the gastric pH conditions, the 5-FU release was <10%, whereas in intestinal pH conditions the HNT-based nanocomposite hydrogel provided a sustained release for over 70 h [90].

CAM is a topoisomerase-I inhibitor used for metastatic CRC. Like 5-FU, CAM is a poorly water-soluble drug with substantial toxicity to healthy tissues. To overcome these drawbacks, nanoclays, such as HNTs, can be applied as nanocarriers for CAM delivery. Recently, Rizzo *et al.* [88] developed an innovative HNT-reinforced supramolecular gel for sustained-release of CAM. It was prepared by the self-assembly of the fluoromethoxycarbonyl amino acid, Fmoc-L-phenylalanine (Fmoc-F). The presence of HNTs within the hydrogel matrix reduced the thermal stability and improved the gel strength. Release assays conducted in physiological conditions showed that CAM hydrolysis did not occur, and that CAM was released from HNTs at a sustained rate [88]. In a more recent study, CAM was immobilized within the lumen of chitosan (CS) oligosaccharide (COS)-modified MHNTs also conjugated to FA. This cancer-targeted nanocomposite was also prepared with magnetic properties. The CAM-loaded magnetic nanocomposite showed a sustained release over 60 h. The percentage of CAM released at pH 5 (acidic pH of the TME) was higher than that released at pH 6.8 and pH 7.4. Additionally, the nanocomposite significantly inhibited the growth of human colon carcinoma cells (Caco-2 cells) [92].

Irinotecan (IRN) is another potent topoisomerase-I inhibitor, which was loaded into the hollow cavity of HNTs. HNTs were coated with an acid-resistant anionic copolymer, Eudragit S100, to protect the IRN from the stomach conditions, and promote IRN release specifically in the intestine. The Eudragit S100-coated HNTs avoided IRN release in the stomach (only 0.7% was released in 2 h), and released their cargo specifically in the intestine (ca. 70% was released in 2 h) [93].

PTX is an antimicrotubular agent used in the treatment of a broad spectrum of solid cancers. Nevertheless, the clinical application of PTX has been hindered by its extremely low water solubility and its low oral bioavailability [35,86,94,95]. This latter biopharmaceutical limitation stems from the susceptibility of PTX to the action of cytochrome P450 metabolic enzymes present in the intestines and liver. Additionally, parts of the gastrointestinal tract, namely the intestine, liver, and kidney, show higher expression of the multi-drug efflux pump transporter, P-glycoprotein, which also contributes to the PTX low bioavailability [30,86,94,95]. Several nanoclay-based efforts have been carried out to deliver PTX to cancer cells. In a study by Dong *et al.* [94], an oral PTX-loaded bioadhesive nanocarrier was developed and tested against the CRC cell lines (Caco-2 and HT-29). PTX was loaded into poly(D,L-lactide-co-glycolic acid) (PLGA) modified MMT spherical NPs (PLGA-MMT NPs). The *in vitro* release experiments from PLGA-MMT NPs showed a biphasic profile with an initial burst release followed by a slow release, due to the presence of the PLGA copolymer. PLGA also enhanced the hydrophilicity and the stability of the nanocarrier. The cellular uptake efficiency of PLGA-MMT NPs was increased from 57% to 177% for Caco-2 cells and from 11% to 55% for HT-29 cells. Overall, the PLGA-MMT NPs displayed an improved residence time thanks to the MMT mucoadhesive properties [94]. In another study, Bothiraja *et al.* [95] incorporated PTX into the interlayer space of MMT via an ion exchange reaction. Subsequently, the PTX-MMT nanocarrier was coated with CS (PTX-MMT-CS). The resulting nanocarrier showed a controlled release of PTX and reduced toxicity. The *in vitro* assays in human colon cancer cells (COLO-205) revealed that the PTX-MMT-CS nanocarrier improved the anticancer activity of PTX, by at least 10% when compared to free PTX. The CS coating reduced the half-maximal inhibitory concentration ( $IC_{50}$ ) value of the PTX-MMT-CS nanocarrier. The amino groups in the nanocarrier structure formed hydrogen bonds with the glycoproteins present on the surface of cancer cells, producing a bioadhesive clay cluster [95]. To maximize the release of PTX in the intestines, Yendluri *et al.* [30] loaded PTX into poly(methacrylic acid-co-methyl methacrylate) (PMMM)-coated HNTs capped with DX end stoppers. PMMM polymer is only soluble in alkaline conditions (pH > 6.8) (Fig. 20A). The release profile showed that the nanocarrier avoided any PTX release at the stomach pH and released PTX in the intestinal pH at a sustained rate for

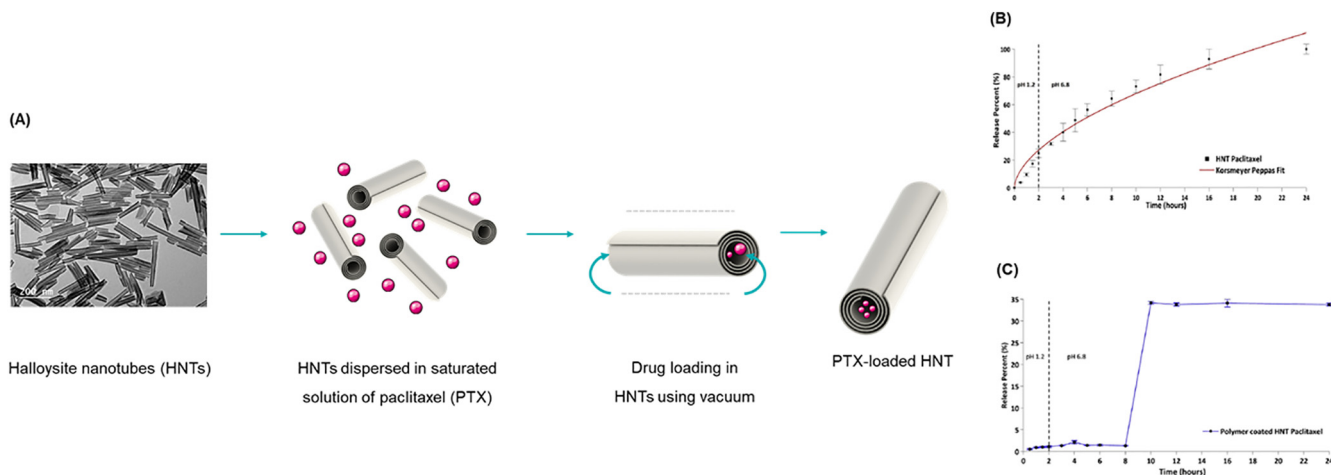


**Fig. 20.** Paclitaxel (PTX) loaded halloysite clay nanotubes (HNTs). (A) PTX loaded into the lumen using the vacuum method. (B) Release profile of PTX-loaded HNTs in media at pH 1.2 and 6.8 at 37 °C (adapted from [30]). (C) PTX pH-responsive release from poly(methacrylic acid-co-methyl methacrylate) (PMMM)-modified HNTs (adapted from [30]).

24 h (Fig. 20C). Moreover, in the same study, the authors described the production of a PTX tablet formulation. HNTs were integrated in the composition of the tablets, and acted not only as sustained drug delivery system, but also as a compression excipient. The tablets showed a sustained release for over 250 h [30].

Atorvastatin (ATV) and celecoxib (CEL) are two off-label anticancer drugs with some potential to be used in CRC treatment. Li *et al.* [86] used a microfluidic technique to encapsulate HNTs inside a pH-responsive hydroxypropyl methylcellulose acetate succinate (HPMACS) polymer, producing a “nano-in-micro” composite microsphere preparation for the simultaneous oral delivery of ATV and CEL. These microspheres disintegrated only when exposed to alkaline conditions (pH 7.4) thus avoiding the premature release of the drugs in the stomach. The microspheres allowed ATV and CEL release in simulated intestinal media (pH 7.4) where they inhibited the proliferation of colon cancer cells [86].

The above-mentioned studies suggest that nanoclays, specifically HNTs and MMT, may be used to develop oral nanocarriers. These clay nanocarriers must protect the anticancer drugs from premature release and degradation in the stomach, while allowing a precise release in the colon or rectum. In this way, anticancer drug-loaded nanoclays may help therapeutic approaches against cancer in these locations.

**3.3.2.3. Gastric cancer.** Gastric cancer still has a significant impact globally. In 2018, gastric cancer was responsible for over 1 million new cases and an estimated 783,000 deaths, making it the third deadliest cancer worldwide [2,7]. Early diagnosis is fundamental for the success of gastric cancer treatment, given that radical surgery is the only realistic treatment option in early stages. However, the overwhelming majority of gastric cancer cases are diagnosed when the cancer is at an advanced stage, due to the lack of clinical symptoms at earlier stages. Consequently, anticancer drugs are mostly used to prolong the life of patients and improved their quality of life [7]. To improve the anticancer efficacy of DOX and develop an innovative treatment option for gastric cancer, DOX-loaded HNTs were modified with soybean phospholipid (DOX-HNTs-LIP). The LIP package protected the DOX-HNTs from direct contact with sodium, chloride, and other charged ions in the blood, thus avoiding triggering any thrombosis [96]. The nanocomposite showed good hemocompatibility because the LIP exerted its protective function. The DOX-HNTs-LIP also showed a pH-responsive release. *In vivo* experiments were conducted in a gastric cancer-

bearing mice to evaluate the anticancer activity and the *in vivo* biodistribution of DOX-HNTs-LIP. In contrast to free DOX, the nanocomposite showed a superior inhibition on the growth of MCF murine gastric cancer cells. Furthermore, the survival time of the gastric cancer-bearing mice was significantly prolonged by treatment with the nanocomposite [7].

**3.3.2.4. Breast cancer.** Breast cancer is the most frequent and deadliest cancer type among women, although it can also rarely occur in men [2]. The term breast cancer includes different types of tumors that stem from the various cells composing the breast tissue. According to the histopathological classification, breast cancers can be classified into three main molecular subtypes, that also show a specific phenotype: luminal (estrogen or progesterone-receptor positive), non-luminal human epidermal growth factor receptor type 2 positive (HER2+), and triple-negative breast cancer [43]. Most breast cancers are estrogen receptor expressing luminal tumors, undergoing rapid growth in response to estrogen stimulation. These hormone-sensitive cancers respond best to endocrine therapies that inhibit estrogen synthesis. Anti-estrogens or aromatase inhibitors are two classes of drugs used in breast cancer endocrine therapy [45]. Tamoxifen (TMX) is a non-steroidal anti-estrogen drug that competes with estradiol for the estrogen receptor. TMX is used in the treatment of breast cancer in both premenopausal and postmenopausal women. In general, the administration of TMX is recommended for at least 5 years. Considering that TMX involves a long-term treatment, the favored route of administration is *via* oral tablets. Hence, to achieve a successful treatment, it is necessary to overcome the challenges associated with the oral route of administration, reduce the TMX side effects, and increase its efficacy [97]. In a study by Kevadiya *et al.* [97], TMX was intercalated within the interlayer space of MMT. The TMX-MMT composite was further modified with poly( $\epsilon$ -caprolactone) (PCL), producing microcomposite particles for oral administration (Fig. 21A). The microcomposite particles showed a controlled release pattern for up to 72 h due to the additional coating with the hydrophobic polymer, PCL (Fig. 21B). The pharmacokinetic profile was studied after a single oral administration of the microcomposite particles to a rat model. The pharmacokinetic results revealed that, in contrast to free TMX, the plasma TMX levels were within the therapeutic window in the rats (Fig. 21C). Additionally, the microcomposite particles displayed lower genotoxicity when compared with free TMX. The reasons behind the

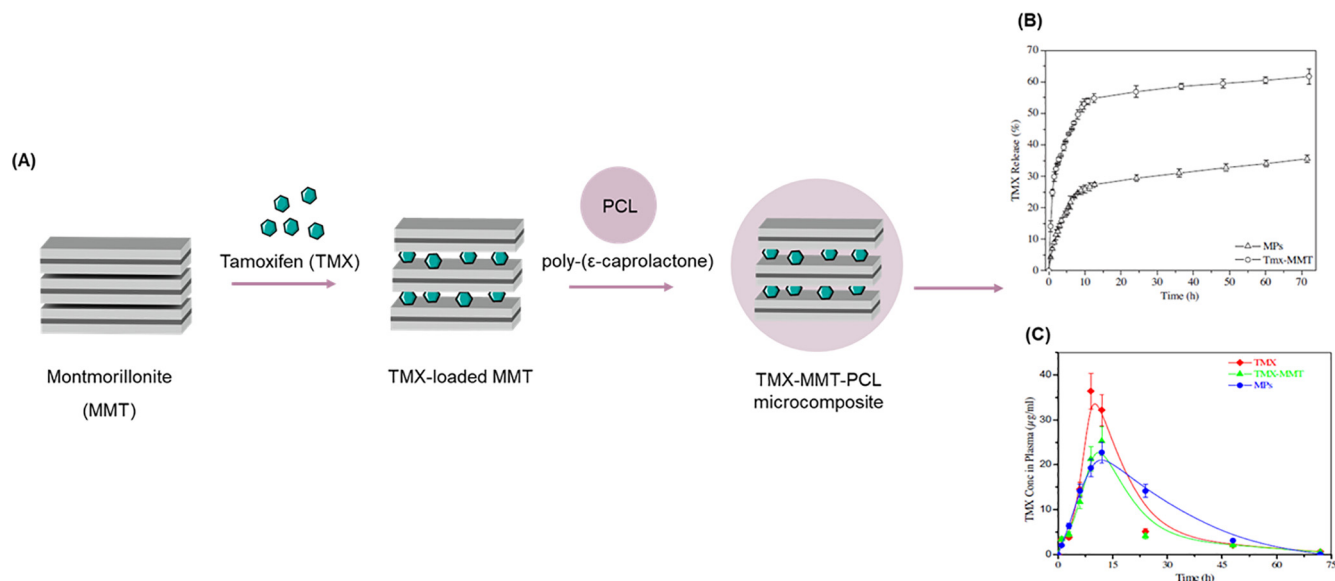


**Fig. 21.** Microcomposite particles composed of poly-(ε-caprolactone) (PCL), and tamoxifen (TMX)-loaded montmorillonite (MMT). (A) Preparation method. (B) Microcomposite particles release profile in intestinal conditions (pH 7.4 at 37 °C) (adapted from [97]). (C) Pharmacokinetic profile of the microcomposite particles after oral administration to Wistar rats (adapted from [97]).

lower genotoxicity were proposed to be the protection of the TMX within the interlayer space of MMT, the effects of MMT *per se*, and the PCL coating [97]. Aromatase is an enzyme responsible for estrogen biosynthesis. Aromatase inhibitors are used in postmenopausal patients with breast cancer who are resistant to anti-estrogen therapy. Exemestane is one example of a steroidal aromatase inhibitor which is used in breast cancer therapy. However, exemestane has low bioavailability due to its poor water solubility. When orally administered, exemestane is susceptible to the first-pass effect where most of the drug is removed by the liver [45]. Li *et al.* [45] developed an MMT-PLGA nanocomposite to enhance the oral bioavailability of exemestane, reduce the variations in drug plasma levels, and minimize the side effects. This nanocomposite displayed hydrophobicity, high surface area, and swelling capacity, leading to a reduction in the initial burst release, and prolonged the release rate of the drug. Moreover, the MMT-PLGA nanocomposite displayed mucoadhesive properties. Furthermore, the nanocomposite reduced the viability of human breast cancer cells (MCF-7) [45]. For non-luminal HER2 + breast cancer, *i.e.*, a type of breast cancer that over-expresses human epidermal growth factor receptor-2 (HER2), the best treatment choice is immunotherapy with trastuzumab. Trastuzumab is a humanized monoclonal antibody designed to specifically target HER2 receptors, which are transmembrane protein kinases involved in the signaling cascade responsible for the proliferation of breast cancer cells. Sun *et al.* [43] developed a trastuzumab decorated MMT-PLGA nanocomposite for the targeted delivery of an anticancer drug, PTX. Trastuzumab has a dual function, *i.e.*, not only does it target cancer cells over-expressing HER2 and inhibit proliferation, but also attracts immune cells that can kill the cancer cells. The coupling of a selective ligand to the surface of the MMT-PLGA nanocomposite significantly improved the cellular uptake. An *in vitro* assay performed in breast cancer cells over-expressing HER2 (SK-BR-3), the anticancer therapeutic efficacy of the PTX-loaded MMT-PLGA nanocomposites decorated with trastuzumab was 13.1 times higher when compared to free PTX [43].

Triple-negative breast cancer has a poor prognosis. CPT, docetaxel, and DOX are examples of anticancer drugs used in triple-negative breast cancer treatment. CPT is a platinum-based anticancer drug that binds to DNA and blocks its replication, conse-

quently inhibiting cellular division. CPT has some limitations due to its severe side effects and nonspecific biodistribution. Kouser *et al.* [98] described a strategy to produce a nanocomposite hydrogel film from carboxymethyl cellulose (CMC), hydroxyethyl cellulose (HEC), acrylonitrile (ACN), sustainable polyols, and sodium MMT (NaMMT) for the controlled release of CPT. The CPT-loaded nanocomposite hydrogel acted as a pH-responsive reservoir for the sustained release of CPT, and efficiently inhibited the growth of MCF-7 cells. The mechanism of the sustained CPT release was proposed to be due to the intermolecular interactions created by the dispersion of NaMMT within the polymer matrix [98].

Docetaxel is another anticancer drug frequently used in the treatment of triple-negative breast cancer. However, the poor water solubility of docetaxel and its severe side effects limit its clinical application. Feng *et al.* [99] developed a nanocomposite between MMT-poly(lactide) and d-α-tocopheryl polyethylene glycol 1000 succinate (TPGS, a vitamin E derivative). The MMT-PLA-TPGS nanocomposite was designed for the oral administration of docetaxel. The MMT-PLA-TPGS nanocomposite showed higher cytotoxicity than free docetaxel, in MCF-7 cells. The *in vivo* studies showed that the MMT-PLA-TPGS nanocomposite had a 26.4-fold longer half-life compared to free docetaxel and improved the oral bioavailability of the drug [99].

The clinical application of DOX is limited by its cardiotoxicity, short plasma half-life, and poor specificity. Nanoclays have been investigated to overcome the severe side effects of DOX. Kohay *et al.* [42] used an amphiphilic block copolymer poly(ethylene)glycol-phosphatidylethanolamine (PEG-PE) to produce micelles. Subsequently, DOX was incorporated into the core of the PEG-PE micelles, and these DOX-loaded micelles were further modified by adsorption of MMT, forming an organic-inorganic nanocomposite for DOX delivery. Two DOX formulations based on different PEG-PE/MMT ratios were studied. In the low polymer loading composite (LOW), the surface of MMT was partially coated with polymer and its interlayer space also incorporated a monolayer of polymer. In the case of the high polymer loading composite (HIGH), a bilayer of polymer covered the surface of MMT, and two layers of polymer were embedded in the interlayer space of MMT. In both cases, the external coat of the composite determined the interaction between DOX and MMT, and consequently the rate

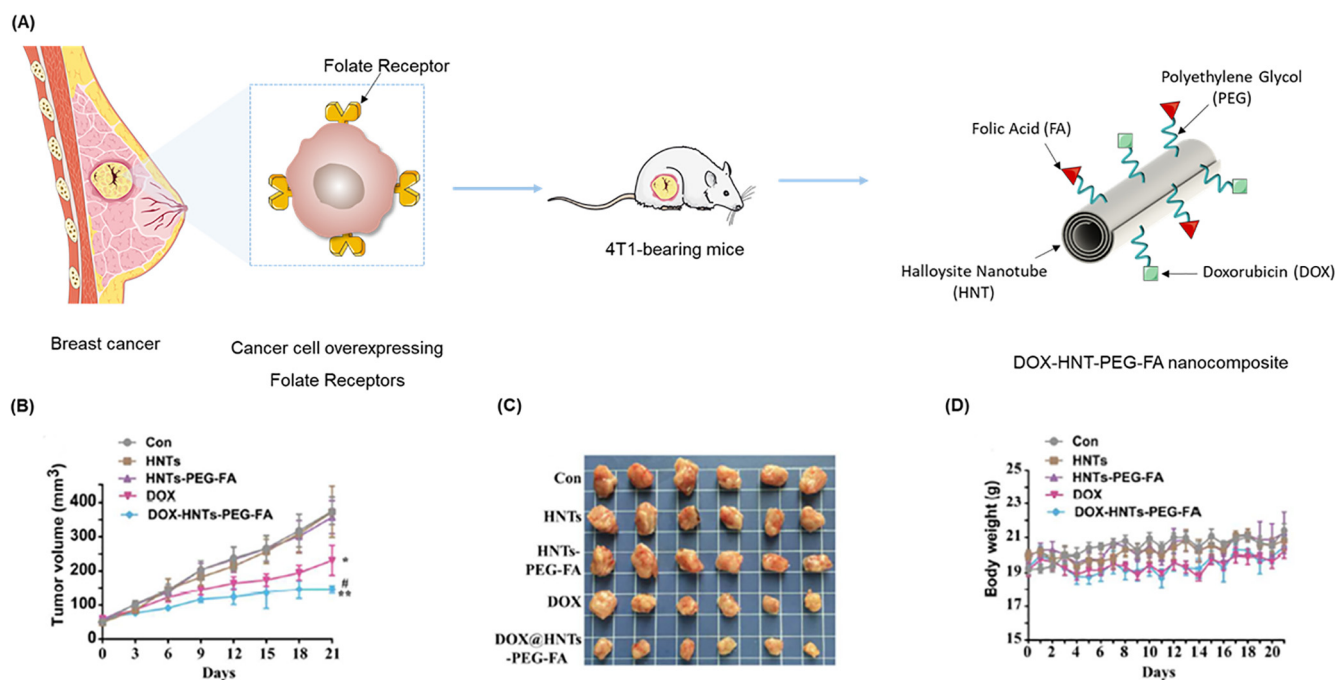


**Fig. 22.** Doxorubicin (DOX)-loaded PEGylated halloysite clay nanotubes (HNTs) conjugated to folic acid (FA) (DOX-HNT-PEG-FA) for targeted breast cancer therapy. (A) Preparation method. (B) *In vivo* antitumor effect of DOX-HNT-PEG-FA nanocomposites in 4T1 breast cancer-bearing mice, expressed as tumor volume (mm<sup>3</sup>) (adapted from [8]). (C) Photograph of excised 4T1 breast cancer solid tumors on the 22<sup>nd</sup> day after treatment (adapted from [8]). (D) Change in tumor weight of each group of mice during the study (adapted from [8]).

of DOX release. In the LOW composite a direct interaction between DOX and MMT occurred due to partial polymer coverage, while in the HIGH composite the interaction was mediated by the embedded and external polymer bilayers. The release rate was inversely correlated with the strength of the DOX interaction with MMT, meaning that a higher and faster release rate in the HIGH composite implied a weaker interaction, compared to the LOW composite. However, the release rate of both composites were inferior to DOX-M micelles but superior to a DOX-MMT nanocomposite. *In vitro* experiments compared the performance of LOW, HIGH and DOX-MMT formulations in DOX-sensitive cells (MCF-7) and DOX-resistant cells (A2780-ADR). All the formulations showed higher cytotoxicity when compared to free DOX. In MCF-7 cells, the HIGH composite showed the highest cytotoxicity. In the case of A2780-ADR cells, the increased amount of PEG-PE copolymer delayed the internalization of the formulation, thus the LOW composite showed a higher cytotoxic effect despite its slower release. They concluded that the cytotoxic effect in sensitive cells mainly depended on the release rate of DOX, whereas in resistant cells the interaction between the composite and cells was the most important factor. The release rate of DOX, the cellular uptake, and the cytotoxicity of the nanocomposites were influenced by the PEG-PE micelles/MMT ratios [42].

The clinical limitations of DOX may be overcome by using cancer-targeted nanocarriers. In 2018, Wu and co-workers developed DOX-loaded PEGylated HNTs conjugated with FA (HNT-PEG-FA) as nanocarriers for targeted breast cancer therapy (Fig. 22A). The HNT-PEG-FA showed a sustained and controlled release over 35 h at acidic pH. *In vitro* assays showed that HNT-PEG-FA inhibited proliferation and promoted apoptosis in breast cancer cells over-expressing FR. In contrast, the HNT-PEG-FA displayed only low cytotoxicity towards cells lacking FR. Studies performed on 4T1 breast cancer-bearing mice showed that the DOX-loaded HNT-PEG-FA nanocarriers inhibited tumor growth and increased the expression of cleaved caspase-3. Moreover, *in vivo*

experiments showed that HNT-PEG-FA reduced the cardiotoxicity seen with free DOX (Fig. 22B, C) [8].

Yang *et al.* [100] also created a nanocarrier based on HNTs for DOX delivery against breast cancer. HNTs were functionalized with COS instead of CS because of its low molecular weight, and to enhance the antitumor efficacy of DOX through the targeting both mitochondria and nuclei. The nanocarrier showed acceptable biocompatibility, reduced hemolysis rate, and suitable drug release kinetics. *In vitro* studies with MCF-7 cells demonstrated that the DOX-HNT-COS nanocarrier had a different action from free DOX, because it induced apoptosis, increased ROS generation, damaged mitochondria, and also acted on the nucleus in this cell line. *In vivo* antitumor studies in 4T1 breast cancer-bearing mice, also showed that the DOX-HNT-COS nanocarrier differed from free DOX, because it showed better inhibition of tumors, accompanied by less damage to cardiomyocytes. This nanocarrier also showed the absence of toxicity in other vital organs [100].

The above results have shown that nanocarriers based on MMT or HNTs can be used for the delivery of anticancer drugs in breast cancer treatment. They can release anticancer drugs in a controlled manner, decrease the side effects, protect anticancer drugs from degradation, prolong the circulation half-life, increase the solubility of insoluble drugs, and decrease renal clearance.

**3.3.2.5. Pancreatic cancer.** Pancreatic cancer is one of the deadliest cancers accounting for 331,000 deaths each year worldwide [2]. Current treatment approaches, including surgery, chemotherapy, and radiotherapy are not very effective compared to most tumor types. Chemotherapy is the main treatment option when surgery cannot totally remove the tumor, or when the cancer has already undergone metastasis [101]. GEM is one of the most common anticancer drugs used for pancreatic cancer treatment [81]. However, GEM has a very short plasma half-life (*ca.* 15 min) and is rapidly metabolized. Thus, high doses of GEM are repeatedly administered to guarantee the desired therapeutic effect, but this causes marked toxicity and low

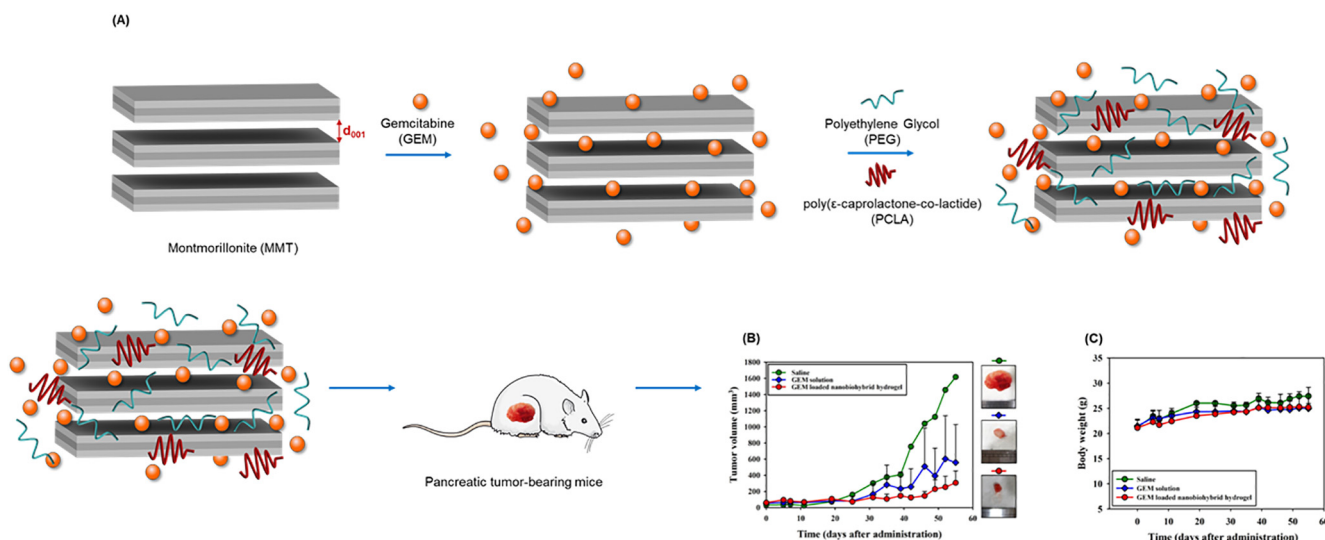


**Fig. 23.** Gemcitabine (GEM)-loaded montmorillonite (MMT) nanohybrid hydrogel (A) Schematic representation of the preparation. (B) *In vivo* antitumor effect obtained from the treatment with the nanobiohybrid hydrogel in pancreatic tumor-bearing mice, expressed as tumor volume ( $\text{mm}^3$ ) (adapted from [102]). (C) Alteration in tumor weight of each group of mice during the study (adapted from [102]).

patient compliance [102]. Hydrogel matrices are one of many strategies that have been tested to maximize the effects of GEM and minimize the side effects. Hydrogels are three-dimensional polymeric networks with good biocompatibility and are biodegradable in physiological conditions since they are mainly composed of water and possess the ability to transport molecules through the bloodstream and to penetrate into tissues [103].

Phan *et al.* [102] produced a nanobiohybrid hydrogel for the controlled release of GEM, and to overcome its clinical limitations in pancreatic cancer treatment. GEM was simultaneously inserted into the interlayer spaces of MMT and adsorbed onto its surface. Subsequently, the obtained GEM-MMT nanocomposites were dispersed into a temperature-responsive tri-block co-polymer hydrogel, poly( $\epsilon$ -caprolactone-co-lactide)-b-poly(ethylene)-glycol-b-poly( $\epsilon$ -caprolactone-co lactide) (PCLA-PEG-PCLA) (Fig. 23A). The *in vitro* release profile of GEM showed that the nanobiohybrid hydrogel lessened the initial burst release compared to the pristine hydrogel. As a result, the GEM-loaded nanobiohybrid hydrogel showed a better antitumor effect in pancreatic tumor-bearing mice, with a sustained release of GEM that maintained an appropriate drug concentration for an extended period (Fig. 23B, C). The presence of MMT was essential for the efficient loading and controlled release of GEM, and to considerably increase the stability of the hydrogel [102].

**3.3.2.6. Brain cancer.** Glioma is a general designation for tumors that arise within the brain at the level of glial cells, and includes glioblastomas, oligodendrogliomas and ependymomas [104]. Overall, gliomas show the worst clinical prognosis in adults and children [105]. Cervini-Silva *et al.* [75] studied the effects of BENT on human glioblastoma cells (U251). *In vitro* tests showed that BENT specifically interacted with the U251 cells, inhibiting their proliferation by controlling metabolic growth signaling [75].

6-Mercaptopurine (6-MP) is an antimetabolite drug with a hydrophobic nature, that readily binds to plasma proteins. Due to these features, 6-MP demonstrates a short plasma half-life and low bioavailability. To address these drawbacks, MMT-PLLA microcomposite spheres were tested as carriers for 6-MP to provide and maintain its therapeutic plasma concentration, without periods of overdosing or underdosing. The viability of human neuroblastoma cells (IMR32) was decreased after exposure to the 6-MP-loaded

MMT-PLLA microcomposite spheres. The release profile of 6-MP from the microcomposite spheres did not exhibit an initial burst release but showed a controlled release with 22% of 6-MP released in the first 10 h followed by a 52% sustained release over 68 h. Furthermore, the oral administration of the microcomposite spheres to Wistar rats led to a significant decrease in 6-MP toxicity. The microcomposite spheres significantly decreased the high peak of the plasma concentration ( $C_{\text{max}}$ ), and the total area under the curve (AUC), while increasing the mean residence time (MRT) of 6-MP in the plasma [106].

LAP is another nanoclay that could be useful for the treatment of glioma due to its stability, and the impressively elevated SSA of LAP nanoscale disks. Studies have shown that LAP has potential as a nanocarrier for anticancer drug delivery. In one study carried out by Wang *et al.* [107], LAP exhibited a high DOX entrapment efficiency (EE) (98.3%) and a pH-responsive sustained release of DOX, which resulted in a better therapeutic effect when compared to free DOX [107]. LAP can be modified with several targeting ligands to produce a cancer-targeted therapy with improved efficacy. However, this kind of functionalization could reduce the high drug delivery efficiency of LAP. Mustafa *et al.* [41] reported a novel method to optimize the performance of LAP-based nanocarriers without compromising the intrinsic loading capacity of LAP. Poly(amidoamine) dendrimers were attached to LAP nanodisks, forming generation 2 (G2) dendrimer-modified LAP nanodisks (LM-G2) to transport DOX (DOX-LM-G2). The DOX-LM-G2 system had a high EE of 98.4% (Fig. 24A). The DOX-LM-G2 system exhibited a pH-responsive sustained release pattern, with a higher release in acidic media when compared to DOX-LAP nanocomposite, over the same time interval (Fig. 24B). Additionally, it was shown that the DOX-LM-G2 particles were internalized by the cancer cells, with better growth inhibition when compared to free DOX (Fig. 24C). Considering that the dendrimers did not compromise the high EE, and also possessed abundant functional groups, LM-G2 nanodisks could be used as an adaptable delivery system for several anticancer drugs used in cancer therapy [41]. LAP was also shown to maintain the morphology of the polymer vesicles due to the rigid nature of its disks. *In vitro* studies showed that the DOX-loaded LAP-PLGA-F68 nanocomposite vesicles were successfully internalized by C6 rat fibroblast glioma cells, supporting the possible application of these vesicles in cancer therapy [40].

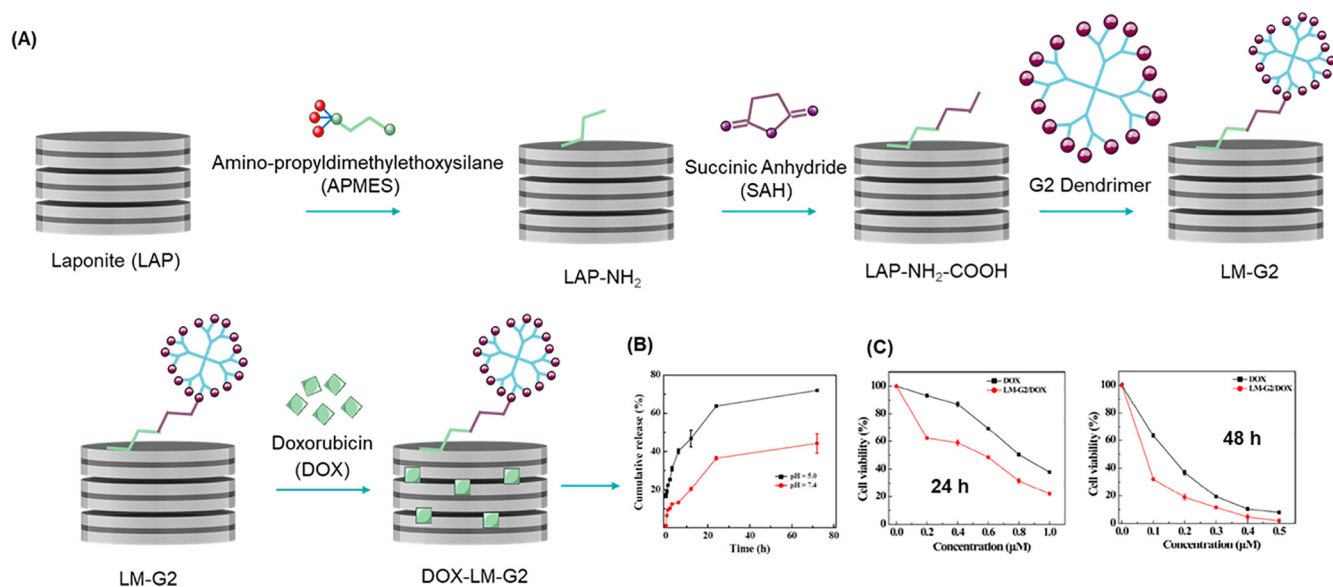


**Fig. 24.** Dendrimer-modified laponite (LAP) nanodisks (LM-G2) for doxorubicin (DOX) delivery. (A) Schematic illustration of the preparation. (B) The release profile of DOX from LM-G2 under acidic (pH 5.0) and physiological conditions (pH 7.4) (adapted from [41]). (C) *In vitro* cytotoxicity of DOX-LMG2 and free DOX tested in KB cells at several concentrations after 24 h and 48 h of exposure (adapted from [41]).

**3.3.2.7. Skin cancer.** Skin cancers have a high incidence rate in the order of 1.3 million new cases per year (Bray, 2018 #179). There are three main types of skin cancer, squamous cell carcinoma, basal cell carcinoma, and melanoma. Although melanoma skin cancer (MSC) is less common than the other skin cancer types, it has the highest mortality. MSC begins in melanocytes, which are the melanin producing cells in the skin. However, the MSC cells can readily invade surrounding tissue and disseminate, which makes this type of cancer much more aggressive when compared to other skin cancers. There are different therapeutic approaches for MSC, and their choice depends on the stage of the disease.

Chemotherapy with anticancer drugs, such as DOX, is one of the standard treatments for advanced MSC, but it is not particularly

successful [89]. Hosseini *et al.* [46] used BENT nanoclays to create a nanocomposite for DOX delivery and tested its anticancer activity on MSC cells. The nanocomposite was developed through electrostatic interactions between the positively charged DOX molecules and the negatively charged BENT surface (Fig. 25A). The authors demonstrated that DOX was slowly released from the DOX-BENT nanocomposite under physiological conditions (pH 7.4) and achieved a faster release rate in the tumor environment (pH 6.5) (Fig. 25B). The *in vitro* anticancer activity of this nanocomposite was evaluated using highly metastatic mouse melanoma cells (B16F10), and the results showed that its activity was higher than free DOX (Fig. 25C). These results suggested that DOX-BENT nanocomposite could be an alternative approach for the local

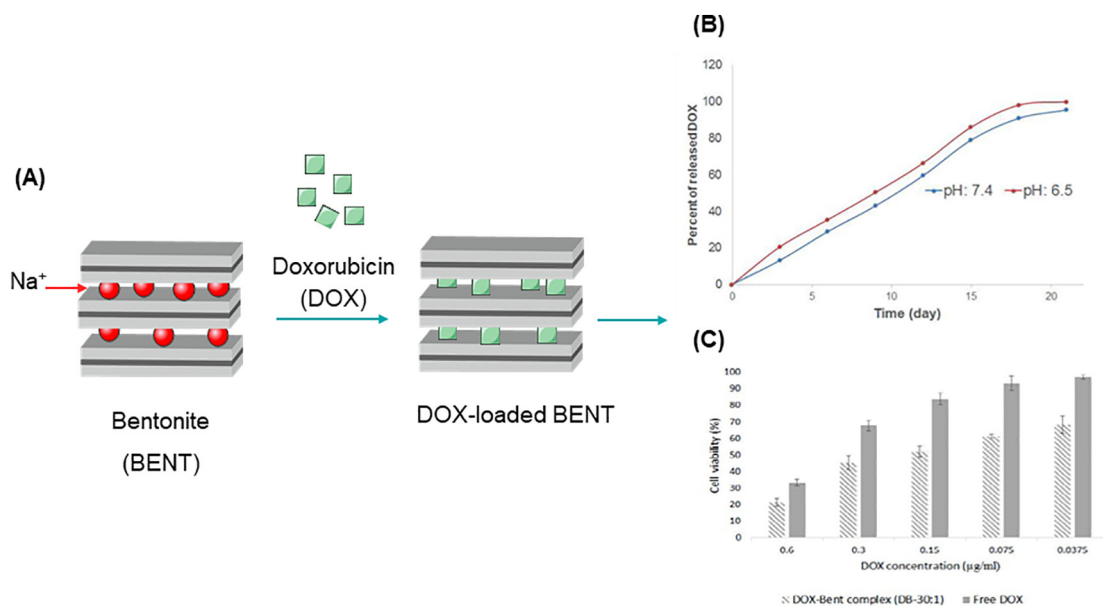


**Fig. 25.** Doxorubicin (DOX) loaded bentonite (BENT). (A) Adsorption of DOX via electrostatic interactions. (B) The release profile of DOX from BENT under different pH conditions (pH 6.5 and pH 7.4) (adapted from [46]). (C) Inhibition of the cell growth of B16F10 cells by DOX-loaded BENT and free DOX after 48 h of exposure (adapted from [46]).

treatment of MSC and that this nanoclay-based composite could minimize the side effects of DOX. The authors suggested that the DOX-BENT nanocomposite aqueous suspension should be injected in and around the melanoma tumor site to achieve an effective melanoma treatment [46].

**3.3.2.8. Thyroid cancer.** Thyroid cancer ranks ninth worldwide in incidence, accounting for over 567,000 cases. The incidence rate in women is 3-fold higher when compared with men [2]. The thyroid gland is a follicular endocrine gland located in the anterior region of the trachea. It contains two main types of cells, follicular epithelial cells and parafollicular cells (C cells), from which distinct cancer types can develop, which show differences in prognosis and treatment approaches [108]. The treatment options for thyroid cancer can include, surgery, administration of radioactive iodine isotopes, external beam radiation therapy, chemotherapy, or gene therapy. However, some of these options involve complex processes and are associated with significant side effects. Generally, a combination of chemotherapy with external beam radiation therapy is used for thyroid cancers with poor prognosis [109]. There are three main types of thyroid cancers, differentiated, medullary, and anaplastic. Differentiated cancers (including papillary, follicular, and Hürthle cell) develop from follicular epithelial cells and are the most common. Medullary cancers are responsible for only 4% of thyroid cancers and arise from C cells. Anaplastic cancers are rare, have a poor prognosis, and can develop from both follicular epithelial cells or C cells [108].

DOX is an anticancer drug often used in the treatment of thyroid cancer. Zhang *et al.* [109] developed DOX-loaded nanocarriers to target papillary thyroid cancer cells. Firstly, the interlayer space of kaolinite was expanded from 0.72 nm to 0.85 nm by modification with methoxy groups to increase the loading capacity. Then, after loading DOX, PEG was conjugated onto the external surface of methoxy-intercalated kaolinite (Kaolin<sub>MeOH</sub>) to increase its hydrophilicity, prolong its circulation time, and lessen its opsoniza-

tion. Follicular epithelial cells have a strong tendency to capture iodine ions in order to synthesize thyroid hormones (triiodothyronine (T3) and its prohormone, thyroxine (T4)). For this reason, the obtained nanocomposites were coated with potassium iodide (KI) to specifically target papillary thyroid cancer cells (Fig. 26). There was a rapid DOX release rate in simulated tumor intracellular conditions (pH 5.5), while in normal physiological conditions (pH 7.4) a slower DOX release was observed. The Kaolin<sub>MeOH</sub> was positively charged at lower pH values, which lessened the electrostatic interactions with the positively charged DOX. The DOX-Kaolin<sub>MeOH</sub>-KI nanocomposite showed a pH-responsive controlled release, good physiological stability, and the ability to accelerate DOX release in the tumor microenvironment. The CLSM and TEM images of papillary thyroid cancer cells showed that the DOX-Kaolin<sub>MeOH</sub>-KI nanocomposite was internalized *via* endocytosis. The nanocomposites also exhibited a dose-dependent *in vitro* therapeutic activity. Additionally, the performance of the nanocomposite was improved by the KI functionalization, which conferred active targeting properties onto the nanocomposite. The anti-metastatic activity of the nanocomposite was evaluated in monolayer scratch healing and cell migration experiments. The nanocomposite substantially inhibited the repair of the *in vitro* monolayer scratch. In the migration experiments, the nanocomposites demonstrated inhibition of cellular migration. Furthermore, a biodistribution analysis was conducted in two distinct *in vivo* experiments, an active transport study in New Zealand white rabbits and a passive study in mini pigs. In the first study, after intravenous administration, there was a significant accumulation of DOX-Kaolin<sub>MeOH</sub>-KI in the thyroid gland. In the second study, a marked accumulation was observed within the thyroid gland after DOX-Kaolin<sub>MeOH</sub>-KI was directly injected into the thyroid gland of mini-pigs. These results suggest that DOX-Kaolin<sub>MeOH</sub>-KI could be exploited as an efficient targeted thyroid cancer therapy [109].

The study discussed above provides evidence that the use of a selective ligand (KI) in the nanocomposite was essential to achieve tumor-targeted accumulation with minimal toxicity. Generally,

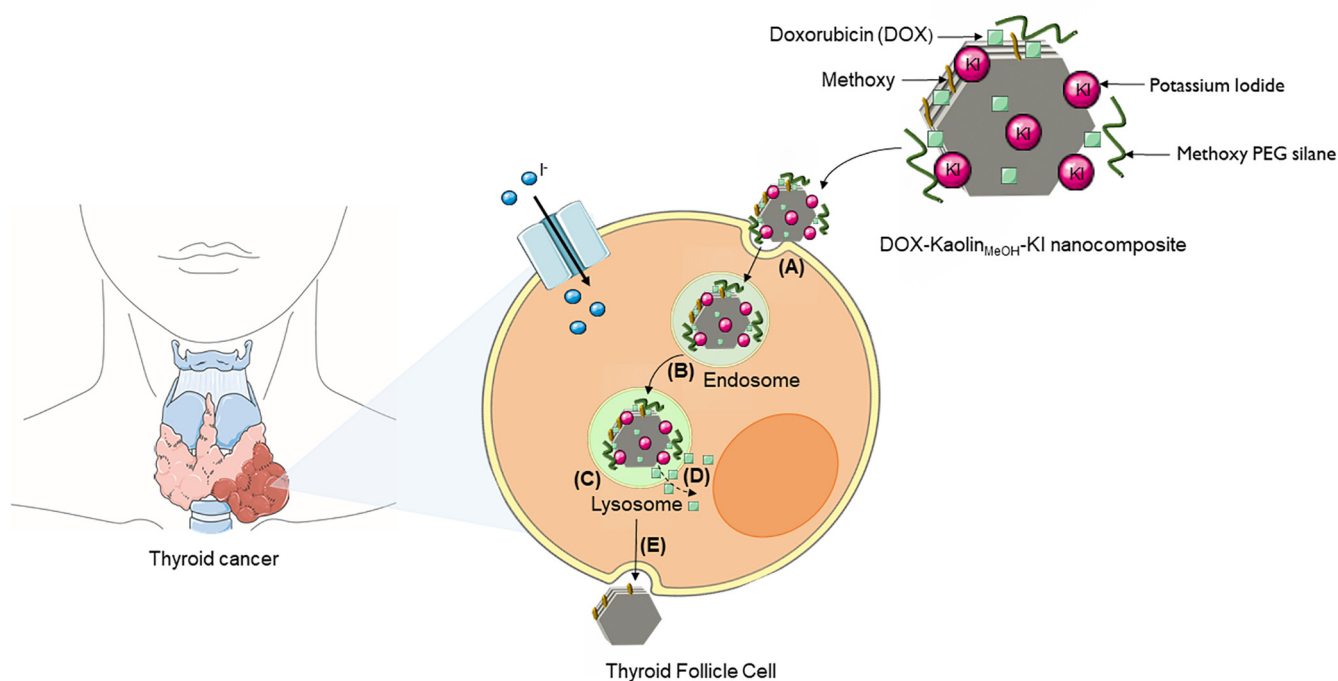


**Fig. 26.** Mechanism of the intracellular delivery of doxorubicin (DOX) from the DOX- Kaolin<sub>MeOH</sub>- potassium iodide (KI) nanocomposite. (A) Non-receptor mediated endocytosis. (B) Membrane surrounds the DOX-Kaolin<sub>MeOH</sub>-KI nanocomposite in endosomes followed by internalization. (C) Formation of a lysosome containing the DOX-Kaolin<sub>MeOH</sub>-KI nanocomposite. (D) Release of DOX. (E) Kaolin<sub>MeOH</sub> leaves the cell.

kaolinite can act as an efficient and low-toxicity drug delivery vehicle. The use of nanoclays could increase the water solubility of anticancer drugs, facilitate their interaction with cancer cells, and control their release in the cancer microenvironment while minimizing their accumulation in healthy tissues. Furthermore, the ability of kaolinite-based nanocomposites to incorporate NPs with magnetic properties, tumor selective ligands, and anticancer drugs can enable diagnostic imaging, targeted therapy, and drug delivery at the same time.

**3.3.2.9. Bone cancer.** Osteosarcoma (OSA) is the most frequent type of bone cancer generally occurring in children and young adults. Surgery must be able to remove all sites of the clinically detectable tumor mass, although tumor recurrence is still frequent if the treatment comprises only surgery. Thus, adjuvant chemotherapy is often used in combination with surgery to inhibit micrometastasis before and/or after surgery. Despite some progress in the treatment of OSA, innovative treatments and preventive approaches are still required [110,111]. HNTs have been studied as nanocarriers for anticancer drugs, such as methotrexate (MTX), quercetin (QUE), taurolidine, and artemisinin, aimed at the treatment of OSA. Cytotoxic assays have shown that nanocomposites could modify OSA cell morphology and inhibit their proliferation. A drug release test was conducted on MTX-loaded HNTs, showing an initial burst release, where 70% of the loaded MTX was released in 1 h, and 95% after 24 h [110]. In order to control the release of MTX, HNTs were alternately modified with positively charged polyvinylpyrrolidone (PVP) polyelectrolyte and with the negatively charged poly(acrylic acid) (PAA) polyelectrolyte via the LbL method (Fig. 27). *In vitro* experiments showed that the polyelectrolyte coatings provided a sustained release of MTX over 160 min, without affecting its ability to inhibit the growth of OSA cells [111].

### 3.3.3. Naturally-occurring compounds

Curcumin (CUR) is a phenolic compound obtained from the rhizomes of *Curcuma longa*. Several studies have demonstrated that CUR has anti-inflammatory, antioxidant, and anticancer activities, with several mechanisms of action directed at different cellular targets. However, therapeutic applications of CUR are limited by its poor water solubility, chemical instability, and rapid metabolic degradation [112]. Nanocarriers based on nanoclays have been tested to widen the therapeutic applications of CUR. MMT has been studied as a potential carrier for CUR. Madusanka *et al.* [113] reported the use of CMC combined with MMT as a nanocarrier for the delivery of water-insoluble CUR. Because CMC has emulsifying properties, it was used as an intermediary to promote the binding of CUR to MMT, thus improving the drug solubility. Additionally, the curcumin-loaded MMT-CMC nanocomposite showed an ability to control the release of CUR with a release of 60% during

150 min in acidic media (pH 5.4) [113]. Hydrophilic biopolymers have received increased attention due to their ability to render nanocarriers more biocompatible and biodegradable. Furthermore, biopolymers can increase the water solubility of the nanocarriers and their colloidal stability within the bloodstream. CS is a hydrophilic biopolymer often used to functionalize nanocarriers, due to its biocompatibility, biodegradability, and mucoadhesive properties. Furthermore, CS is only in an ionized state in acidic conditions, which makes it ideal to interact with the cancer cells, because at low pH, CS is positively charged and forms electrostatic interactions with the negatively charged cellular membranes [8]. Khatun *et al.* [114] developed MMT-CS nanocomposites for the controlled delivery of CUR. After 6 h, the cumulative release varied depending on the pH. Thus, the release of curcumin ranged from 70% to 90% in acidic conditions (pH 1.2), whereas in alkaline pH it ranged from 45% to 60%. This pH-dependent release was a consequence of a difference in the CS swelling behavior in acidic and alkaline conditions. CS swells readily in acidic media, and its residual amino groups become protonated, leading to a faster CUR release rate. Moreover, the nanoclay-based nanocomposite reduced the viability of MCF-7 and Hep G2 cells [114]. Researchers have also shown that HNTs are excellent candidates to deliver CUR since these nanocarriers can enhance its oral bioavailability [112,115–120]. The surface of CUR-loaded HNTs was modified with a mucoadhesive poly(methylvinyl ether-co-maleic acid) polymer (PMVEMA) to increase the interaction with the intestinal epithelium, and promote a better CUR penetration into the intestinal cell monolayer. The interactions of PMVEMA-modified HNTs with Caco-2 cells and human colon adenocarcinoma cells (HT29-MTX) which mimic the absorptive enterocytes and mucus-producing goblet cells, respectively, showed that modification with the mucoadhesive PMVEMA resulted in a 13-fold increase in CUR permeability. Subsequently, the CUR-HNT-APTES-PMVEMA nanocomposite was encapsulated with the pH-responsive HPMCAS using a microfluidic technique (Fig. 28A). The obtained spherical nanocomposite particles had a homogeneous particle size distribution (Fig. 28B). The *in vitro* release studies showed a pH-responsive CUR release (Fig. 28C). The pH-responsive CUR release was useful to protect CUR from the harsh environment in the stomach and release it only in the intestinal environment [112]. In one study designed to mimic not only the well-known carbohydrate-lectin interaction, but also the glycocluster phenomenon, the authors designed a new nanocarrier based on HNTs to transport phenolic compounds like CUR. Thus, carbohydrate-cyclodextrin units were covalently attached to the HNT surface. Later, CUR was incorporated inside the two types of available cavities, the hydrophobic cavity of cyclodextrin and the lumen of the HNTs [115]. In a different approach, CUR was covalently attached to HNTs, using pH-responsive disulfide bonds that enabled a dual specific release

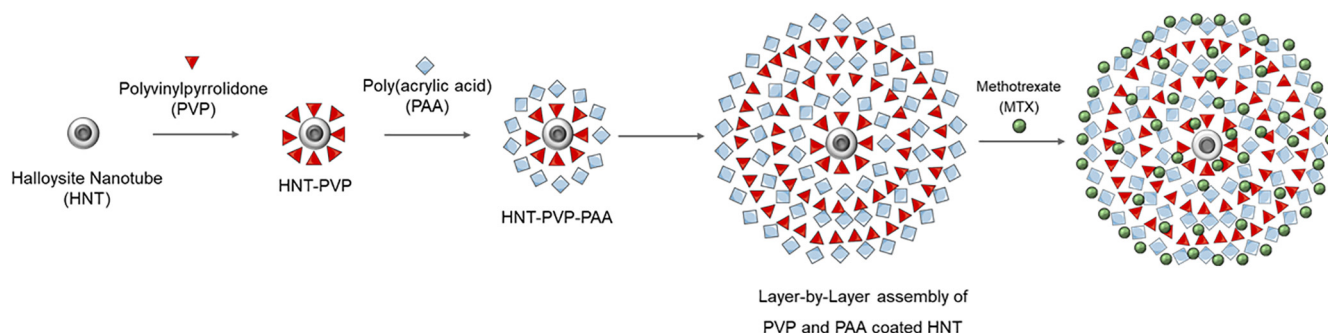


**Fig. 27.** Schematic representation of halloysite clay nanotubes coated with opposite charged polyelectrolytes, polyvinylpyrrolidone (PVP), and poly(acrylic acid) (PAA), by the layer-by-layer (LbL) self-assembly technique, followed by methotrexate (MTX) loading.

mechanism triggered by different pH values and glutathione (GSH) concentrations. The resulting dual-responsive nanocarriers showed a significantly enhanced release of CUR at low pH and high concentrations of GSH [121]. The CUR-HNT nanocomposites exhibited high cytotoxicity towards two hepatocellular carcinoma cell lines after 48 h of incubation, suggesting their potential in the treatment of hepatocellular carcinoma [116]. Another strategy for the pH-responsive release of CUR was developed via CUR interacting with the hydroxyl groups present in both the internal and external surfaces of HNTs.

Additionally, CUR can also be used in the synthesis of gold nanoparticles (Au NPs) associated with HNTs. The obtained HNT-based nanocomposites were coated with the cationic biopolymer CS (Fig. 29A). The presence of both Au NPs and CS conferred near-infrared-light-and pH-responsive properties. In fact, the CUR release was higher at acidic pH (pH 5.5) than at alkaline pH (pH 7.4) (Fig. 29B). Also, the nanocomposite exhibited a higher anticancer activity against MCF-7 cells at intracellular tumor pH 5.5 compared to extracellular pH 7.4 (Fig. 29C). Moreover, the designed nanocomposites could be used as photosensitizers in photothermal therapy (PTT) [120]. Liu *et al.* [117] developed an innovative nanocarrier based on HNTs that involved CS used as a coating. Initially, the hydroxyl groups on the surface of HNTs were converted to carboxyl groups (COOH) using succinic anhydride. Then, CS was grafted onto the HNT-COOH to decrease its toxicity, increase its stability, and improve the loading efficiency of CUR. The chitosan-grafted HNTs (HNT-CS) showed improved values of EE (90.8%) and drug loading (DL) (3.4%) in contrast to pristine

HNTs. In addition, the HNT-CS exhibited satisfactory stability in serum without any significant hemolytic effects. The CUR release from HNT-CS showed specific toxicity towards several cancer lines, with the highest anticancer activity against EJ human bladder carcinoma cells [117]. CUR was also efficiently encapsulated into cellulose-HNT composite hydrogels. Cellulose hydrogels modified with HNTs showed higher EE (21%) than pure cellulose hydrogels (17%), since the composite hydrogels contained two components (HNTs and cellulose) both with high adsorption capacity. In the drug release studies, cellulose-HNT composite hydrogels allowed CUR controlled release with a maximum release (62.1%) at 20 h. Moreover, the CUR-loaded composite hydrogels showed strong inhibition of MCF-7 cells, while still showing cytocompatibility to mouse embryonic osteoblast precursor cells (MC3T3-E1) [119]. HNTs coated with polyelectrolytes multilayers have been used to transport CUR. HNTs were alternately coated with positively charged and negatively charged electrolytes via the LbL procedure. The HNT coating reduced the release rate of CUR and was 20% lower than uncoated HNTs for 24 h. Also, the CUR-loaded LbL-coated HNTs were successfully internalized by MCF7-cells, releasing CUR over 24 h with a sustained pattern [118].

Resveratrol (RSV) is a polyphenolic natural compound which has been recognized as an effective anticancer and antiproliferative agent. However, its pharmacological use has been limited by its low stability and poor water solubility. RSV was loaded into the hollow cavity of HNTs to improve its bioactivity and avoid its rapid metabolism. The LbL method was used to coat HNTs with protamine salt (PRM) and dextran sulfate sodium (DXS), a cationic

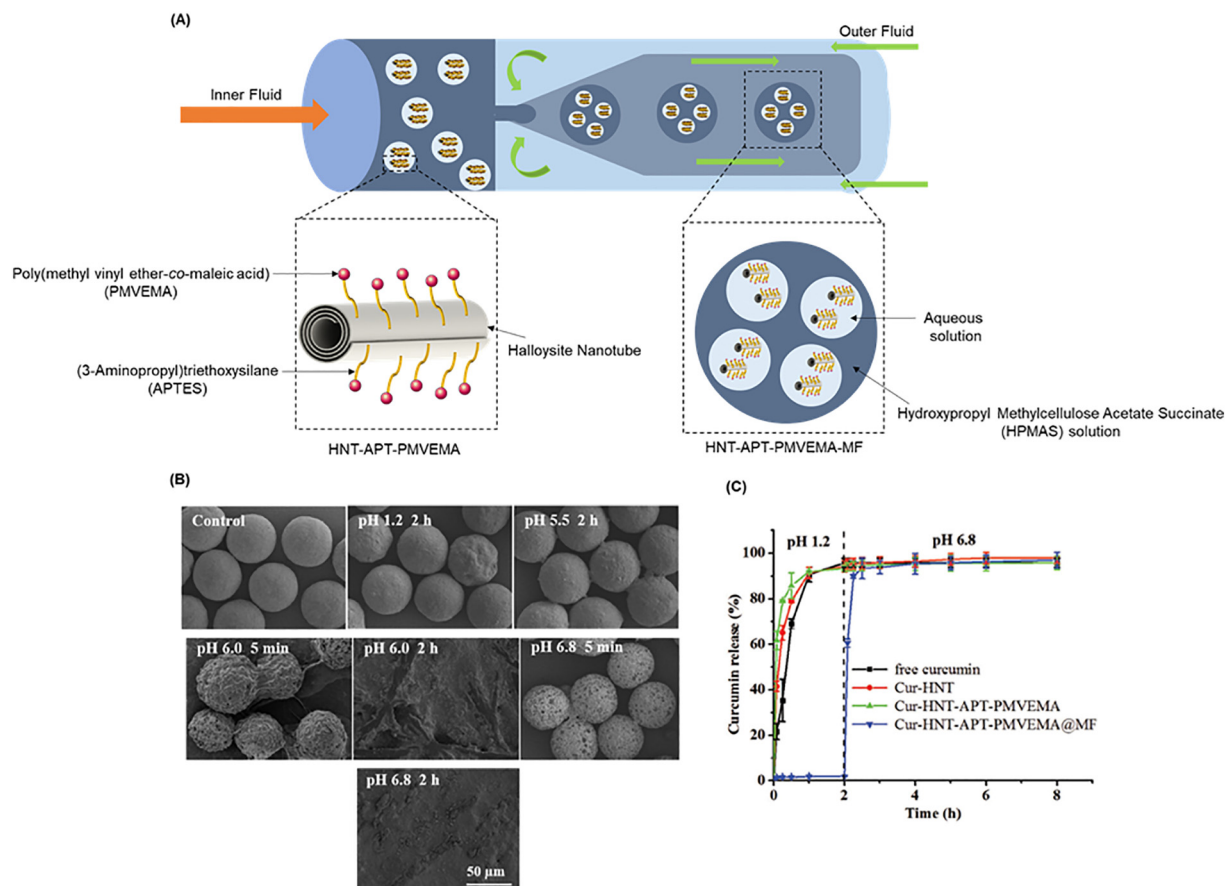


**Fig. 28.** Curcumin (CUR)-loaded aminopropyltrimethoxysilane (APT) and poly(methylvinyl ether-co-maleic acid) (PMVEMA)-modified halloysite clay nanotubes (HNTs) nanocomposites (CUR-HNTs-APT-PMVEMA). (A) Schematic representation of the microfluidic preparation. (B) Scanning electron microscopy (SEM) images of the surface morphology of CUR-HNTs-APT-PMVEMA microspheres at different conditions (pH 12, pH 5.5, and pH 6.8) (adapted from [112]). (C) The release profiles of CUR from CUR-HNTs, CUR-HNTs-APT-PMVEMA, and CUR-HNTs-APT-PMVEMA microspheres (adapted from [112]).

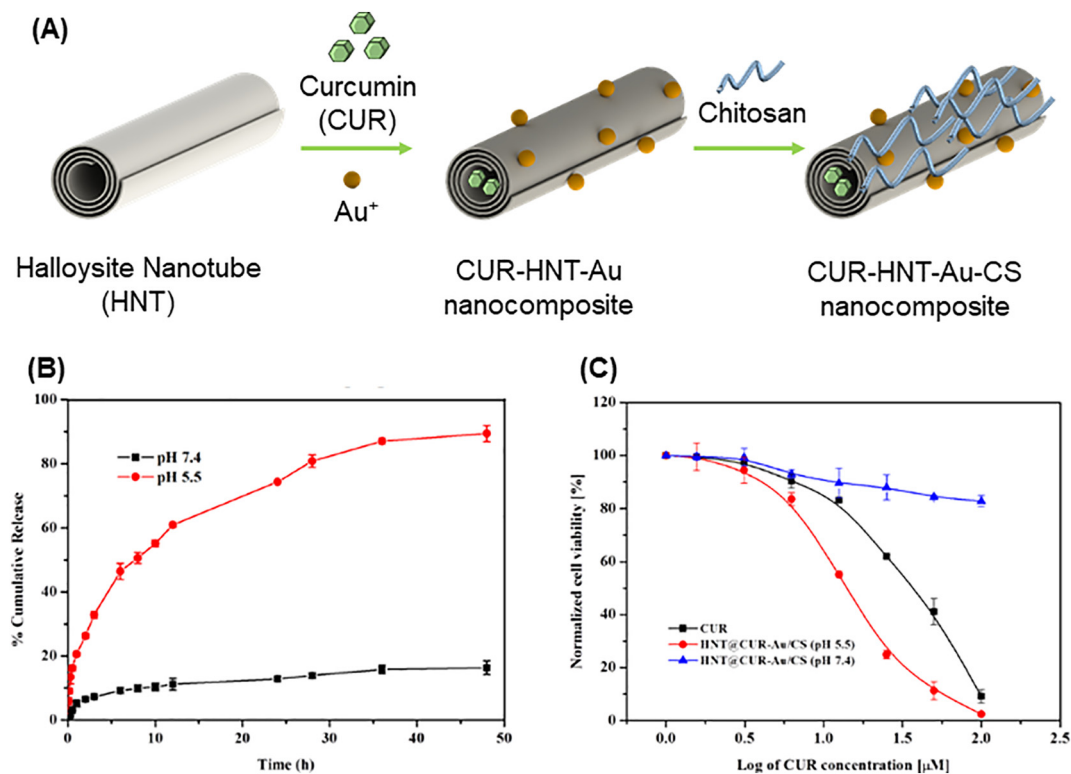


**Fig. 29.** Curcumin (CUR)-loaded chitosan (CS)-coated halloysite clay nanotubes (HNTs)/gold nanoparticles (Au) (CUR-HNT-Au-CS) nanocomposite. (A) Schematic illustration of the preparation. (B) The release profile of CUR at pH 5.5 and 7.4 from CUR-HNTs-Au-CS nanocomposite (adapted from [120]). (C) *In vitro* cytotoxicity of CUR released from the CUR-HNTs-Au-CS nanocomposite. The cytotoxicity was tested on MCF-7 cells after an incubation for 48 h (adapted from [120]).

and an anionic polyelectrolyte, respectively. The LbL-modification of the external surface of HNTs allowed the controlled release of RSV with a slow and constant pattern over 48 h. In addition, *in vitro* experiments in MCF-7 cells showed that the RSV-loaded LbL-coated HNTs produced increased apoptosis in MCF-7 cells [122].

Saponins (SAP) are secondary metabolites produced by several different plant species to protect themselves from stressful conditions. SAPs are chemically defined as heterosides, with a sugar residue bound to a genin residue that can be a triterpene or a steroid. Several studies have shown that steroidal SAPs can exert cytostatic or cytotoxic effects on cancer cells. SAP can interact with the high concentration of cholesterol present in the plasma membrane of cancer cells. Nevertheless, SAPs may also cause membrane damage to normal cells, possibly leading to tissue necrosis, and reducing the therapeutic index. It should be noted that intravenous administration of SAPs is highly toxic due to their pronounced hemolytic activity. Thus, the use of nanocarriers is a possible option to overcome the toxic effects of SAPs, control the release, and avoid their degradation at physiological pH. Akbal *et al.* [123] used MMT modified with human serum albumin (MMT-HSA) to form nanocomposites that could be loaded with SAPs and investigated the cytotoxicity against human colorectal adenocarcinoma cells (DLD-1) and L929 fibroblasts. The results showed that the SAPs-loaded MMT-HSA nanocomposites caused dose-dependent cancer cell death and did not induce any toxicity to healthy cells. The use of MMT-HSA nanocomposites improved the anticancer efficacy of SAPs and could be an alternative approach for CRC treatment [123].

*Serratia marcescens* bacterial cells naturally produce prodigiosin, which is a secondary metabolite with anticancer activity against several human cancer cell lines. Nonetheless, the clinical use of prodigiosin has been limited by its hydrophobicity, poor

absorption, and low bioavailability. These limitations could be overcome using HNTs as nanocarriers. Guryanov *et al.* [124] showed that prodigiosin could be adsorbed onto the external surface and simultaneously encapsulated into the lumen of HNTs, resulting in nanocomposites with good bioavailability. Furthermore, the nanocomposite showed cytotoxic activity against Caco-2 cells and human colon carcinoma cells (HCT116) without damaging healthy cells [124].

Overall, the strategies discussed in this section have suggested the usefulness of MMT and HNTs as efficient nanocarriers for the delivery of different natural compounds to cancer cells.

### 3.3.4. Biopharmaceutical agents

**3.3.4.1. Enzyme delivery.** Proteins are rather unstable outside the body, being highly susceptible to enzyme action, and sensitive to marked changes in pH or temperature. Moreover, many proteins are characterized by rapid clearance and low permeability through biological membranes. Given that proteins have major problems regarding their stability, their therapeutic application requires special care.

There has been increasing interest in the use of enzyme-based agents for cancer therapy. Some specific types of enzymes can exert an effective anticancer action over a long period and with fewer side effects when compared to conventional anticancer drugs. The anticancer properties of several enzymes, such as lactase, glutaminase, binase, arginase, methioninase, or uricase have been well-documented. The preferred route of administration for enzymes is the parenteral route. However, this route may be limited by the side-effects and discomfort suffered during the intravenous infusion. Thus, less invasive routes of administration, such as the oral route may be preferable [24,125,126]. The administration of enzymes *via* the oral route presents several difficulties, such as the loss of therapeutic activity, likely degradation in the

gastrointestinal tract, and possible side effects. One viable strategy is the immobilization of enzymes inside neutral nanocarriers, which could prevent their degradation and reduce possible side effects. Furthermore, nanocarriers could specifically increase the concentration of the enzyme in cancer cells through sustained and targeted release [24,125,126].

HNTs are promising nanocarriers for cancer-targeted enzyme delivery [126]. The opposite charges present between the inner and outer surfaces of the HNTs could enable the selective adsorption of either negatively or positively charged enzymes. The identity of the enzymes and the pH conditions in which the adsorption procedure is carried out, affect the results [125]. pH conditions will affect the charge of the amino acids present in the enzyme structure, and consequently the electrostatic interactions between the enzyme and the HNT surface. Accordingly, if the pH of the enzyme solution is above the isoelectric points (pI) of the protein, the enzyme will be negatively charged and interact more efficiently with the positively charged lumen of the HNTs. On the other hand, if the pH of the solution is below the pI of the enzyme, it will be positively charged and interact better with the negatively charged external surface of the HNTs (Fig. 30). Typically, the charge of the HNT surface area is often negative, leading to suboptimal adsorption of negatively charged enzymes, which could range from 6 to 7 wt%. This is a rather low value when compared to the adsorption of positively charged enzymes onto HNTs, which can range from 15 to 25 wt% [125]. It has been shown that approximately one-third of negatively charged proteins show an initial burst release within the first 5 to 10 h, followed by a more prolonged release pattern. This means that the remaining two-thirds of the protein remains functional in the HNT lumen with a slower release rate. These features suggest the use of HNTs as functional enzymatic nanoreactors [125].

Some applications of the HNTs as an enzymatic nanoreactor have already been reported for cancer therapy. For example, Kim *et al.* [127] and Khodzhaeva *et al.* [126] demonstrated the immobilization of laccase or binase onto HNTs, respectively, for enzyme-based cancer therapy [126,127]. In the first study, a new promising theranostic nanoplatform was described to improve the efficiency and specificity of laccase delivery. Laccase is a polyphenol oxidase with antiproliferative activity, especially for cancers over-expressing estrogen receptors (e.g., cervical and breast cancer). The laccase lowers the interaction between estrogen and estrogen receptor by degrading estrogen, which is a natural phenolic compound. In order to improve the anticancer activity and achieve a targeted release, laccase (pI 3.0) was immobilized inside the lumen of HNT by electrostatic bonding. HNTs were modified with CS and Fe<sub>3</sub>O<sub>4</sub> NPs before the immobilization of laccase. The CS coating enabled the covalent loading of laccase mediated by a cross-linking agent, glutaraldehyde. The modification of HNTs with SPIONs (Fe<sub>3</sub>O<sub>4</sub> NPs) conferred magnetic properties to the nanocarriers, enabling a specific release mechanism triggered by an external magnetic field. Additionally, SPIONs allowed monitoring of the treatment *in vivo* due to their MRI contrast imaging properties (Fig. 31A). The authors produced an actively targeted theranostic nanoplatform with efficient antiproliferative and apoptotic activities against cell lines over-expressing estrogen receptors, such as HepG2 cells (Fig. 31C) [127]. On the other hand, in the second study, the immobilization of binase on HNTs was an excellent example of an enzymatic nanoreactor used in CRC treatment. The guanyl-preferring ribonuclease isolated from *Bacillus pumilus*, called binase (pI 9.5), has an anticancer activity against cancers expressing the rat sarcoma virus (*ras*) oncogene. Mutations in the *ras* oncogene are present in >30% of all cancers and are present in 90% of cancers with a poor prognosis, such as CRC. These mutations result in a permanently activated state of the RAS protein, which is important because the cells proliferate in an uncontrolled

manner and acquire resistance to chemotherapy [128]. To prevent this scenario, the administration of binase could be a viable strategy due to its ability to block the downstream signaling pathway associated with the RAS protein. As described by Khodzhaeva *et al.* [126], binase was immobilized within the HNT lumen to avoid its degradation by proteases and prolong its release time. Considering that binase is a positively charged enzyme, its loading through electrostatic interactions with the positively charged lumen of HNTs is challenging. Nevertheless, the molecular size of binase (3.3 nm) allowed its easy insertion into the HNT lumen, which have a diameter of approximately 15 nm. In this study, the authors employed dextrin stoppers at the ends of the HNTs to prevent the early release of binase. The immobilization of binase inside the HNTs significantly increased the cytotoxicity towards CRC cells (Colo 320) due to increasing the cell uptake and prolonging the release time. The binase-HNT complex reduced cell viability by 60%, whereas free binase reduced cell viability by only 25%. Considering the biodegradability of HNTs, the development of rectal suppositories containing binase-HNTs complexes could be a promising enzymatic approach for CRC treatment [126]. These two studies showed that the immobilization of laccase and binase within the hollow cavities of HNTs could create enzymatic nanoreactors against different cancer cell lines.

**3.3.4.2. Gene delivery.** Gene therapy is an approach seeking to modulate gene expression levels, often by introducing exogenous nucleic acids into specific cells to treat human monogenic or multifactorial disorders [129]. In order to correct a genetic defect that causes a disorder, gene therapy can employ different types of biologically active nucleic acids, which can affect the transcriptional, post-transcriptional, or translational regulation of gene expression. For the last 20 years, several clinical trials have been carried out to prove the efficacy and safety of gene therapy. Although monogenic disorders are gaining more attention, more than half (67%) of the ongoing gene therapy clinical trials have been focused on multifactorial diseases, in particular cancer [130]. The occurrence of gain-of-function mutations can activate proto-oncogenes, and loss-of-function mutations can inactivate tumor suppressor genes, and either or both can promote carcinogenesis. These genetic alterations promote uncontrolled cell proliferation, reduce the effective performance of the immune system, and cause an accumulation of driver and passenger mutations [6,72]. Initially, the accumulation of mutations in cells happens randomly. Next, a selection process of mutations that produce an excessive increase in the number of malignant cells takes place. The steadily growing malignant cells (except for hematological cancers) develop into an abnormal cell mass called a tumor. Because the cancer development process depends on gene mutations, gene therapy is starting to play an important role in cancer therapy [131]. In gene therapy, the delivery of exogenous nucleic acids into cells in order to affect gene expression is challenging. Naked nucleic acids have a hydrophilic nature, large molecular size, and are very unstable due to their ready degradation by nucleases *in vivo*. For this reason, in gene therapy, the main challenge is to overcome the cellular, tissue, and enzymatic barriers to deliver genes into the targeted cells, which can be partly achieved by selecting effective gene carriers [131,132]. Gene carriers can be biological or chemical and can be classified into viral vectors and non-viral vectors [129,131,132]. Viral vectors have been the primary molecular carriers with an ability to transfer genes into human cells and have been investigated in >60% of clinical trials so far [131]. Viral vectors integrate their viral cargo into the target cell genome, and they are recognized for their capacity to transform a wide variety of cell types. Although viral vectors remain the most often used for gene delivery, these carriers have high associated risks, including strong immunogenicity and the capacity to trigger insertional mutagenic

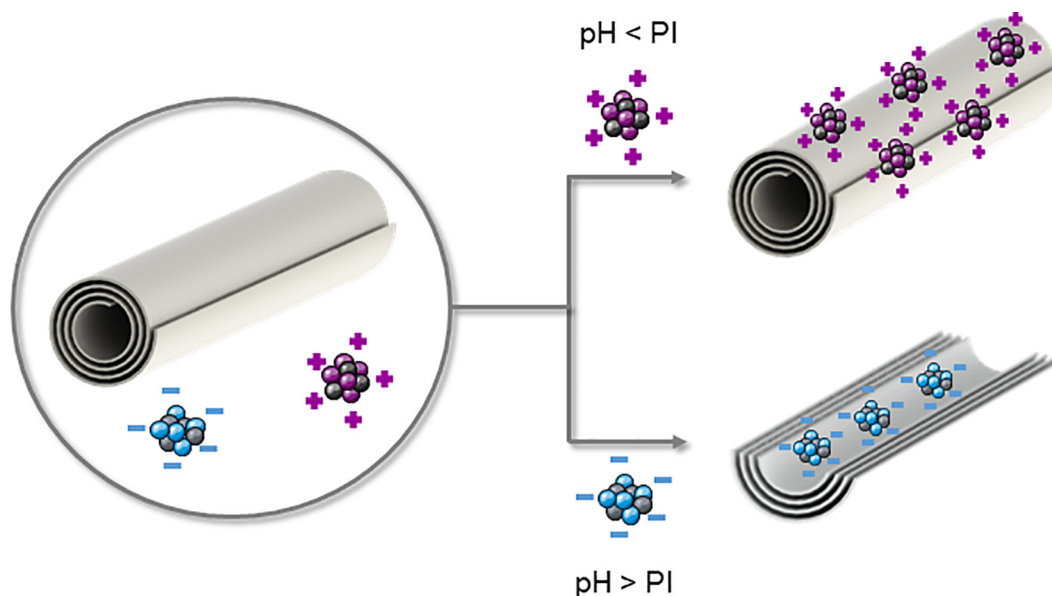


**Fig. 30.** Illustration of the immobilization of enzymes on halloysite clay nanotubes (HNTs). Negatively charged enzymes interact more efficiently with the positively charged lumen of HNTs. On the other hand, positively charged enzymes interact more efficiently with the negatively charged external surface of HNTs.

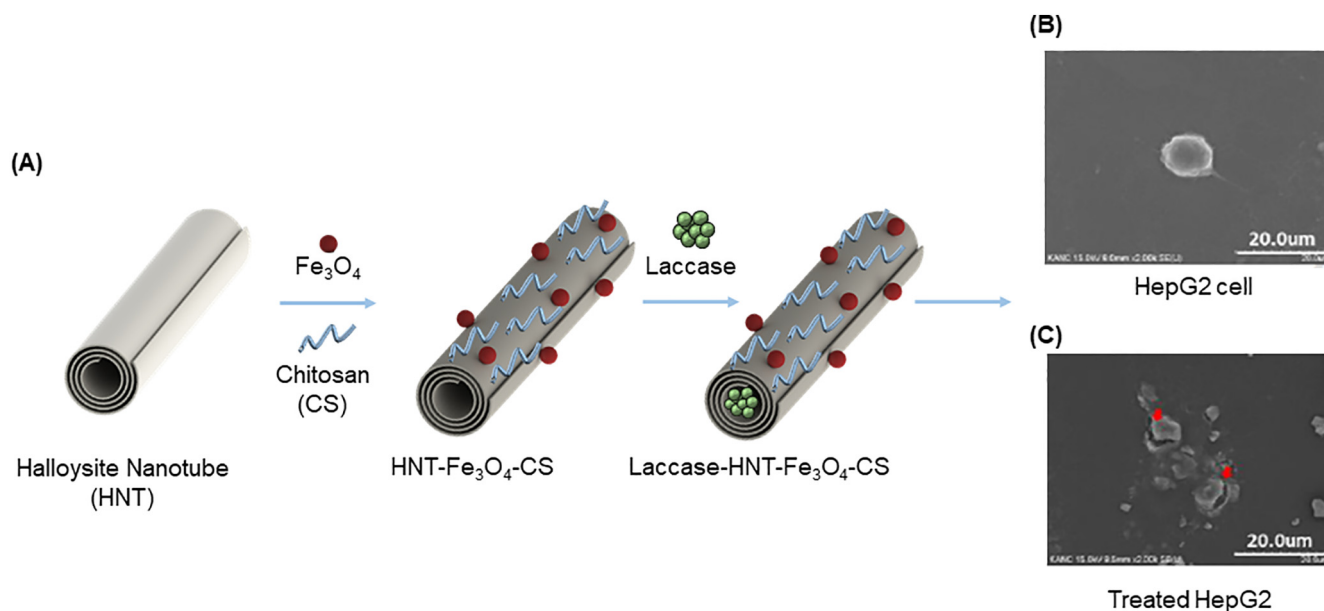


**Fig. 31.** Laccase-halloysite clay nanotubes (HNTs)- $\text{Fe}_3\text{O}_4$  nanoparticles (NPs)-chitosan (CS) (Laccase-HNT- $\text{Fe}_3\text{O}_4$ -CS) complex. (A) Schematic illustration of the preparation. (B) Untreated HepG2 cells (adapted from [127]). (C) Morphological changes in HepG2 cells induced by the release of laccase from the HNT- $\text{Fe}_3\text{O}_4$ -CS complexes (adapted from [127]). Red arrows indicate cell damage.

events, which may alter the expression of proto-oncogenes or tumor suppressor genes, and they have been known to be carcinogenic [132]. These associated risks encouraged the development of non-viral vectors. In contrast to viral vectors, non-viral vectors show higher biosafety, lower immunogenicity, and easier preparation [129]. Unfortunately, non-viral vectors sometimes have a lower transfection efficiency, and are not easy to track *in vivo*, imposing clinical limitations. To circumvent these disadvantages, new strategies are being developed such as the chemical synthesis of inorganic particles with adjustable shape, composition, and physicochemical properties [129,133]. Given the large size and negative charge of nucleic acids, the surface of the synthesized inorganic particles is often functionalized with positively charged

groups or cationic polymers to allow nucleic acid complex formation [132]. Many natural inorganic NPs show satisfactory cell uptake and good biosafety. However, these NPs have not been widely studied as gene vectors. Nanoclays are a particular example that have been shown to be a promising non-viral gene vector [132].

Antisense oligodeoxynucleotides (ASODNs) and small interfering RNAs (siRNAs), are widely used molecules for gene therapy, especially in cancer treatment. These nucleic acids show a strong ability to silence the expression of oncogenic factors [74,134,135]. ASODNs are single-strand DNA molecules with 15 to 30 nucleotides that can be delivered into the cytoplasm to bind to complementary regions of a target messenger RNA (mRNA), thus

inhibiting the gene expression [134]. A preliminary study on the application of HNTs as a nanocarrier for the intracellular delivery of ASODNs was carried out by Shi *et al.* [134]. To facilitate the loading and delivery of ASODNs, the HNTs were functionalized with APTES (Fig. 32A). Then, ASODNs were labeled with fluorescein for intracellular tracking. The complex showed a good ability for the intracellular delivery of ASODNs to HeLa cells (*ca.* 98.7%) and better antitumor activity compared to free ASODNs (Fig. 32B, C) [134]. siRNAs are endogenous small non-coding RNAs of *ca.* 21 nucleotides, with the ability to silence the expression of target genes. siRNAs have a sequence-specific action, to induce gene knockdown, and inhibit gene expression. This mechanism has been exploited to silence specific genes involved in cancer progression [74,135]. Wu *et al.* [74] prepared modified HNTs to deliver survivin siRNA to pancreatic cancer cells (PANC-1) and decrease the levels of the survivin protein, which inhibits apoptosis and stimulates cancer cell proliferation. In this work, HNTs were modified with PEI polymer using the LbL-method. Mercaptoacetic acid capped (CdSe) quantum dots were attached by non-covalent electrostatic interaction to the survivin siRNA to visualize the transfection, and then bound to the PEI-HNTs. The HNT-based multifunctional complex exhibited high transfection efficiency in PANC-1 cells (95.6%), showing that the functionalization with PEI significantly increased the delivery efficiency. The *in vitro* cytotoxicity assay showed increased apoptosis and improved anticancer activity of survivin siRNA. Furthermore, according to Western blot analysis, after 72 h of exposure to the complex, the survivin protein levels in PANC-1 cells were reduced by *ca.* 90%. These results suggest that the HNT-based multifunctional complex silenced the *surviving* gene and decreased the survival of pancreatic cancer cells [74].

The coating of short HNTs with cationic PEI was also used to improve the transfection efficiency [129]. PEI-modified HNTs were used for the transfection of green fluorescence protein (GFP) labeled DNA. In their study, shortened HNTs with a length of approximately 200 nm were coated with PEI not only to enhance the transfection efficiency, but also to avoid cell injury and inflam-

mation. The resulting complexes showed a high DNA transfection efficiency (44.4%) in HeLa cells and exhibited good biocompatibility [129].

In another recent study, a dendrimer of poly(amidoamine) grafted HNTs (HNT-PAMAM) for the intracellular delivery of vascular endothelial growth factor (VEGF) siRNA (siVEGF) (Fig. 33A) [132]. The *in vitro* assays, with human breast cancer MCF-7 cells, showed a cellular uptake of 94.3% for siVEGF-HNT-PAMAM and a reduction of 78% in VEGF mRNA expression (Fig. 33B). The significant depletion in the expression levels of VEGF induced apoptosis in breast cancer cells. Regarding the *in vivo* anticancer assays, the results showed that siVEGF-HNT-PAMAM significantly reduced the tumor volume by 55.1%, and inhibited angiogenesis (Fig. 34). These results suggest that siVEGF-HNTs-PAMAM could be a promising therapeutic strategy for breast cancer [132].

In 2019, Liu *et al.* used HNTs to load the receptor-interacting protein kinase 4 (RIPK4) siRNA in order to treat bladder cancer. This specific RNA molecule targets the *RIPK4* oncogene, which is often up-regulated in bladder cancer. The RIPK4 siRNA was encapsulated within the lumen of the HNTs to increase the serum stability and improve target silencing. It was shown that the HNTs could deliver RIPK4 siRNA in an efficient and specific manner into bladder cancer cells. Also, the *in vitro* and *in vivo* results in this study showed that the siRNA-HNT complex reduced the expression levels of RIPK4 protein, resulting in the inhibition of bladder cancer progression [132].

MMT can also be used as a gene vector [136,137]. Lin *et al.* [136] design a vector for gene delivery using hexadecyltrimethylammonium (HDTMA) attached to MMT. Given that the MMT surface and the DNA molecules are both negatively charged, the functionalization of MMT with HDTMA is useful to increase its affinity with DNA molecules. Moreover, HDTMA expands the interlayer space of MMT, thus increasing the loading capacity. Electrophoresis showed that the DNA-MMT-HDTMA complex could protect the DNA molecules. *In vitro* assays using human dermal fibroblasts demonstrated that the MMT-HDTMA complex was successfully transfected into

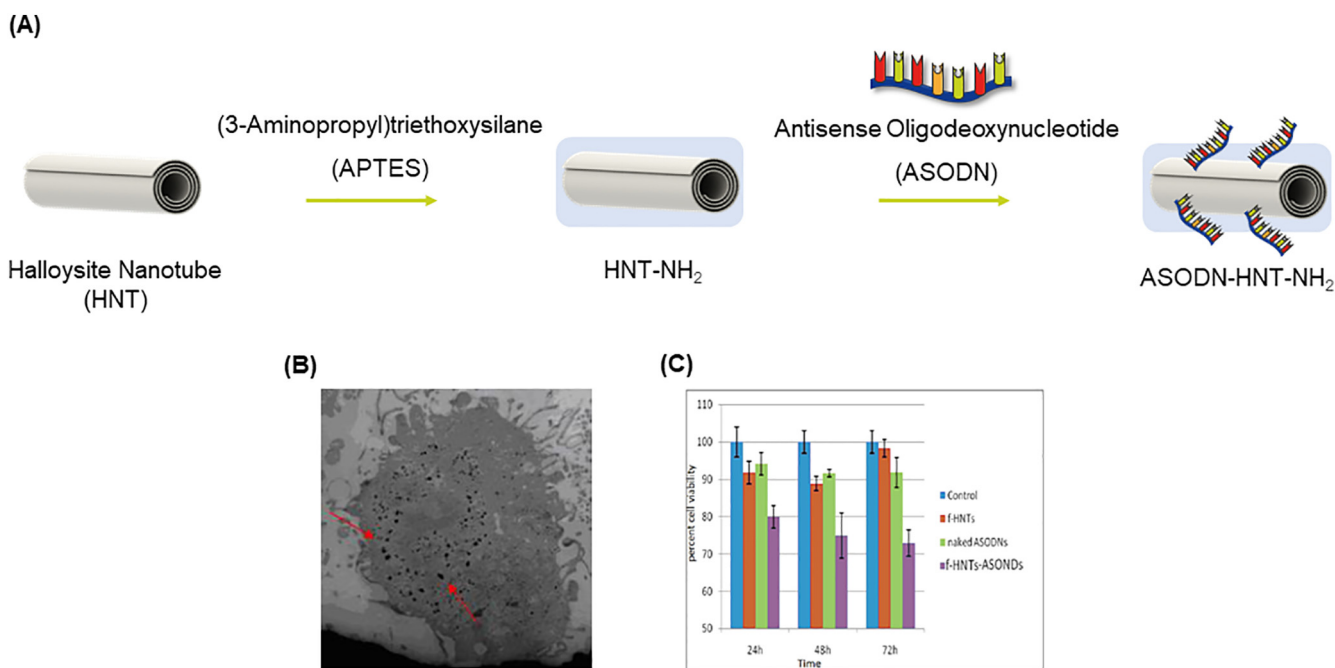


**Fig. 32.** Antisense oligodeoxynucleotides (ASODNs)-halloysite clay nanotubes (HNTs) complex. (A) Illustration of the preparation steps. (B) Transmission electron microscopy (TEM) image of the intracellular uptake of ASODNs-HNTs complexes by HeLa cells (adapted from [134]). (C) HeLa cell viability after treatment with HNT-NH<sub>2</sub>, naked ASODNs, and ASODNs-HNTs complexes for different time intervals (24, 48, and 72 h) (adapted from [134]).

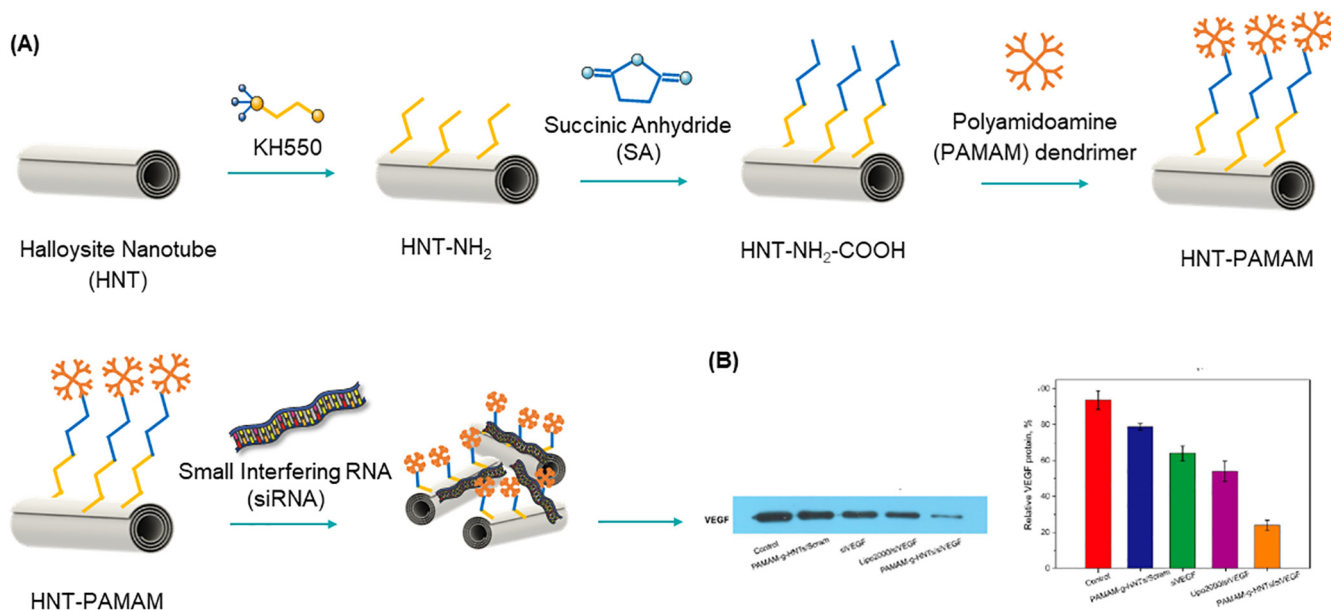


**Fig. 33.** Vascular endothelial growth factor (VEGF) siRNA (siVEGF)-halloysite clay nanotubes (HNTs)-poly(amidoamine) (PAMAM) (siVEGF-HNTs-PAMAM) complex. (A) Scheme of the preparation. (B) VEGF protein expression and VEGF mRNA levels in MCF-7 cells, adapted from [132]

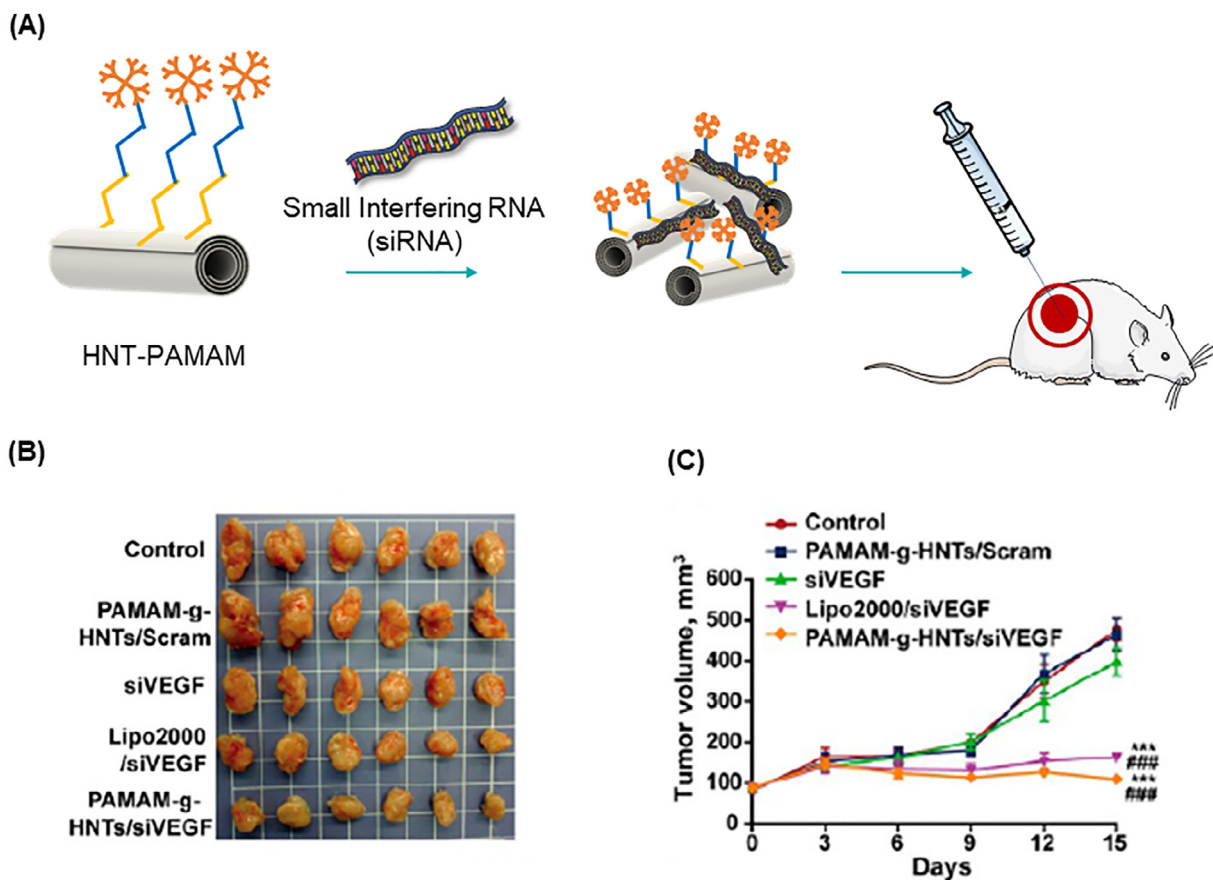


**Fig. 34.** Vascular endothelial growth factor (VEGF) siRNA (siVEGF)-halloysite clay nanotubes (HNTs)-poly(amidoamine) (PAMAM) (siVEGF-HNTs-PAMAM) complex. (A) Schematic illustration of the administration to 4T1 breast cancer-bearing mice. (B) Photograph of excised 4T1 breast cancer solid tumors (adapted from [132]). (C) *In vivo* antitumor effect obtained after treatment with siVEGF-HNTs-PAMAM complex in 4T1 breast cancer-bearing mice, expressed as tumor volume (mm<sup>3</sup>) (adapted from [132]).

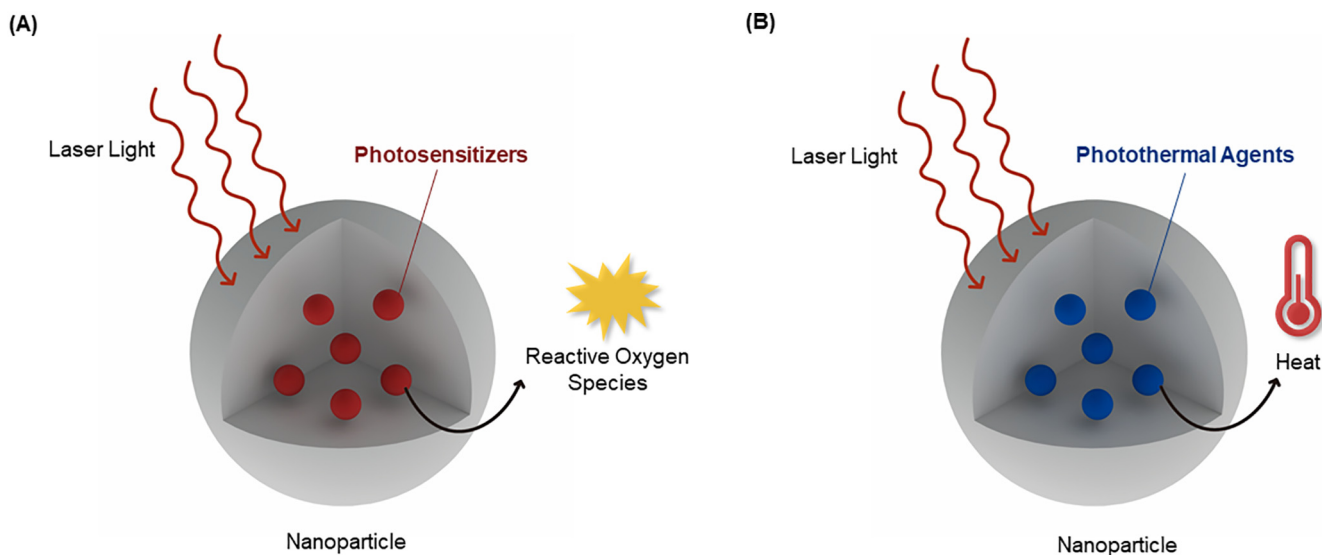


Fig. 35. Schematic representation of the mechanism of action of cancer phototherapy. (A) Photodynamic therapy (PDT). (B) Photothermal therapy (PTT).

the nucleus of the cells [136]. In one study carried out by Sironmani *et al.* [137], silver nanoparticles (Ag NPs) were stabilized onto MMT to transport a plasmid vector containing the complementary DNA of GFP (pcDNA-GFP). The pcDNA-GFP-MMT-Ag complex was characterized by a shift in the plasmon resonance to a longer wavelength. This shift typically occurs in the presence of DNA. This result suggested that the pcDNA-GFP-MMT-Ag complex could also be used for diagnostic purposes. Moreover, the pcDNA-GFP-MMT-Ag complex showed satisfactory results in transfection assays, and could be a promising gene vector [137].

### 3.3.5. Phototherapy

Many therapies designed for different types of cancer treatment are under investigation [138,139]. Amongst all these therapies, phototherapy has shown promising results. Cancer phototherapy involves the administration of light-responsive molecules followed by light irradiation at a specific wavelength to the tumor location. Ideally the molecules selectively accumulate in the tumor site and combined with spatially-confined light irradiation provide a level of dual selectivity [140,141]. The therapeutic action is localized because the molecules that could possibly accumulate in other locations are not exposed to light irradiation. The *in vivo* application of phototherapy usually requires the use of longer wavelengths to facilitate light penetration into the tissue. In the human body, the main tissue chromophores (hemoglobin, myoglobin, and melanin) strongly absorb UV and visible light, while water absorbs light with wavelengths above 900 nm. Therefore, the most appropriate phototherapeutic agents are those that have strong absorption in the near-infrared wavelengths (650 nm to 900 nm), a region known as the biological transparency window [142]. Using NIR light guarantees minimal interaction with biological components and deeper tissue penetration, allowing the activation of phototherapeutic agents that accumulate in the tumor area [140,143]. Generally, two types of phototherapeutic agents have been distinguished: photosensitizers for photodynamic therapy (PDT); and photothermal agents for PTT (Fig. 35) [141].

In PDT, upon light irradiation, the administered photosensitizers lead to the production of cytotoxic ROS, which cause the destruction of the tumor by affecting three main targets: cancer cells; the microvasculature; and elements of the host inflammatory and immune systems (Fig. 35A). The ROS responsible for the therapeutic effect in PDT are a result of the transfer of energy from the

excited photosensitizer to molecular oxygen to produce singlet oxygen. Electron transfer reactions can also produce hydroxyl radicals and superoxide anions. PDT differs from anticancer drugs because it does not have any toxic effects on biological systems in the absence of light, and, contrary to the ionizing radiation used in radiotherapy, it does not damage intervening normal tissue. Additionally, PDT leads to outstanding functional and cosmetic recovery, less long-term morbidity, and enhances the patient quality of life. It should be noted that the level of cytotoxicity resulting from PDT is dependent on the photosensitizer optical properties, its concentration, location, the period between photosensitizer administration and light activation, and the concentration of oxygen present in the tumor location [139,141].

Indocyanine green (ICG) is a photosensitizer approved by the Food and Drug Administration (FDA) for medical applications. ICG has been investigated for anticancer PDT since it produces cytotoxic effects when activated by light. However, the clinical use of ICG is still cumbersome due to its instability in physiological conditions. ICG has only poor stability in aqueous solution, particularly when exposed to light. Therefore, the application of nanocapsules to encapsulate ICG has been investigated to overcome the limitations associated with this photosensitizer [139,141]. Li *et al.* [141] loaded negatively charged ICG into the positively charged lumen of HNTs *via* electrostatic interactions to enhance the photochemical stability of ICG. HNTs were functionalized with a polyanionic coating of poly(sodium-p-styrene sulfonate) (PSS). The PSS coating increased the zeta potential of the HNTs from  $-32$  mV to  $-52$  mV, improving the biocompatibility and dispersion stability. The resulting ICG-HNT-PSS nanocomposite showed a higher photosensitizing effect than free ICG. The encapsulation of ICG into HNTs prevented the photochemical degradation of ICG (lower photobleaching), especially in aqueous media. The PDT effects of the ICG-HNT-PSS nanocomposite were examined using giant unilamellar vesicles (GUVs) as model membranes. When exposed to NIR light, the GUVs underwent a rapid morphological alteration, confirming the ability of the nanocomposites to cause oxidative membrane damage [141]. The ICG-HNT-PSS nanocomposites were also decorated with the membranes from human breast carcinoma cells (MDA-MB-436) (Fig. 36A). This modification increased the biocompatibility of the nanocomposites and improved the targeting towards MDA-MB-436 cells (Fig. 36B). *In vitro* PDT was performed by irradiating MDA-MB-436 cells with

808 nm NIR light at a power density of  $300 \text{ mW/cm}^2$  for 160 s. Under these conditions, the MDA-MB-436 cells displayed significant membrane disintegration. The study also reported *in vivo* PDT using the membrane-coated ICG-HNTs-PSS nanocomposite administered by tail-vein injection plus 808 nm NIR laser irradiation at a safe irradiance of  $300 \text{ mW/cm}^2$  for 300 s. A significant tumor volume reduction (ca. 95%) occurred after 14 days compared to control, ICG, and uncoated ICG-HNT-PSS (Fig. 37). These results suggested that membrane-coated the ICG-HNT-PSS nanocomposites could be a targeted therapy for breast cancer [141].

In PTT, photothermal agents are used to convert light into heat inside the tumor, resulting in the thermal ablation of cancer cells by the irreversible damage produced at a high temperature. The amount of damage depends on the thermal energy that is delivered, the rate of delivery, *i.e.*, the power density, and the thermal sensitivity of the target tissue. With temperatures ranging from  $41 \text{ }^\circ\text{C}$  to  $47 \text{ }^\circ\text{C}$ , irreversible cellular damage occurs only after prolonged exposure (longer than 60 min), while at temperatures above  $50 \text{ }^\circ\text{C}$ , the required time to produce irreversible damage decreases exponentially. Above  $50 \text{ }^\circ\text{C}$ , protein denaturation leads to coagulation necrosis. Moreover, mild hyperthermia promotes mitochondrial dysfunction and inhibition of DNA replication. It is accepted that cancer cells are more thermosensitive compared to healthy cells, due to their high metabolic stress, reduced heat-dissipating capacity, and the acidity of the TME [144–146]. PTT is similar to PDT; in that it is highly selectivity due to confinement of the laser irradiation on the tumor location. Furthermore, photothermal agents should possess suitable optical properties and a high photothermal energy conversion efficiency. Their accumulation in the tumor site and suitable intracellular distribution are crucial for the success of the treatment [145,146].

Nanomaterials have been widely explored as a new generation of photothermal agents. Nanomaterials are less susceptible to photobleaching and can accumulate in the tumor site through either passive or active targeting. For example, Au NPs have been extensively explored as photothermal agents, due to their tunable plasmon resonance properties, high absorption coefficients in the NIR

region, and efficient photothermal conversion. Moreover, gold is an element with inert chemical reactivity and acceptable biocompatibility. The use of Au NPs is based on an optical phenomenon known as localized surface plasmon resonance (LSPR). The LSPR absorption of Au NPs can be easily tuned to the NIR region, by changing the morphology of the NPs. For example, the LSPR absorption of Au NPs can be adjusted to the NIR region by lengthening the structure of the NPs along a single direction [140,147]. Wu *et al.* [146] used a simple process to stabilize Au NPs using PAL as a template. Firstly, the negatively charged surface of PAL was altered to become positively charged by the sequential deposition of polymers with an opposite charge on its surface, using the LbL method. Then, the LbL-coated PAL surface was uniformly decorated with small Au NPs (diameter ca.15.0 nm) linked to each other to produce tube-like Au-PAL nanocomposites (Fig. 38). The fibrous morphology of the PAL template allowed the successful adjustment of the LSPR peak to the NIR region (ca. 670 nm). The nanocomposite rapidly absorbed NIR light and efficiently converted the light into thermal energy. In this study, the temperature of the Au-PAL nanocomposite increased from room temperature to  $53 \text{ }^\circ\text{C}$  after irradiation with an 808 nm NIR laser at  $0.5 \text{ W/cm}^2$ . The photothermal activity was tested using A549 cells and A549 lung cancer-bearing nude mice. A549 cells were incubated with a suspension of the nanocomposite ( $100 \text{ } \mu\text{g/mL}$ ) and irradiated with an 808 nm laser at a power density of  $0.5 \text{ W/cm}^2$  for 15 min. These conditions induced an almost total loss of cancer cell viability. In lung cancer-bearing mice, an intratumoral injection of Au-PAL nanocomposite caused tumor ablation after laser irradiation. Moreover, there was an absence of re-growth for at least 10 days, suggesting that the PTT ablation could also inhibit cancer cell metastasis [146].

Tube-like Au-PAL nanocomposites have also been tested in a combination of chemotherapy and PTT (chemo-PTT). In one study by Zhao *et al.* [147], MTX was intercalated and adsorbed in the channels, and the surface of PAL was decorated with Au NPs (MTX-Au-PAL). In an *in vitro* cytotoxicity assay in HeLa cells, the MTX-Au-PAL nanocomposite induced a rapid loss of cell viability

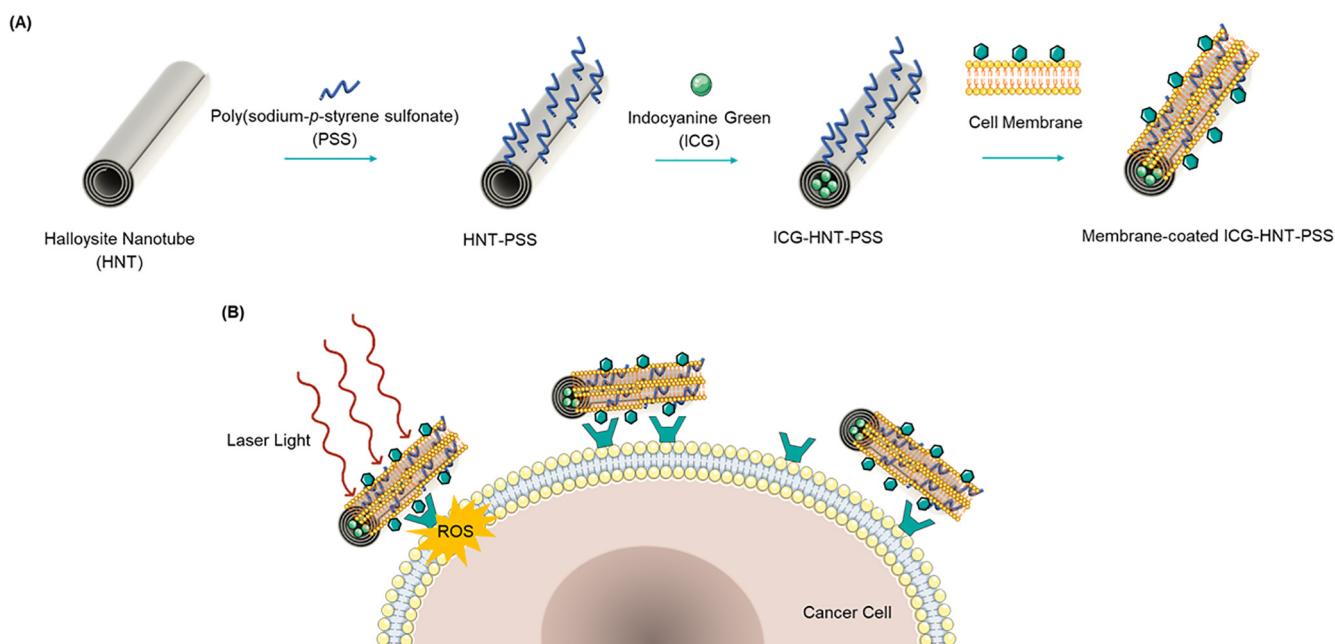


**Fig. 36.** Membrane-coated indocyanine green (ICG)-loaded poly(sodium-p-styrene sulfonate) (PSS)-modified halloysite clay nanotubes (HNTs) (ICG-HNT-PSS). (A) Schematic illustration of the preparation. (B) Specific targeting effect of membrane-coated ICG-HNT-PSS nanocomposite on the cancer cell membrane and membrane cellular damage triggered by laser light irradiation.

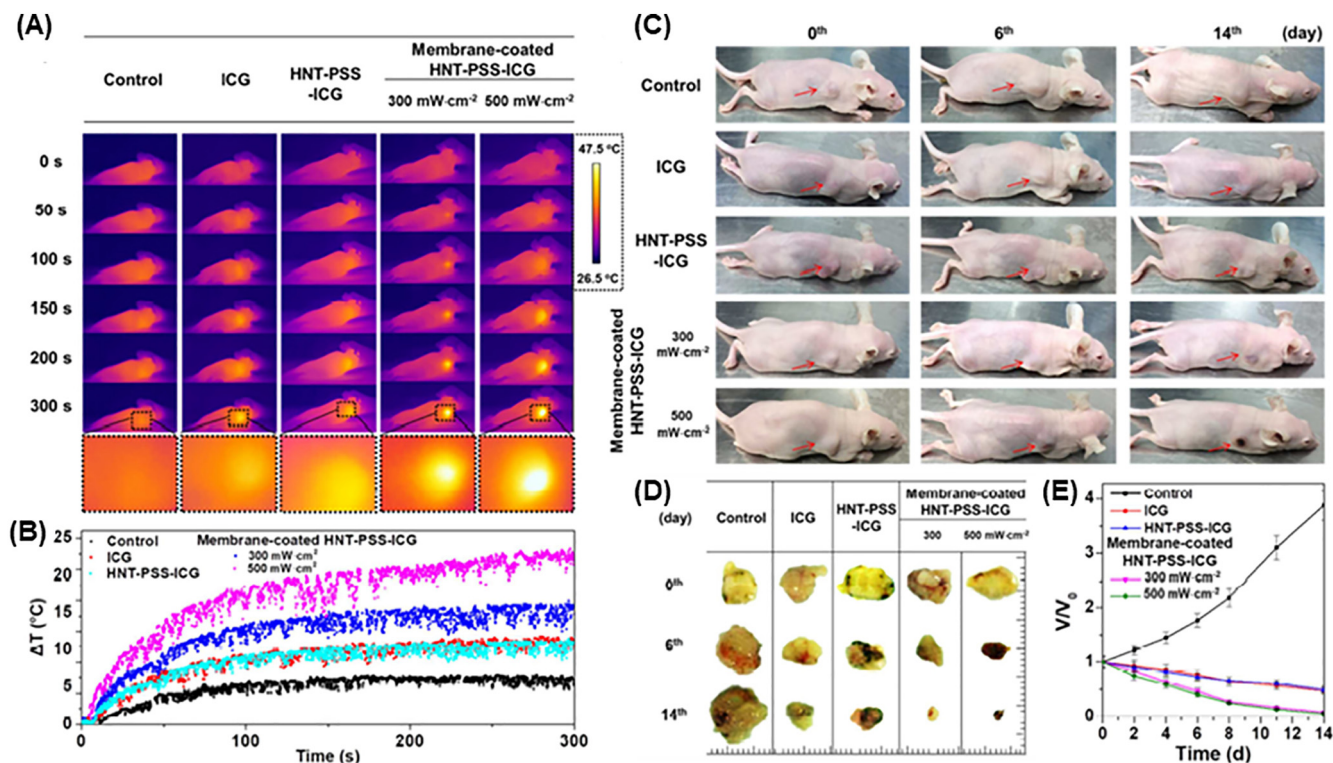


**Fig. 37.** Photothermal therapy (PTT) with indocyanine green (ICG)-loaded poly(sodium-p-styrene sulfonate) (PSS)-modified halloysite clay nanotubes (HNTs) (ICG-HNT-PSS). (A) Photothermal imaging and (B) temperature variation in mice from groups control, ICG, ICG-HNTs-PSS and membrane-coated ICG-HNTs-PSS plus 808 laser irradiation (300 mW/cm<sup>2</sup>) for 300 s. (C) Photographs of representative mice from groups control, ICG, ICG-HNTs-PSS and membrane-coated ICG-HNTs-PSS on the 0<sup>th</sup>, 6<sup>th</sup> and 14<sup>th</sup> days. (D) Photographs of excised tumors from the mice at 24 h after administration of ICG, ICG-HNTs-PSS and membrane-coated ICG-HNTs-PSS on the 0<sup>th</sup>, 6<sup>th</sup> and 14<sup>th</sup> days. (E) *In vivo* antitumor effect expressed as the average values of the relative tumor volume  $V/V_0$ , where  $V$  is the tumor volume at the test time points and  $V_0$  is the initial tumor volume. Reproduced from [141].

in comparison to free MTX. A 24-hour incubation of MTX-Au-PAL nanocomposite with HeLa cells produced a cytotoxic effect after laser irradiation for 15 min [147]. Similarly, Zhang *et al.* [148] described a different chemo-PTT nanocomposite for breast cancer, in which gold nanorods (GNR) and DOX were simultaneously loaded in the lumen and surface of HNTs, respectively. The external surfaces of HNTs were also grafted with the targeting ligand FA *via* a reaction with bovine serum albumin (BSA). This additional functionalization enabled the recognition of cancer cells over-expressing FR and improved the tumor-targeting ability (Fig. 39A). *In vitro* experiments showed that the Au-DOX-HNT-BSA-FA nanocomposite displayed strong chemotherapeutic and phototherapeutic efficacy against MCF-7 cells, which over-expressed FA receptors. Before the laser irradiation, the cell survival rate was 73%, but after exposure to 808 nm NIR laser at

1 W/cm<sup>2</sup> for 8 min, the apoptosis rate increased, and the survival rate was only 7.4%. These results suggested that both the DOX and GNRs contained in the Au-DOX-HNT-BSA-FA nanocomposite played a role in apoptosis induction and cell death after light irradiation. At first, the release of DOX from the nanocomposite led to a low level of apoptosis, whereas the subsequent laser exposure enhanced the apoptosis due to a pronounced rise in the temperature. Furthermore, 4T1 breast cancer-bearing mice were intravenously injected with Au-DOX-HNT-BSA-FA nanocomposite (20 mg/kg) and exposed to 808 nm laser at 1 W/cm<sup>2</sup> (Fig. 39B, C, D). The intravenous administration of the chemo-PTT nanocomposite combined with laser irradiation caused a 79% reduction in the average tumor volume. By contrast, when using the Au-HNT-BSA-FA nanocomposite followed by laser irradiation (DOX was absent), the decrease of the average tumor volume was only

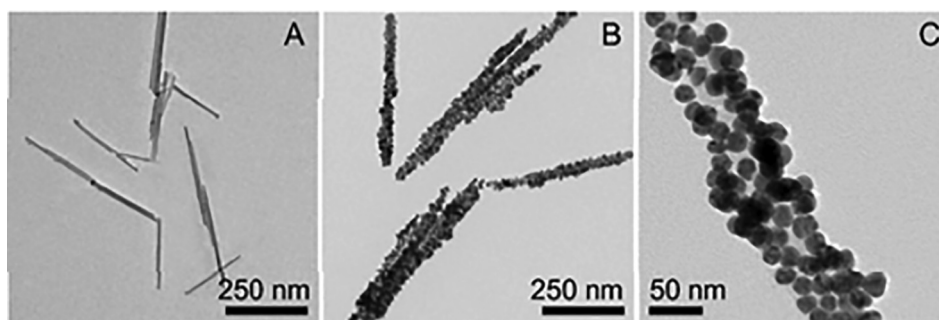


**Fig. 38.** Transmission electron microscopy (TEM) images of (A) pristine palygorskite (PAL) and (B, C) gold nanoparticles (Au NPs)-PAL nanocomposite. Reproduced from [146].

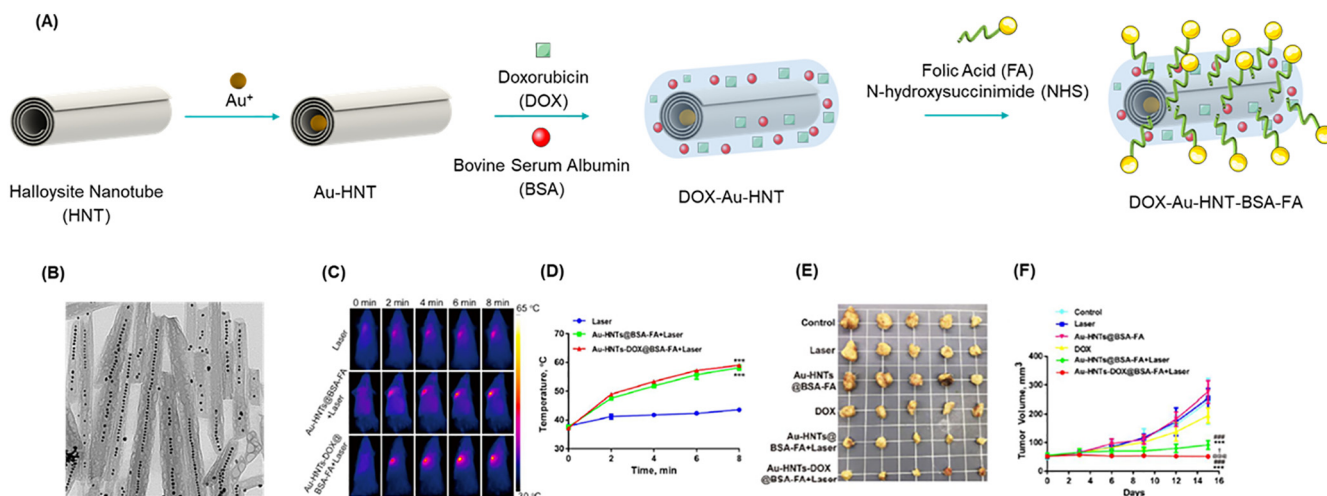


**Fig. 39.** Gold nanoparticles (Au NPs)-loaded halloysite clay nanotubes (HNTs) decorated with bovine serum albumin (BSA), doxorubicin (DOX) and the folic acid (FA) ligand (Au-DOX-HNT-BSA-FA) nanocomposite. (A) Schematic illustration of the preparation. (B) Transmission electron microscopy (TEM) images of HNTs used as template for the *in situ* growth of 6-nm diameter gold nanoparticles. (C) Infrared thermal images of Au-DOX-HNT-BSA-FA nanocomposite in 4T1 breast cancer-bearing mice. (D) Temperature variation in the mouse tumor during laser irradiation. (E) Photographs of excised 4T1 breast cancer solid tumors on the 16th day after the administration of Au-HNT-BSA-FA, DOX, Au-HNT-BSA-FA with laser irradiation and Au-DOX-HNT-BSA-FA nanocomposite with laser irradiation. (F) *In vivo* antitumor effect obtained from treatment with Au-HNT-BSA-FA, DOX, Au-HNT-BSA-FA with laser irradiation and Au-DOX-HNT-BSA-FA nanocomposite with laser irradiation in mice, expressed as tumor volume ( $\text{mm}^3$ ). Reproduced from [148].

67.4%. Also compared to free DOX, the Au-DOX-HNT-BSA-FA nanocomposite decreased the tumor volume more prominently and did not cause any decrease in body weight (Fig. 39E, F) [148]. Together, the mentioned two studies outline the use of nanoclays as platforms to achieve simultaneous delivery of anticancer drugs and photothermal activation. The combination of chemotherapy and PTT leads to a considerable increase in cancer treatment efficacy with a reduced presence of side effects.

Magnetic NPs (MNPs) are another example of nanomaterials that have been applied as photothermal agents. Anirudhan *et al.* [142] explored the magnetic hyperthermia properties of MNPs for tumor ablation. The authors studied the *in vitro* heating behavior of carboxymethyl chitosan (CMCS)-capped-MNPs intercalated in MMT (MMT-CMCS-MNPs). When these nanocomposites were exposed to an alternating electromagnetic field, a rapid increase in the temperature, from 25 °C to 40 °C, occurred in 20 min. After 40 min, the temperature reached 45 °C which remained constant until the end of the experiment. These results demonstrated that the MMT-CMCS-MNP nanocomposites can regulate the temperature and heat flux, which is a fundamental requirement for PTT [142].

All these studies highlight the potential of cancer phototherapy using nanoclays as templates and nanocarriers for the delivery of photothermal agents and photosensitizers.

### 3.3.6. Co-delivery

Resistance to anticancer drugs has been a major hurdle in cancer treatment. Frequently, conventional treatment with a single therapeutic agent is unable to eliminate all the cancer cells, and the surviving cells give rise to MDR. One strategy to overcome this problem is to use nanocarriers for the co-delivery of anticancer drugs or other anticancer bioactive molecules in a combination therapy. Ideally, chemotherapy with a combination of two or more drugs would provide a synergistic effect between the drugs, and suppress the emergence of drug resistance *via* several pathways [39,149,150].

In 2015 and 2016, the group of Massaro *et al.* developed HNT-based multi-cavity hybrid nanocarriers for the co-delivery of some natural compounds. In their first study, the authors combined sili-

binin (SIL) and QUE, and, in their latest work, SIL and CUR. This group of researchers created multifunctional hybrid nanocarriers through modification of the external surface of HNTs with amphiphilic-CD molecules. Spectroscopy and chromatography revealed that SIL was preferentially bound within the lumen of the HNTs, while QUE and CUR were encapsulated in the hydrophobic cavity of the CDs. These distinct interactions allowed a targeted drug release in different environments. *In vitro* release experiments demonstrated an enhanced release of SIL in gastric pH (pH 1.0), whereas the release of QUE and CUR was higher in the intestinal fluid pH (pH 7.4). The multifunctional HNT-based hybrid nanocarrier showed higher cytotoxicity towards anaplastic thyroid cancer cells (8505C) compared to the free natural compounds. Fluorescence microscopy showed the intracellular presence of the hybrid nanocarriers near the cell nucleus, showing their successful internalization by thyroid cancer cells. In a recent study, Massaro *et al.* [150] added mannose to the core of CDs. This functionalization increased the cellular internalization of the hybrid nanocarriers due to carbohydrate receptor-mediated endocytosis. The mannose units specifically bind to the lectin concanavalin A, a carbohydrate-binding protein widely expressed on the surface of cancer cells [149,150].

Cancer patients often have a weakened immune system making them more susceptible to infections. Therefore, antibiotics are frequently administered to cancer patients who are receiving chemotherapy. Zeynabad *et al.* [39] reported an innovative antibacterial nanocomposite that could be included in multi-agent cancer therapy. MMT nanoclay was used as the nanocarrier, since MMT interacts with bacterial cells *via* electrostatic forces. Silica-based co-polymers were inserted into the interlayer space of MMT *via* an ion-exchange mechanism. The resulting nanocomposites were loaded with two anticancer drugs, DOX and MTX, as well as an antibiotic, CIP, with an EE of *ca.* 95.0% for all the drugs. There was an increased drug release when the pH was reduced, which was useful because of the higher acidity of cancer cells compared with healthy cells. In addition, the simultaneous release of DOX and MTX from the nanocomposite led to higher cell death in breast cancer cells (T47D) when compared to the free drugs individually. The CIP released from the nanocomposite showed an antimicrobial

activity towards both *Escherichia coli* and *Pseudomonas aeruginosa* Gram-negative bacteria [151]. The same authors developed another pH-responsive co-delivery nanocomposite, but this time used LAP. In this work, LAP was modified with two kinds of cationic vinyl monomers using a cation exchange procedure. After that, MTX and CIP were loaded separately into the nanocomposite. The EE of both drugs was >90%. The nanocomposite, apart from the higher drug release at acidic pH, also exhibited an effective antimicrobial action towards both *E. coli* and *P. aeruginosa*. Moreover, the nanocomposite enhanced the cytotoxicity of MTX and CIP, inducing apoptosis in MCF-7 cells [39]. Recently, Kar *et al.* [44] evaluated the potential of MMT that was organically modified with cetyltrimethylammonium bromide (CTAB) (OMMT) for the delivery of MTX and CUR. The anticancer drug and the natural compound were separately intercalated in OMMT. MTX is a folate antagonist; therefore, MTX-OMMT displayed higher uptake in FR-positive cervical cancer cells (HeLa). The exposure of FR-positive HeLa cells and FR-negative breast cancer cells (MCF-7) first to CUR-OMMT and then to MTX-OMMT significantly reduced the cell viability by 94% and 85%, respectively. The exposure of cancer cells to the IC<sub>50</sub> drug concentration of MTX, after pre-exposure to CUR, further enhanced cancer cell death. Thus, pre-treatment with CUR-OMMT followed by MTX-OMMT allowed the use of a lower concentration of MTX, while maintaining the FR targeting ability and the cytotoxic anticancer activity without damaging healthy cells (Fig. 40) [44].

Collectively, these studies confirm the utility of nanoclays as nanocarriers for the simultaneous delivery of two or more anticancer molecules. Nanoclays provided a synergistic therapeutic activity along with reduced side effects.

### 3.3.7. Treatment of cancer-associated chronic pain

Fentanyl is a synthetic opioid used for the relief of cancer-induced pain. Sustained release formulations are preferred for fentanyl administration in order to reduce the frequency of dosing. Currently, the sustained release fentanyl delivery formulations available on the market are based on patches and infusion pumps. These formulations usually contain a drug dose necessary to maintain a therapeutic plasma concentration for over 6 h. However, sustained release drug delivery formulations for oral administration are still not available on the market due to the risk connected to dose-dumping, which results in adverse or even lethal side effects [152]. Bearing this in mind, innovative pellets composed of HNTs and microcrystalline cellulose were developed for fentanyl sustained release. Drug release studies of intact and segmented pellets, which simulated swallowing in the presence or in the absence of chewing, respectively, were performed under three different conditions: pH 6.8, pH 1, and in 48.0% ethanol in order to mimic intestinal conditions, stomach conditions and the administration of the drug with alcohol, respectively. Intact pellets showed a fentanyl sustained release for 3–4 h in all studied conditions, while the segmented pellets showed a complete release after 2–3 h. Thus, the nanocomposite exhibited controlled fentanyl release properties, which was the main goal of the experiment [152]. Nevertheless, further research is needed to evaluate the potential of halloysite-based oral fentanyl formulations for the treatment of cancer-associated chronic pain.

## 4. Nanoclays as theranostic nanoplateforms

Recent decades have seen significant technological progress, enabling the development of innovative cancer therapeutic interventions. In this context, the design of multifunctional nanodelivery systems able to carry several types of cargos at the same time has laid the foundation for the concept of theranostic nano-

medicine [89]. A theranostic nanoplateform simultaneously allows diagnostic and therapeutic functions. Accordingly, theranostic nanoplateforms can detect and target tumors, and monitor the response to treatment. Moreover, these all-in-one nanoplateforms enable the tracking of the release of anticancer agents in real-time [9,12]. Nanoclays, particularly HNTs, have the potential to be used in the design of theranostic nanoplateforms. HNTs have a hollow tubular morphology and tunable surface chemistry, enabling the simultaneous delivery of imaging contrast and anticancer agents.

In one study by Guo *et al.* [121], FA and MNPs were grafted onto the external surface of HNTs *via* amide bonds, while DOX was adsorbed onto the surface of HNTs *via* electrostatic interactions. In the *in vitro* experiments, the multifunctional nanoplateform produced by Guo *et al.* showed significant cytotoxic effects towards HeLa cells, with the potential to be applied in cancer therapeutics. Furthermore, the MNPs grafted onto HNTs functioned as an imaging contrast agent, thus enabling the simultaneous detection of tumors by MRI [121]. In another recent study, carbon dots (CDs) were covalently attached to the external surface of HNTs (HNT-CDs), producing a nanoplateform with excellent photoluminescent properties (Fig. 41). The HNT hybrid acted as a non-viral vector to deliver calf thymus DNA, and showed *in vitro* antioxidant activity, as well as an intracellular imaging ability [133].

Another nanoclay with the potential to be used in theranostic nanoplateforms is MMT. In a work by Bekaroğlu *et al.* [153], a computer tomography (CT) contrast material and DOX were adsorbed to the surface of MMT, producing a nanoplateform with drug-release and medical imaging capability. This MMT-based theranostic nanoplateform was also used for transcatheter arterial embolization. In this clinical procedure, particles are injected to obstruct tumor arterial vessels, reducing the oxygen and nutrient supply, which consequently leads to the progressive shrinkage of the tumor. In a rabbit kidney model, a preliminary evaluation showed the total occlusion of the first renal artery and renal arterial branches. The CT contrast material adsorbed to MMT enabled the visualization of the embolization (Fig. 42). Besides, this theranostic nanoplateform allowed a follow-up using a cone beam CT scan, enabled the early identification of pathological lesions, and an early intervention to prevent local recurrence [153].

PAL was also used in the development of a prospective theranostic nanoplateform. PEI was uniformly distributed on the surface of PAL *via* a covalent grafting process. Then, the PEI-modified PAL was decorated with fluorescein isothiocyanate (FI) and FA to target and detect cancer cells over-expressing the FR. CLSM images and inductively coupled plasma optical emission spectroscopy (ICPOES) data revealed that the PAL-based theranostic nanoplateform was internalized by FR-over-expressing HeLa cells. These results showed that the PAL-based theranostic nanoplateform could be used for early tumor diagnosis. Furthermore, these nanoplateforms could be candidates for targeted anticancer drug delivery due to their mesoporous structure, combining in a single structure cancer diagnosis and therapy [154].

Recently, Zhang *et al.* [155] intercalated dodecylamine into the interlayer of a Kaolin<sub>MeOH</sub> intermediate to prepare dodecylamine-modified kaolinite (Kaolin C<sub>12</sub>N). This modification was used to increase the interlayer space to 4.16 nm and expose the Si-OH groups on the internal surface of kaolinite, allowing the loading of compounds to be carried. DOX was loaded in the interlayer space of Kaolin-C<sub>12</sub>N and the outer surface of the nanocomposites was functionalized with Mn<sub>3</sub>O<sub>4</sub> magnetic nanoparticles plus KI, forming a promising targeted theranostic nanoplateform to be used against papillary thyroid cancer therapy. DOX-Kaolin C<sub>12</sub>N-Mn<sub>3</sub>O<sub>4</sub>-KI showed better *in vitro* anticancer activity than free DOX towards papillary thyroid cancer cells (TPC-1). DOX-Kaolin C<sub>12</sub>N-Mn<sub>3</sub>O<sub>4</sub>-KI exhibited a cell inhibition rate of 79%, while free

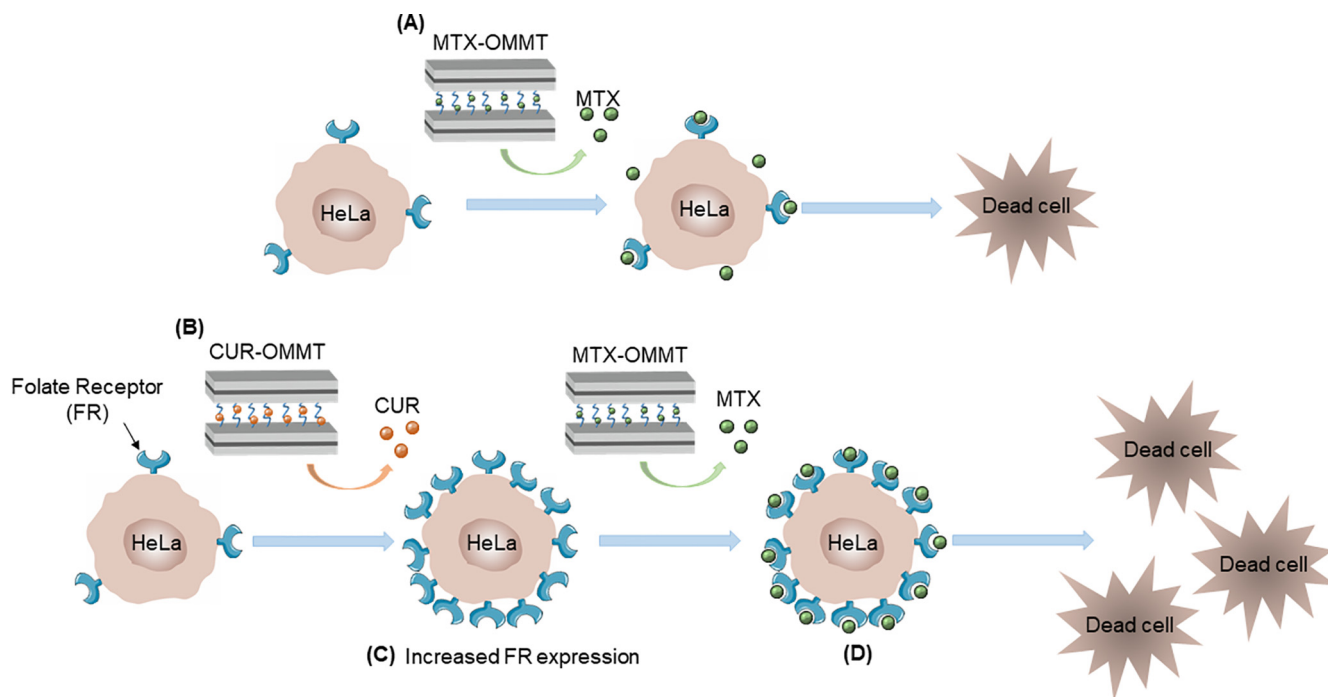


**Fig. 40.** Organically modified montmorillonite (MMT) with cetyltrimethylammonium bromide (CTAB) loaded with methotrexate (MTX). (A) Schematic illustration of MTX loading. (B) Curcumin (CUR) loading. (C) CUR enhanced the expression of folate receptor (FR) on the surface of HeLa cells. (D) Increased uptake and MTX anticancer therapeutic activity.

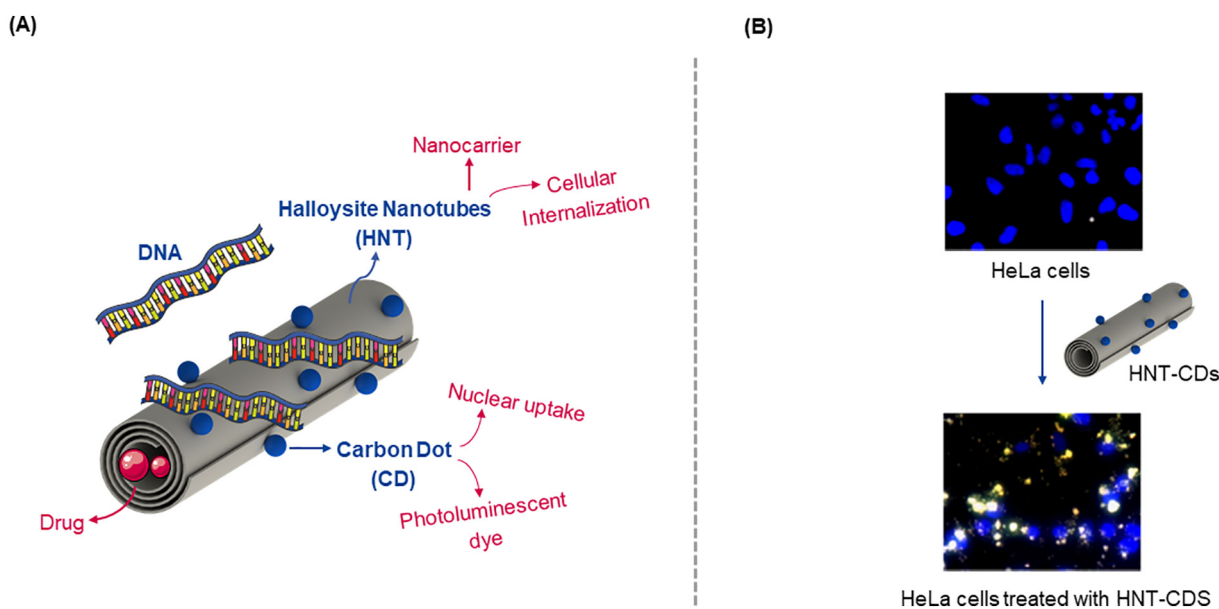


**Fig. 41.** Theranostic nanoplatform composed of halloysite clay nanotubes (HNTs) decorated with carbon dots (CDs) (HNT-CDs). (A) Illustration of the preparation. (B) Fluorescence microscopy images of HeLa cells treated with HNT-CDs (adapted from [133]).

DOX displayed a rate of only 43%. Moreover, images of the tumor sections of thyroid cancer-bearing mice demonstrated that the theranostic nanoplatform caused a significant tumor shrinking (75%) and an accumulation in the tumor tissue [155].

Overall, there is substantial evidence reporting the use of nanoclays as innovative theranostic nanoplatforms. These nanoplatforms can enable an evaluation of the therapeutic success, opening new avenues in precision medicine.

## 5. Nanoclays toxicological evaluation

The increasing interest in biomedical applications of nanoclays requires more toxicological studies to confirm the suitability for clinical applications. Several studies have examined the *in vitro* toxicological profiles of different nanoclays and their derived nanocomposites. *In vitro* assays have mainly been used for screening and for generating more comprehensive toxicological

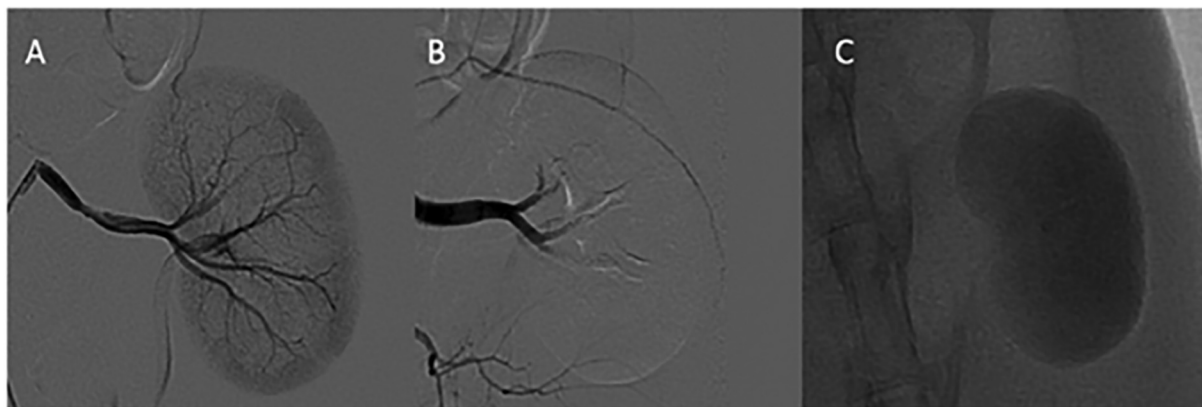


**Fig. 42.** Montmorillonite (MMT) for kidney embolization. Angiograms of the kidney: (A) before arterial embolization renal arteries are open; (B) after embolization, showing a total occlusion of the renal arteries; (C) fluorogram shows attenuation in embolized kidney. Reproduced from [153].

data, providing evidence of any biological damage and the mechanism of action responsible for the toxic effects. Although most of the research about the toxicity of nanoclays has focused on *in vitro* assays, these results require further confirmation using *in vivo* assays. *In vivo* toxicology allows studying the complex interactions between the nanostructure and tissues and organs in animal models, providing information on biodistribution, clearance, immune response, and metabolism. Therefore, understanding the correlation between the properties of nanoclays and their *in vitro* and *in vivo* behavior is crucial to evaluate their toxicity. The *in vitro* and *in vivo* toxicity of nanoclays have been explored in the scientific literature, and the main toxicological findings regarding nanoclays are described below.

### 5.1. *In vitro* toxicological assays

#### 5.1.1. Cytotoxic analysis in healthy cells

Human lymphocytes treated with different concentrations of kaolinite ranging from 3.9  $\mu\text{g}/\text{mL}$  to 500  $\mu\text{g}/\text{mL}$  did not show significant changes in cell viability. Besides, it was reported that the degree of hemolysis was <5% for all tested concentrations. Therefore, kaolinite was classified as a hemocompatible material [19]. Furthermore, in another study, kaolinite did not demonstrate any cytotoxic effects in mammalian cells at concentrations between 50  $\mu\text{g}/\text{mL}$  and 200  $\mu\text{g}/\text{mL}$  [156].

Studies were performed on human umbilical vein endothelial cells (HUVECs) to investigate the cytotoxicity of different concentrations (from 2.5  $\mu\text{g}/\text{mL}$  to 200  $\mu\text{g}/\text{mL}$ ) of FITC-functionalized HNTs (FITC-HNT). After 24-hour exposure to FITC-HNT, the HUVECs exhibited cell viability values above 85%. However, there was a decrease in cell viability when cells were subjected to long incubation periods. After 72-hour exposure to a high concentration (200  $\mu\text{g}/\text{mL}$ ) of FITC-HNTs, the HUVEC viability was approximately 62% [157]. In monkey kidney epithelial cells (Vero cells), pristine HNTs, and HNTs modified with  $\text{Fe}_3\text{O}_4$  NPs did not show any cytotoxic effects [158]. In another study, human normal liver cells (L02) treated with pristine HNTs and HNTs bi-functionalized with PEG and FA at a concentration of 500  $\text{mg}/\text{mL}$  for 24 h showed cell viability over 90% [8]. More recently, the viability of human skin fibroblasts (HSF) did not change in the presence of prodigiosin-loaded HNTs at a concentration of 10  $\mu\text{g}$  per  $10^5$  cells [124].

Cytotoxicity experiments using MMT have been the most common due to its commercial availability. The cytotoxic effects of MMT on Chinese hamster ovary cells (CHO) were only evident at concentrations above 1000  $\mu\text{g}/\text{mL}$ , and for a long exposure time (>24 h) [159]. Furthermore, in the same study, the genotoxicity

of MMT was evaluated. MMT did not induce any DNA damage in CHO cells and was not mutagenic in *Salmonella typhimurium* [159]. However, some healthy cells showed a more acute toxic response when exposed to MMT. MMT significantly reduced the proliferation of human normal intestinal cells (INT-407) at concentrations above 100  $\mu\text{g}/\text{mL}$  after 24-hour and 72-hour exposure times. Besides, MMT inhibited colony formation of INT-407 cells after 10 days at the lowest concentration (5  $\mu\text{g}/\text{mL}$ ). A significant reduction in the INT-407 cell viability was evident after 24-hour and 72-hour exposure to MMT at a concentration of 1000  $\mu\text{g}/\text{mL}$ . These results suggested that MMT displays significant cytotoxicity towards normal cells only after a long exposure to high concentrations [160]. Furthermore, the cytotoxic effects of MMT in mouse embryonic fibroblasts (NIH 3T3) and human embryonic kidney cells (HEK 293) were investigated [161,162]. The cytotoxicity of MMT was correlated with the tendency of nanoclays to aggregate into micro-sized clusters, which accumulated around cells in culture media with elevated NaCl concentrations. Instead of causing direct cytotoxic effects, MMT clusters could block membrane channels, disturb cellular metabolism and cytoskeleton organization, and inhibit proliferation and colony formation. The LDH assay revealed that cell membrane damage only occurred at very high concentrations (1000  $\mu\text{g}/\text{mL}$ ) of MMT after 48 h to 72 h of exposure. Additionally, significant cellular ROS production was observed only for concentrations above 50  $\mu\text{g}/\text{mL}$  after 48 h of exposure to MMT [160].

LAP did not exhibit significant effects on the morphology, viability, or proliferation of human mesenchymal stem cells (HMSCs) and human adipose-derived stem cells (HASCs) at concentrations below 100  $\mu\text{g}/\text{mL}$  during 7 days of exposure. The metabolic activity of HMSCs cells and HASCs was reduced to 50% after exposure to LAP concentrations of 4  $\text{mg}/\text{mL}$  and 1  $\text{mg}/\text{mL}$ , respectively [163,164]. Moreover, LAP did not exhibit toxicity to MC3T3-E1 cells since the overall viability remained unchanged at high doses (>35  $\text{mg}/\text{mL}$ ) [165].

#### 5.1.2. Cytotoxic analysis in cancer cells

The first step of nanoclays internalization by mammalian cells is the adsorption of protein corona via electrostatic interactions to the nanoclays surface [166]. This protein-nanoclays interaction is influenced by the physicochemical properties of nanoclays (chemical composition, surface-area-to-volume ratio, charge, and size). Nanoclays may also adsorb cellular membrane lipids [59]. Subsequently, nanoclays are internalized by mammalian cells via endocytic mechanisms and transported by lysosomal vesicles. Nanoclays are internalized by more than one mechanism due to

their wide range of shapes and sizes [81]. For instance, fibrous nanoclays as sepiolite are spontaneously internalized and excluded by mammalian cells [59]. In Castro-Smirnov *et al.* [59] study, after 6 h of exposure it was possible to observe by TEM the full uptake of sepiolite by hamster fibroblasts (V79 cell line). Sepiolite is internalized by clathrin-mediated endocytosis and macropinocytosis. In the study of Liu *et al.* [81], organosilane-modified HNTs labeled with FITC were internalized by A549 cells by caveolae- and clathrin-dependent endocytosis and transported by the cytoskeleton (actin filaments and microtubules) via Golgi apparatus and lysosomes, without entering in the cell nucleus [81]. Inside the cells, nanoclays intrinsically impact a series of cellular functions, notably ROS generation, whose production is directly proportional to the concentration of nanoclays delivered [166].

Several cancer cell lines, including lung cancer, CRC, gastric cancer, breast cancer, pancreatic cancer, cervical cancer, prostate cancer, esophageal cancer, and differentiated thyroid cancer were tested and showed almost no biological response when exposed to kaolinite at a concentration of 200  $\mu\text{g}/\text{mL}$ . The cell viability of the cancer cell lines was mostly above 85%. Esophageal cancer cells showed the highest cell viability (99.8%), and lung cancer cells the lowest cell viability value (61.3%) [29].

Bi-functionalized HNTs with FA and FITC were taken up by murine CRC cells (CT-26) and showed no signs of cytotoxicity at concentrations below 150  $\text{mg}/\text{mL}$  after 48 h of exposure [3]. In another work, CLSM results confirmed that FITC-functionalized HNTs were internalized by HeLa and MCF-7 cells. HNTs were concentrated around the nucleus of HeLa and MCF-7 cells and did not cause cellular damage or inhibit cellular proliferation. Even high concentrations of HNTs (75  $\mu\text{g}/\text{mL}$ ) did not show any toxicity, and at least 90% of the cells remained viable [55]. HNTs exhibited a similar biocompatible profile in human colon cancer cells (HCT116) and the HepG2 cell line. However, at a concentration of 1000  $\mu\text{g}/\text{mL}$ , HNTs significantly inhibited the proliferation of lymphocytes [167].

Several studies have shown that the functionalization of nanoclays with organosilanes,  $\text{Fe}_3\text{O}_4$  NPs, or polycations can cause some toxicity to cancer cells. A 24-hour exposure to pristine HNTs at a concentration of 500  $\mu\text{g}/\text{mL}$  did not cause cytotoxic effects. In contrast, HNTs modified with the organosilanes (trimethoxy(propyl)silane (TMPS) or triethoxy(octyl)silane (EOS)) induced apoptosis and caused toxicity to cancer cells. The functionalization of HNTs with  $\text{Fe}_3\text{O}_4$  NPs increased the cytotoxicity of the nanocomposite on A549 cells [158]. Cationic polyelectrolytes, such as PEI, poly(diallyldimethyl-ammonium) (PDADMAC), and PAH adsorbed onto the HNT surface significantly increased the toxicity of HNTs, inducing cellular and nuclear damage to A549 cells [168]. By contrast, PEG-coated HNTs (HNT-PEG) showed excellent biocompatibility towards cancer cells. After 72-hour exposure to HNT-PEG, HeLa and HepG2 cells showed cell viability above 80% for concentrations up to 0.5  $\text{mg}/\text{mL}$  [169,170]. In MCF-7 cells, after 72-hour exposure to HNT-PEG at a concentration not exceeding 0.1  $\text{mg}/\text{mL}$ , the survival rate was >70% [171]. The absence of cytotoxicity was verified in human ovarian carcinoma cells (SKOV-3) and osteosarcoma cells (MG-83) in the presence of HNT-PEG at a concentration ranging from ca. 0.3 to 1.5  $\text{mg}/\text{mL}$  for 6 to 72 h. Overall, pristine and modified HNTs can show some time and dosage-dependent toxicity [169,170].

There is some conflicting evidence concerning the cytotoxicity of MMT. Low concentrations of MMT inhibited cell proliferation of HepG2 cells by approximately 65%. Genotoxicity studies revealed that MMT was potentially genotoxic to HepG2 cells. In contrast, in Caco-2 cells, after a 24-hour exposure time, MMT did not induce any DNA damage.

The fibrous morphology of sepiolite and PAL has raised some concerns about their toxicity. Despite several experiments and

the International Agency for Research on Cancer (IARC) consistently having regarded sepiolite as safe and non-carcinogenic, its fibrous structure still raises questions regarding a potential asbestos-like effect [15,172]. The exposure of several human cancer cell lines, including U251, PC-3, human leukemia (K-562), colon cancer (HCT-15), MCF-7, and lung adenocarcinoma (SKLU-1) to sepiolite and PAL, resulted in the inhibition of cellular proliferation. Both sepiolite and PAL caused a similar cytotoxic effect in U251, whereas in PC-3 cells, different mortality rates were observed. When exposed to sepiolite, K-562, HCT-15, and MCF-7 cells showed significant growth inhibition, which did not occur in the presence of PAL. SKLU-1 cells showed cytotoxicity seven times higher when treated with PAL. Generally, all cell lines showed increased growth inhibition after exposure to both fibrous clays [173].

Studies in human osteosarcoma cells (U2OS) showed that these cells generated ROS and inflammatory cytokines after exposure to sepiolite. However, sepiolite exposure did not inhibit the cell cycle progression, cause any DNA damage, or induce apoptosis in U2OS cells and SV40-transformed human fibroblasts (GC92) [172]. These results suggested that sepiolite does not possess a significant risk for genome integrity. However, a long-period of exposure to sepiolite could indirectly affect the genome, for example, due to the production of ROS [172]. The cytotoxicity of allophane was investigated in A549 cells. The A549 cell viability remained >70% after exposure to allophane at concentrations below 3160.0  $\mu\text{g}/\text{mL}$ . These findings suggest that allophane is a biocompatible nanomaterial [48].

## 5.2. *In vivo* toxicological assays

The number of *in vivo* experimental toxicology studies using nanoclays in the scientific literature is rather low in comparison to the number of *in vitro* studies, and the results reported are variable, because different nanoclays, administration routes, and concentrations have been tested. Furthermore, the toxicity of nanoclays is also influenced by the type of used modifier [174,175].

HNTs were used in the production of ceramics for thousands of years, so, taking into account this continued manipulation by human hands, the topical contact with HNTs was considered safe. More importantly, halloysite as traditional Chinese medicine (mineral medicine) was used in human therapy for thousands of years in Asia countries, and it is recognized that halloysite has the functionality of promoting wound healing, hemostasis in skin and organ, treatment of dysentery, and so on. Therefore, oral uptake and skin contact of halloysite at certain dose was safe. *In vivo* experiments employing different laboratory organisms have proved the high overall biocompatibility of HNTs. *Caenorhabditis elegans* is a nematode worm that is naturally found in soil. *C. elegans* is optically transparent and dark-field microscopy allowed the visualization of HNT distribution in this *in vivo* model. *C. elegans* feeds on *E. coli*, so *E. coli* was coated with HNTs functionalized with PAH and PSS via the LbL method. The obtained HNT-coated bacterial food was used to deliver HNTs, at a concentration range of 0.05–0.1  $\text{mg}/\text{mL}$  into the intestines of *C. elegans*. These concentrations were shown to be safe and did not damage *C. elegans* organisms. However, concentrations between 0.5 and 1  $\text{mg}/\text{mL}$  irritated the intestinal cells of *C. elegans*, disturbing its feeding behavior and reducing its body length. However, the *C. elegans* life-span and reproduction rate remained unaltered [176].

Another *in vivo* experiment performed using *Paramecium caudatum*, a habitual freshwater protozoan, showed that HNTs were more biocompatible than other nanoclays, such as kaolinite, MMT, or BENT, and graphene oxide [18]. The *in vivo* toxicity of HNTs was also studied in the early development stage of zebrafish embryos. The survival rate of zebrafish embryos and larvae showed

no effects at different developmental stages when exposed to several concentrations of HNTs, ranging from 0.25 to 10.0 mg/mL. Furthermore, HNTs showed the ability to increase the hatching rate of zebrafish embryos and did not interfere with the morphological development of zebrafish at a concentration below 25.0 mg/mL. HNTs were also ingested by zebrafish larvae and accumulated mainly in the gastrointestinal tract (GI). The fluorescence intensity of FITC-modified HNTs was progressively reduced over time, suggesting that the HNTs could be excreted by the zebrafish larvae [157].

The single oral administration of HNTs (50 and 300 mg/kg body weight) every day during ca. 1 month induced liver toxicity and caused lung fibrosis in mice due to accumulation of insoluble  $Al^{3+}$  ions [177,178]. Furthermore, HNTs orally administered also in mice at concentrations >50 mg/kg body weight caused Al and Si accumulation, inducing oxidative stress in the mice stomach and small intestine; however, after a recovery period (ca. 1 month), the hepatic, lung, and gastrointestinal tissue damages were reversed [179,180]. These acute toxic effects did not occur when mice were treated with lower doses of HNTs (<5 mg/kg body weight). Besides, studies concerning the inhalation of HNTs were also performed in mice. Inhaled HNTs induced sub-chronic toxicity in rodents due to the accumulation of p62, that can be reversed after the oral administration of trehalose [181]. Moreover, in another work, the intratracheal instillation of HNTs in mice was used as an alternative to inhalation [182]. This administration of etched HNTs (with an increase surface area) caused pulmonary inflammation, but did not cause pulmonary or systemic genotoxicity. The heavy metals and corresponding ions released from clays have negative influence of the cell and tissue. However, for purified HNTs sample supplied by Applied Minerals Inc and the deposition in Yunnan Province of China, the content of heavy metals is below 0.01 wt% of Ti, Pb, Cd, Cr, and As. So, the tiny content of heavy metals ions of HNTs would show very negligible effect on the drug activities and *in vivo* toxicity. Overall, the information regarding the risks of occupational exposure to HNTs are limited, thus it is recommended to avoid their inhalation [183].

Regarding MMT, it can cause toxic effects in cellular models (e.g., oxidative stress). However, the oral administration of different doses of MMT in mice, ranging from 5.0 to 1000.0 mg/kg, did not induce significant toxicity, revealing that, sometimes, opposite toxicological effects may be witnessed in experiments performed *in vitro* and *in vivo* [160,184]. In Sprague-Dawley rats, the oral ingestion of MMT up to a dose of 5700.0 mg/kg body weight did not induce significant toxic effects, namely alterations in body weight or food consumption [159]. The dietary consumption of MMT by pregnant Sprague-Dawley rats was considered safe and did not cause metal accumulation [185]. In another study, oral administration of MMT modified with organic quaternary ammonium compounds (Cloisite® 30B, the commercial formulation used as an additive for plastics) in Wistar rats did not induce genotoxicity, and no systemic toxic effects were observed at a dose <1000 mg/kg body weight [186]. It was possible to conclude, using inductively coupled plasma mass-spectrometry, that the modified MMT did not accumulate in the liver and kidneys; instead, the modified MMT is excreted in the rats' feces. MMT was already used in animal feeds and prevented mycotoxin-induced toxicity in rats [187,188] and pigs [189]. In a short-term clinical trial, the oral administration of MMT as a supplement revealed promising results for the prevention of aflatoxicosis in children, and was considered safe at a dose up to 1.5 g/day for 2 weeks [175,190]. According to the hematological data in Lee *et al.* [191] study, the intravenous administration of MMT did not induce significant toxicity when compared to the control (PBS buffer). Nevertheless, the intravenous administration of MMT (14.29 mg/kg body weight) reduced the concentration of potassium ( $K^+$ ) and increased the alanine

transaminase enzymatic activity. Despite this, MMT was considered non-toxic; however its administration to rats with cardiovascular diseases is discouraged [191].

## 6. Conclusions and future trends

Nanoclays may have a wide range of applications in oncology. Thus, the production of cancer cell spheroids using nanoclays could lead to the reduction of the number of animals required in *in vivo* experiments, making preclinical drug development more effective and sustainable.

Concerning cancer diagnosis, nanoclays can be used to stabilize imaging contrast agents. Moreover, nanoclays can also be used in biosensors to detect cancer biomarkers and circulating tumor cells, suggesting a future role in cancer detection and monitoring.

The delivery of anticancer drugs and bioactive agents (e.g., natural compounds, biopharmaceutical, and phototherapeutic agents) is still challenging, and further advances are necessary to improve therapeutic performance. Given the physiological changes that occur during carcinogenesis, the tumor can be diverse, and its microenvironment can be unique. Examples of those characteristics are defects in the tumor vasculature, higher enzyme activity, low pH in the tumor microenvironment, elevated glutathione, and higher concentrations of ROS. These biological alterations can be used often to construct stimulus-responsive therapeutic approaches.

The dispersed aqueous clay properties: particle size, shape, adsorption ability, surface area, cation exchange capacity and charge, allow for a transportation of a wide range of anticancer drugs and bioactive agents to the tumor location. Nanoclays can provide controlled and sustained drug release profiles, which minimize premature release and maximize concentration of the anticancer cargo molecule in the tumor site. Nanoclays can transport proteins and genes, protecting these biomacromolecules against enzymatic degradation, and improving their therapeutic action. Moreover, clays can act as templates for photosensitizers and photothermal agents, making them less susceptible to bleaching and increasing their tumor-targeting ability. The charge of the anticancer guest molecule is not a determining factor, as both positive and negative molecules have been loaded efficiently into- or onto-nanoclays exploiting their dual charge nature. The versatile physicochemical features obtained when HNTs are combined with other structures, such as quantum dots, allow for the efficient co-delivery of two or more molecules with synergistic anticancer effects. The co-delivery of anticancer molecules ultimately enhances the therapeutic efficiency while reducing side effects.

The application of nanoclays requires understanding their physicochemical properties. The physicochemical properties of nanoclays (surface area, type of exchangeable cations, hydrophilicity / hydrophobicity, zeta potential, interlayer space, and porosity) can be tuned *via* functionalization, with target ligands, polymers, and amphiphile molecules. These modifications are useful to improve the anticancer activity of the guest molecules, provide a controlled release, designing stimuli-responsive nanocarriers, achievement of an improved targeting effect, and lowered the side effects of the drugs. These modifications may also enable the design of theranostic nanoplateforms that combine diagnostic and therapeutic functions.

The anticancer efficacy of nanoclays has been tested on conventional 2D cell cultures. This type of *in vitro* model exhibits some limitations when attempting to mimic the tumor microenvironment. To overcome the constraints associated with 2D cell cultures, experiments using 3D *in vitro* tumor models, which incorporate multiple cell types to better mimic the biological and biochemical diversity are required. Also, further *in vivo* studies

concerning the anticancer efficacy of nanoclays *per se* or as delivery carriers for bioactive molecules are necessary.

The safety of nanoclays needs to be further investigated. Pharmacokinetic (absorption–distribution–metabolism–excretion studies), pharmacodynamic and biopersistence investigations have to be performed for understanding of preclinical toxicological data and promoting translation to clinical trials.

Considering the available toxicological outputs, despite being generally hemocompatible, the parenteral administration of nanoclays possesses a risk of toxicity due to the possibility of thrombosis occurrence, and the potential for Al- and Si-ions accumulation. However, we cannot disqualify the use of nanoclays for intramuscular injections and short-term treatments *via* blood injection. The oral and topical administration routes are the most prospective for nanoclay pharmaceutical formulations. Clays are already used as compression excipients in tablets, cosmetics and as additives in oral veterinary formulations [175,189]. We envisage a wider use of nanoclays for oral delivery in the form of tablets. We also think that the topical administration of nanoclays on skin has a potential to be translated to clinical research due to their ethnopharmacological use in pelotherapy (application of medicinal thermal muds compromising geomaterials and thermo-mineral medicinal water through the skin) [28] and the use of certain types of nanoclays as functional excipients in cosmetic formulations [25,35]. The transdermal administration (which implicates systemic absorption), or even the intratumoral administration of drug-clay formulations may be applied in the treatment of solid cancers (*e.g.*, skin cancers). Besides, the topical cream and spray applications *via* the skin or as rectal or vaginal suppository (without systemic absorption) may be considered for the treatment of different disorders. Montmorillonite is already an ingredient in skin products commercialized by famous brands, so we can predict new healthcare formulations containing nanoclays. Here, we discussed the role of nanoclays in cancer research, diagnosis, and therapy, and their promising applications, due to biocompatibility, enhanced intracellular penetration, drug loading capacity, and tunable physicochemical properties including selection of the carrier shapes of sizes in a submicron level.

### Declaration of Competing Interest

The authors declare that they have no known competing financial interests or personal relationships that could have appeared to influence the work reported in this paper.

### Acknowledgments

Irina Pereira and Miguel Pereira-Silva acknowledge the Ph.D. research grants SFRH/BD/136892/2018 and SFRH/BD/148771/2019, respectively, funded by *Fundação para a Ciência e a Tecnologia I.P. (FCT)* and *Programa Operacional Capital Humano (POCH)*. Professor Mingxian Liu acknowledges the National Natural Science Foundation of China (52073121) and the National Natural Science Foundation of Guangdong Province (2019A1515011509).

### Conflict of interest

None.

### References

- [1] T. Date, V. Nimbalkar, J. Kamat, A. Mittal, R.I. Mahato, D. Chitkara, J. Control. Release 271 (2018) 60–73, <https://doi.org/10.1016/j.jconrel.2017.12.016>.
- [2] F. Bray, J. Ferlay, I. Soerjomataram, R.L. Siegel, L.A. Torre, A. Jemal, CA Cancer J. Clin. 68 (2018) 394–424, <https://doi.org/10.3322/caac.21492>.
- [3] W. Grimes, Y. Luo, A. McFarland, D. Mills, Appl Sci 8 (2018) 281, <https://doi.org/10.3390/app8020281>.
- [4] M.J. Mitchell, C.S. Chen, V. Ponmudi, A.D. Hughes, M.R. King, J. Control. Release 160 (2012) 609–617, <https://doi.org/10.1016/j.jconrel.2012.02.018>.
- [5] M.J. Mitchell, C.A. Castellanos, M.R. King, Biomaterials 56 (2015) 179–186, <https://doi.org/10.1016/j.biomaterials.2015.03.045>.
- [6] E. Pérez-Herrero, A. Fernández-Medarde, Eur. J. Pharm. Biopharm. 93 (2015) 52–79, <https://doi.org/10.1016/j.ejpb.2015.03.018>.
- [7] K. Li, Y. Zhang, M. Chen, Y. Hu, W. Jiang, L. Zhou, S. Li, M. Xu, Q. Zhao, R. Wan, Int. J. Nanomed. 13 (2018) 19–30, <https://doi.org/10.2147/IJN.S143928>.
- [8] Y.-P. Wu, J. Yang, H.-Y. Gao, Y. Shen, L. Jiang, C. Zhou, Y.-F. Li, R.-R. He, M. Liu, ACS Appl. Nano Mater. 1 (2018) 595–608, <https://doi.org/10.1021/acsnan.7b00087>.
- [9] N. Barkalina, C. Charalambous, C. Jones, K. Coward, Nanomedicine 10 (2014) e921–e938, <https://doi.org/10.1016/j.nano.2014.01.001>.
- [10] A. Wicki, D. Witzigmann, V. Balasubramanian, J. Huwyler, J. Control. Release 200 (2015) 138–157, <https://doi.org/10.1016/j.jconrel.2014.12.030>.
- [11] W. Song, A.C. Anselmo, L. Huang, Nat. Nanotechnol. 14 (2019) 1093–1103, <https://doi.org/10.1038/s41565-019-0589-5>.
- [12] L. Bregoli, D. Movia, J.D. Gavigan-Imedio, J. Lysaght, J. Reynolds, A. Prina-Mello, Nanomedicine 12 (2016) 81–103, <https://doi.org/10.1016/j.nano.2015.08.006>.
- [13] Z. Zhao, A. Ukidve, V. Krishnan, S. Mitragotri, Adv. Drug Deliv. Rev. 143 (2019) 3–21, <https://doi.org/10.1016/j.addr.2019.01.002>.
- [14] Y. Hwang, S.-H. Park, J.W. Lee, Polymers 9 (2017) 13, <https://doi.org/10.3390/polym9010013>.
- [15] O. Pietrement, F.A. Castro-Smirnov, E. Le Cam, P. Aranda, E. Ruiz-Hitzky, B.S. Lopez, Chem. Rec. 18 (2018) 849–857, <https://doi.org/10.1002/tcr.201700078>.
- [16] M.C. Floody, B. Theng, P. Reyes, M. Mora, Clay Miner. 44 (2009) 161–176, <https://doi.org/10.1180/claymin.2009.044.2.161>.
- [17] G. Lazzara, S. Riel, R.F. Fakhruddin, Ther. Deliv 8 (2017) 633–646, <https://doi.org/10.4155/tde-2017-0041>.
- [18] M. Kryuchkova, A. Danilushkina, Y. Lvov, R. Fakhruddin, Environ. Sci. Nano 3 (2016) 442–452, <https://doi.org/10.1039/C5EN00201J>.
- [19] B. Yilmaz, E.T. Irmak, Y. Turhan, S. Doğan, M. Doğan, O. Turhan, Adv. Mater. Sci. 19 (2019) 83–99, <https://doi.org/10.2478/adms-2019-0007>.
- [20] D. Zhang, C.-H. Zhou, C.-X. Lin, D.-S. Tong, W.-H. Yu, Appl. Clay Sci. 50 (2010) 1–11, <https://doi.org/10.1016/j.clay.2010.06.019>.
- [21] C. Viseras, E. Carazo, A. Borrego-Sánchez, F. García-Villén, R. Sánchez-Espejo, P. Cerezo, C. Aguzzi, Clays Clay Miner. 67 (2019) 59–71, <https://doi.org/10.1007/s42860-018-0003-7>.
- [22] E.E. Gaskell, A.R. Hamilton, Future Med. Chem. 6 (2014) 641–655, <https://doi.org/10.4155/fmc.14.17>.
- [23] M.H. Mousa, Y. Dong, I.J. Davies, Int. J. Polym. Mater. Polym. Biomater. 65 (2016) 225–254, <https://doi.org/10.1080/00914037.2015.1103240>.
- [24] G. Lazzara, G. Cavallaro, A. Panchal, R. Fakhruddin, A. Stavitskaya, V. Vinokurov, Y. Lvov, Curr. Opin. Colloid Interface Sci. 35 (2018) 42–50, <https://doi.org/10.1016/j.cocis.2018.01.002>.
- [25] J.D.D. Moraes, S.R.A. Bertolino, S.L. Cuffini, D.F. Ducart, P.E. Bretzke, G.R. Leonardi, Int. J. Pharm. 534 (2017) 213–219, <https://doi.org/10.1016/j.ijpharm.2017.10.031>.
- [26] M. Mousa, N.D. Evans, R.O. Oreffo, J.I. Dawson, Biomaterials 159 (2018) 204–214, <https://doi.org/10.1016/j.biomaterials.2017.12.024>.
- [27] M. Kotal, A.K. Bhowmick, Prog. Polym. Sci. 51 (2015) 127–187, <https://doi.org/10.1016/j.progpolymsci.2015.05.001>.
- [28] M.E. Awad, A. Lopez-Galindo, M. Setti, M.M. El-Rahmany, C.V. Iborra, Int. J. Pharm. 533 (2017) 34–48, <https://doi.org/10.1016/j.ijpharm.2017.09.056>.
- [29] Y. Zhang, M. Long, P. Huang, H. Yang, S. Chang, Y. Hu, A. Tang, L. Mao, Nano Res. 10 (2017) 2633–2643, <https://doi.org/10.1007/s12274-017-1466-x>.
- [30] R. Yendluri, Y. Lvov, M.M. de Villiers, V. Vinokurov, E. Naumenko, E. Tarasova, R. Fakhruddin, J. Pharm. Sci. 106 (2017) 3131–3139, <https://doi.org/10.1016/j.xphs.2017.05.034>.
- [31] Y. Lvov, E. Abdullayev, Prog. Polym. Sci. 38 (2013) 1690–1719, <https://doi.org/10.1016/j.progpolymsci.2013.05.009>.
- [32] A. Stavitskaya, S. Batasheva, V. Vinokurov, G. Fakhruddin, V. Sangarov, Y. Lvov, R. Fakhruddin, Nanomaterials 9 (2019), <https://doi.org/10.3390/nano9050708>.
- [33] M. Hanif, F. Jabbar, S. Sharif, G. Abbas, A. Farooq, M. Aziz, Clay Miner. 51 (2016) 469–477, <https://doi.org/10.1180/claymin.2016.051.3.03>.
- [34] K.A. Zahidah, S. Kakooei, M.C. Ismail, P.B. Raja, Prog. Org. Coat. 111 (2017) 175–185, <https://doi.org/10.1016/j.porgcoat.2017.05.018>.
- [35] R. Yendluri, D.P. Otto, M.M. De Villiers, V. Vinokurov, Y.M. Lvov, Int. J. Pharm. 521 (2017) 267–273, <https://doi.org/10.1016/j.ijpharm.2017.02.055>.
- [36] W. Ma, H. Wu, Y. Higaki, A. Takahara, Chem. Rec. 18 (2018) 986–999, <https://doi.org/10.1002/tcr.201700093>.
- [37] L. Bailey, H.N. Lekkerkerker, G.C. Maitland, Soft Matter 11 (2015) 222–236, <https://doi.org/10.1039/c4sm01717j>.
- [38] H. Pálková, J. Madejová, M. Zimowska, E. Bielańska, Z. Olejniczak, L. Lityńska-Dobrzyńska, E.M. Serwicka, Microporous Mesoporous Mater. 127 (2010) 228–236, <https://doi.org/10.1016/j.micromeso.2009.07.019>.
- [39] F.B. Zeynabad, R. Salehi, M. Mahkam, Appl. Clay Sci. 141 (2017) 23–35, <https://doi.org/10.1016/j.clay.2017.02.015>.
- [40] B.P. Nair, C.P. Sharma, Langmuir 28 (2012) 4559–4564, <https://doi.org/10.1021/la300005c>.
- [41] R. Mustafa, Y. Luo, Y. Wu, R. Guo, X. Shi, Nanomaterials 5 (2015) 1716–1731, <https://doi.org/10.3390/nano5041716>.
- [42] H. Kohay, C. Sarisozen, R. Sawant, A. Jhaveri, V.P. Torchilin, Y.G. Mishaev, Acta Biomater. 55 (2017) 443–454, <https://doi.org/10.1016/j.actbio.2017.04.008>.

- [43] B. Sun, B. Ranganathan, S.S. Feng, *Biomaterials* 29 (2008) 475–486, <https://doi.org/10.1016/j.biomaterials.2007.09.038>.
- [44] S. Kar, B. Kundu, R.L. Reis, R. Sarkar, P. Nandy, R. Basu, S. Das, *Eur. J. Pharm. Sci.* 135 (2019) 91–102, <https://doi.org/10.1016/j.ejps.2019.05.006>.
- [45] Z. Li, K. Liu, P. Sun, L. Mei, T. Hao, Y. Tian, Z. Tang, L. Li, D. Chen, *J. Microencapsul.* 30 (2013) 432–440, <https://doi.org/10.3109/02652048.2012.746749>.
- [46] F. Hosseini, F. Hosseini, S.M. Jafari, A. Taheri, *Clay Miner.* 53 (2018) 53–63, <https://doi.org/10.1180/clm.2018.4>.
- [47] J. Nones, H.G. Riella, A.G. Trentin, J. Nones, *Appl. Clay Sci.* 105–106 (2015) 225–230, <https://doi.org/10.1016/j.clay.2014.12.036>.
- [48] Y. Toyota, Y. Matsuura, M. Ito, R. Domura, M. Okamoto, S. Arakawa, M. Hirano, K. Kohda, *Appl. Clay Sci.* 135 (2017) 485–492, <https://doi.org/10.1016/j.clay.2016.10.037>.
- [49] K.S. Katti, M.S. Molla, F. Karandish, M.K. Haldar, S. Mallik, D.R. Katti, *J. Biomed. Mater. Res. A* 104 (2016) 1591–1602, <https://doi.org/10.1002/jbma.a.35685>.
- [50] S. Kar, M.S. Molla, D.R. Katti, K.S. Katti, *J. Tissue Eng. Regen. Med.* 13 (2019) 119–130, <https://doi.org/10.1002/term.2773>.
- [51] M.A. Theodoraki, C.O. Rezende Jr, O. Chantarasriwong, A.D. Corben, E.A. Theodorakis, *M.L. Alpaugh, Oncotarget* 6 (2015) 21255, <https://doi.org/10.18632/oncotarget.4013>.
- [52] E. Rozhina, S. Batasheva, M. Gomzikova, E. Naumenko, R. Fakhruullin, *Colloids Surf. A* 565 (2019) 16–24, <https://doi.org/10.1016/j.colsurfa.2018.12.038>.
- [53] T. Zhou, L. Jia, Y.F. Luo, J. Xu, R.H. Chen, Z.J. Ge, T.L. Ma, H. Chen, T.F. Zhu, *Int. J. Nanomed.* 11 (2016) 4765–4776, <https://doi.org/10.2147/IJN.S110081>.
- [54] T. Zhu, X. Ma, R. Chen, Z. Ge, J. Xu, X. Shen, L. Jia, T. Zhou, Y. Luo, T. Ma, *Biomater. Sci.* 5 (2017) 1090–1100, <https://doi.org/10.1039/C7BM00031F>.
- [55] V. Vergaro, E. Abdullayev, Y.M. Lvov, A. Zeitoun, R. Cingolani, R. Rinaldi, S. Leporatti, *Biomacromolecules* 11 (2010) 820–826, <https://doi.org/10.1021/bm9014446>.
- [56] Y. Liu, C. Jiao, W. Lu, P. Zhang, Y. Wang, *RSC Adv.* 9 (2019) 18027–18041, <https://doi.org/10.1039/C9RA02467K>.
- [57] J. Dong, Z. Zhao, R. Liu, H. Zhang, Y. Wu, X. Ba, *RSC Adv.* 7 (2017) 55067–55073, <https://doi.org/10.1039/c7ra10210k>.
- [58] A.V. Stavitskaya, A.A. Novikov, M.S. Kotelev, D.S. Kopitsyn, E.V. Rozhina, I.R. Ishmukhametov, R.F. Fakhruullin, E.V. Ivanov, Y.M. Lvov, V.A. Vinokurov, *Nanomaterials* 8 (2018), <https://doi.org/10.3390/nano8060391>.
- [59] F.A. Castro-Smirnov, J. Ayache, J.-R. Bertrand, E. Dardillac, E. Le Cam, O. Piétrement, P. Aranda, E. Ruiz-Hitzky, B.S. Lopez, *Sci. Rep.* 7 (2017) 1–10, <https://doi.org/10.1038/s41598-017-05839-3>.
- [60] A. Erdem, F. Kuralay, H.E. Cubukcu, G. Congur, H. Karadeniz, E. Canavar, *Analyst* 137 (2012) 4001–4004, <https://doi.org/10.1039/c2an35181a>.
- [61] M. Hasanzadeh, N. Shadjou, *Mater. Sci. Eng. C Mater. Biol. Appl.* 61 (2016) 1002–1017, <https://doi.org/10.1016/j.msec.2015.12.020>.
- [62] Y. Li, M.S. Khan, L. Tian, L. Liu, L. Hu, D. Fan, W. Cao, Q. Wei, *Anal. Bioanal. Chem.* 409 (2017) 3245–3251, <https://doi.org/10.1007/s00216-017-0266-1>.
- [63] Y.T. Yaman, O. Akbal, S. Abaci, *Biosens. Bioelectron.* 132 (2019) 230–237, <https://doi.org/10.1016/j.bios.2019.02.058>.
- [64] M. Ikeda, T. Yoshii, T. Matsui, T. Taniida, H. Komatsu, I. Hamachi, *J. Am. Chem. Soc.* 133 (2011) 1670–1673, <https://doi.org/10.1021/ja109692z>.
- [65] A.D. Hughes, J. Mattison, J.D. Powderly, B.T. Greene, M.R. King, *J. Vis. Exp.* (2012), <https://doi.org/10.3791/4248> e4248.
- [66] A.D. Hughes, M.R. King, *Langmuir* 26 (2010) 12155–12164, <https://doi.org/10.1021/la101179y>.
- [67] M.J. Mitchell, C.A. Castellanos, M.R. King, *J. Biomed. Mater. Res. A* 103 (2015) 3407–3418, <https://doi.org/10.1002/jbma.a.35445>.
- [68] A.D. Hughes, J. Mattison, L.T. Western, J.D. Powderly, B.T. Greene, M.R. King, *Clin. Chem.* 58 (2012) 846–853, <https://doi.org/10.1373/clinchem.2011.176669>.
- [69] R. He, M. Liu, Y. Shen, Z. Long, C. Zhou, *J. Mater. Chem. B* 5 (2017) 1712–1723, <https://doi.org/10.1039/C6TB02538B>.
- [70] R. He, M. Liu, Y. Shen, R. Liang, W. Liu, C. Zhou, *Mater. Sci. Eng. C Mater. Biol. Appl.* 85 (2018) 170–181, <https://doi.org/10.1016/j.msec.2017.12.030>.
- [71] X. Li, J. Chen, H. Liu, Z. Deng, J. Li, T. Ren, L. Huang, W. Chen, Y. Yang, S. Zhong, *Colloids Surf. B Biointerfaces* 181 (2019) 379–388, <https://doi.org/10.1016/j.colsurfb.2019.05.068>.
- [72] D. Hanahan, R.A. Weinberg, *Cell* 144 (2011) 646–674, <https://doi.org/10.1016/j.cell.2011.02.013>.
- [73] D.F. Quail, J.A. Joyce, *Nat. Med.* 19 (2013) 1423–1437, <https://doi.org/10.1038/nm.3394>.
- [74] H. Wu, Y. Shi, C. Huang, Y. Zhang, J. Wu, H. Shen, N. Jia, *J. Biomater. Appl.* 28 (2014) 1180–1189, <https://doi.org/10.1177/0885328213501215>.
- [75] J. Cervini-Silva, M.T. Ramírez-Apan, S. Kaufhold, K. Ufer, E. Palacios, A. Montoya, *Chemosphere* 149 (2016) 57–61, <https://doi.org/10.1016/j.chemosphere.2016.01.077>.
- [76] S. Misyak, A. Burlaka, V. Golotiuk, S. Lukin, P. Kornienko, *Galician Med. J.* 23 (2016) 44–47.
- [77] S.N. Abdulljawad, H.-u.-R. Ahmed, *Sci. Rep.* 9 (2019) 5935, <https://doi.org/10.1038/s41598-019-42498-y>.
- [78] S.N. Abdulljawad, H.-u.-R. Ahmed, V.T. Moy, *Sci. Rep.* 11 (2021) 2737, <https://doi.org/10.1038/s41598-021-82441-8>.
- [79] F. García-Villén, E. Carazo, A. Borrego-Sánchez, R. Sánchez-Espejo, P. Cerezo, C. Viseras, C. Aguzzi, *Clay minerals in drug delivery systems*, in: M. Mercurio, B. Sarkar, A. Langella (Eds.), *Modified clay and zeolite nanocomposite materials: environmental and pharmaceutical applications*, 2019, pp. 129–166, <https://doi.org/10.1016/B978-0-12-814617-0.00010-4>.
- [80] L.H. Araujo, L. Horn, R.E. Merritt, K. Shilo, M. Xu-Welliver, D.P. Carbone, *Cancer of the lung: non-small cell lung cancer and small cell lung cancer*, in: J.E. Niederhuber, J.O. Armitage, M.B. Kastan, J.H. Doroshow, J.E. Tepper (Eds.), *Abeloff's Clinical Oncology*, Elsevier, 2020, pp. 1108–1158, e1116, <https://doi.org/10.1016/B978-0-323-47674-4.00069-4>.
- [81] H. Liu, Z.-G. Wang, S.-L. Liu, X. Yao, Y. Chen, S. Shen, Y. Wu, W. Tian, *J. Mater. Sci.* 54 (2019) 693–704, <https://doi.org/10.1007/s10853-018-2775-5>.
- [82] Y. Lee, G.E. Jung, S.J. Cho, K.E. Geckeler, H. Fuchs, *Nanoscale* 5 (2013) 8577–8585, <https://doi.org/10.1039/c3nr02665e>.
- [83] M.R. Dzumakova, E.A. Naumenko, Y.M. Lvov, R.F. Fakhruullin, *Sci. Rep.* 5 (2015) 10560, <https://doi.org/10.1038/srep10560>.
- [84] Y. Toyota, M. Okamoto, S. Arakawa, *Appl. Clay Sci.* 143 (2017) 422–429, <https://doi.org/10.1016/j.clay.2017.04.017>.
- [85] K. Tamas, A. Walenkamp, E. De Vries, M. Van Vugt, R. Beets-Tan, B. Van Etten, D. de Groot, G. Hospers, *Cancer Treat. Rev.* 41 (2015) 671–679, <https://doi.org/10.1016/j.ctrv.2015.06.007>.
- [86] W. Li, D. Liu, H. Zhang, A. Correia, E. Makila, J. Salonen, J. Hirvonen, H.A. Santos, *Acta Biomater.* 48 (2017) 238–246, <https://doi.org/10.1016/j.actbio.2016.10.042>.
- [87] F.-H. Lin, Y.-H. Lee, C.-H. Jian, J.-M. Wong, M.-J. Shieh, C.-Y. Wang, *Biomaterials* 23 (2002) 1981–1987, [https://doi.org/10.1016/S0142-9612\(01\)00325-8](https://doi.org/10.1016/S0142-9612(01)00325-8).
- [88] C. Rizzo, R. Arrigo, F. D'Anna, F. Di Blasi, N. Dintcheva, G. Lazzara, F. Parisi, S. Riel, G. Spinelli, M. Massaro, *J. Mater. Chem. B* 5 (2017) 3217–3229, <https://doi.org/10.1039/C7TB00297A>.
- [89] L.N. Borgheti-Cardoso, J.S.R. Viegas, A.V.P. Silvestrini, A.L. Caron, F.G. Praça, M. Kravicz, M.V.L.B. Bentley, *Adv Drug Deliver Rev* (2020), <https://doi.org/10.1016/j.addr.2020.02.005>.
- [90] K.M. Rao, S. Nagappan, D.J. Seo, C.-S. Ha, *Appl. Clay Sci.* 97–98 (2014) 33–42, <https://doi.org/10.1016/j.clay.2014.06.002>.
- [91] M. Yu, L. Pan, L. Sun, J. Li, J. Shang, S. Zhang, D. Liu, W. Li, *J. Mater. Chem. B* 3 (2015) 9043–9052, <https://doi.org/10.1039/C5TB01513H>.
- [92] P. Dramou, M. Fizir, A. Taleb, A. Itatahine, N.S. Dahiru, Y.A. Mehdi, L. Wei, J. Zhang, H. He, *Carbohydr. Polym.* 197 (2018) 117–127, <https://doi.org/10.1016/j.carbpol.2018.05.071>.
- [93] E. Gianni, K. Avgoustakis, M. Pšenička, M. Pospíšil, D. Papoulis, *J. Drug Deliv. Sci. Technol.* 52 (2019) 568–576, <https://doi.org/10.1016/j.jddst.2019.05.001>.
- [94] Y. Dong, S.-S. Feng, *Biomaterials* 26 (2005) 6068–6076, <https://doi.org/10.1016/j.biomaterials.2005.03.021>.
- [95] C. Bothiraja, U.H. Thorat, A.P. Pawar, K.S. Shaikh, *Mater. Technol.* 29 (2014) B120–B126, <https://doi.org/10.1179/1753555714y.0000000174>.
- [96] S. Maisanaba, K. Hercog, M. Filipic, A. Jos, B. Zegura, *J. Hazard. Mater.* 304 (2016) 425–433, <https://doi.org/10.1016/j.jhazmat.2015.10.018>.
- [97] B.D. Kevadiya, R.P. Thumbar, M.M. Rajput, S. Rajkumar, H. Brambhatt, G.V. Joshi, G.P. Dang, H.M. Mody, P.K. Gadhia, H.C. Bajaj, *Eur. J. Pharm. Sci.* 47 (2012) 265–272, <https://doi.org/10.1016/j.ejps.2012.04.009>.
- [98] R. Kouser, A. Vashist, M. Zafaryab, M.A. Rizvi, S. Ahmad, *ACS Omega* 3 (2018) 15809–15820, <https://doi.org/10.1021/acsomega.8b01691>.
- [99] S.S. Feng, L. Mei, P. Anitha, C.W. Gan, W. Zhou, *Biomaterials* 30 (2009) 3297–3306, <https://doi.org/10.1016/j.biomaterials.2009.02.045>.
- [100] J. Yang, Y. Wu, Y. Shen, C. Zhou, Y.F. Li, R.R. He, M. Liu, *ACS Appl. Mater. Interfaces* 8 (2016) 26578–26590, <https://doi.org/10.1021/acsmi.6b09074>.
- [101] K. McCarthy, W. Zhang, J. Soliz, D. Lovinaria, *Pancreatic surgery in cancer patients: post-surgical care*, in: J.L. Nates, K.J. Price (Eds.), *Oncologic critical care*, 2020, pp. 1809–1823, [https://doi.org/10.1007/978-3-319-74588-6\\_180](https://doi.org/10.1007/978-3-319-74588-6_180).
- [102] V.H.G. Phan, E. Lee, J.H. Maeng, T. Thambi, B.S. Kim, D. Lee, D.S. Lee, *RSC Adv.* 6 (2016) 41644–41655, <https://doi.org/10.1039/c6ra07934b>.
- [103] P.C. Thomas, B.H. Cipriano, S.R. Raghavan, *Soft Matter* 7 (2011) 8192–8197, <https://doi.org/10.1039/C1SM05369H>.
- [104] M.N. Hart, C.K. Petito, K.M. Earle, *Cancer* 33 (1974) 134–140, [https://doi.org/10.1002/1097-0142\(197401\)33:1<134::aid-cnrc282030120>3.0.co;2-i](https://doi.org/10.1002/1097-0142(197401)33:1<134::aid-cnrc282030120>3.0.co;2-i).
- [105] N. Gagliano, G. Aldini, G. Colombo, R. Rossi, R. Colombo, M. Gioia, A. Milzani, I. Dalle-Donne, *Anticancer Drugs* 21 (2010) 140–150, <https://doi.org/10.1097/CAD.0b013e32833498f1>.
- [106] B.D. Kevadiya, S.S. Chettiar, S. Rajkumar, H.C. Bajaj, K.A. Gosai, H. Brambhatt, *Colloids Surf. B Biointerfaces* 112 (2013) 400–407, <https://doi.org/10.1016/j.colsurfb.2013.07.008>.
- [107] S. Wang, Y. Wu, R. Guo, Y. Huang, S. Wen, M. Shen, J. Wang, X. Shi, *Langmuir* 29 (2013) 5030–5036, <https://doi.org/10.1021/la4001363>.
- [108] Q.T. Nguyen, E.J. Lee, M.G. Huang, Y.I. Park, A. Khullar, R.A. Plodkowski, *Am. Health Drug Benefits* 8 (2015) 30.
- [109] Y. Zhang, M. Long, P. Huang, H. Yang, S. Chang, Y. Hu, A. Tang, L. Mao, *Sci. Rep.* 6 (2016) 33335, <https://doi.org/10.1038/srep33335>.
- [110] L. Sun, D.K. Mills, in: *36th Annual International Conference of the IEEE Engineering in Medicine and Biology Society, IEEE*, 2014, pp. 2920–2923, <https://doi.org/10.1109/EMBC.2014.6944234>.
- [111] L. Sun, C. Boyer, R. Grimes, D. Mills, *Curr. Nanosci.* 12 (2016) 207–214, <https://doi.org/10.2174/1573413711666151008014051>.
- [112] N. Kerdakundee, W. Li, J.P. Martins, Z. Liu, F. Zhang, M. Kemell, A. Correia, Y. Ding, M. Airavaara, J. Hirvonen, R. Wiwattanapatapee, H.A. Santos, *Adv. Healthc. Mater.* 6 (2017), <https://doi.org/10.1002/adhm.201700629>.
- [113] N. Madusanka, K.N. de Silva, G. Amarunganga, *Carbohydr. Polym.* 134 (2015) 695–699, <https://doi.org/10.1016/j.carbpol.2015.08.030>.
- [114] B. Khatun, N. Banik, A. Hussain, A. Ramteke, T. Maji, *J. Microencapsul.* 35 (2018) 439–453, <https://doi.org/10.1080/02652048.2018.1524524>.
- [115] M. Massaro, S. Riel, P.L. Meo, R. Noto, G. Cavallaro, S. Milioto, G. Lazzara, *J. Mater. Chem. B* 2 (2014) 7732–7738, <https://doi.org/10.1039/C4TB01272K>.

- [116] M. Massaro, R. Amorati, G. Cavallaro, S. Guernelli, G. Lazzara, S. Milioto, R. Noto, P. Poma, S. Riela, *Colloids Surf. B Biointerfaces* 140 (2016) 505–513, <https://doi.org/10.1016/j.colsurfb.2016.01.025>.
- [117] M. Liu, Y. Chang, J. Yang, Y. You, R. He, T. Chen, C. Zhou, *J. Mater. Chem. B* 4 (2016) 2253–2263, <https://doi.org/10.1039/C5TB02725J>.
- [118] C. Dionisi, N. Hanafy, C. Nobile, M.L. De Giorgi, R. Rinaldi, S. Casciaro, Y.M. Lvov, S. Leporatti, *IEEE Trans. Nanotechnol.* 15 (2016) 720–724, <https://doi.org/10.1109/TNANO.2016.2524072>.
- [119] B. Huang, M. Liu, C. Zhou, *Cellulose* 24 (2017) 2861–2875, <https://doi.org/10.1007/s10570-017-1316-8>.
- [120] K.M. Rao, A. Kumar, M. Suneetha, S.S. Han, *Int. J. Biol. Macromol.* 112 (2018) 119–125, <https://doi.org/10.1016/j.ijbiomac.2018.01.163>.
- [121] M. Guo, A. Wang, F. Muhammad, W. Qi, H. Ren, Y. Guo, G. Zhu, *Chin. J. Chem.* 30 (2012) 2115–2120, <https://doi.org/10.1002/cjoc.201200657>.
- [122] V. Vergaro, Y.M. Lvov, S. Leporatti, *Macromol. Biosci.* 12 (2012) 1265–1271, <https://doi.org/10.1002/mabi.201200121>.
- [123] O. Akbal, T. Vural, S. Malekghasemi, B. Bozdoğan, E.B. Denkbaş, *Appl. Clay Sci.* 166 (2018) 214–222, <https://doi.org/10.1016/j.clay.2018.09.021>.
- [124] I. Guryanov, E. Naumenko, F. Akhatova, G. Lazzara, G. Cavallaro, L. Nigamatyanova, R. Fakhruullin, *Front. Bioeng. Biotechnol.* 8 (2020) 424, <https://doi.org/10.3389/fbioe.2020.00424>.
- [125] J. Tully, R. Yendluri, Y. Lvov, *Biomacromolecules* 17 (2016) 615–621, <https://doi.org/10.1021/acs.biomac.5b01542>.
- [126] V. Khodzhaeva, A. Makeeva, V. Ulyanova, P. Zelenikhin, V. Evtugyn, M. Hardt, E. Rozhina, Y. Lvov, R. Fakhruullin, O. Ilinskaya, *Front. Pharmacol.* 8 (2017) 631, <https://doi.org/10.3389/fphar.2017.00631>.
- [127] M. Kim, S.C. Jee, J.-S. Sung, A.A. Kadam, *Int. J. Biol. Macromol.* 118 (2018) 228–237, <https://doi.org/10.1016/j.ijbiomac.2018.06.074>.
- [128] A. Azmi, *Conquering RAS: From Biology to Cancer Therapy*, Academic Press, 2016.
- [129] Z. Long, J. Zhang, Y. Shen, C. Zhou, M. Liu, *Mater. Sci. Eng. C Mater. Biol. Appl.* 81 (2017) 224–235, <https://doi.org/10.1016/j.msec.2017.07.035>.
- [130] S.L. Ginn, A.K. Amaya, I.E. Alexander, M. Edelstein, M.R. Abedi, *J. Gene Med.* 20 (2018), <https://doi.org/10.1002/jgm.3015> e3015.
- [131] F. Wang, Z. Qin, H. Lu, S. He, J. Luo, C. Jin, X. Song, *J. Gene Med.* 21 (2019), <https://doi.org/10.1002/jgm.3108> e3108.
- [132] Z. Long, Y.P. Wu, H.Y. Gao, Y.F. Li, R.R. He, M. Liu, *Bioconjug. Chem.* 29 (2018) 2606–2618, <https://doi.org/10.1021/acs.bioconjchem.8b00321>.
- [133] M. Massaro, G. Barone, G. Biddeci, G. Cavallaro, F. Di Blasi, G. Lazzara, G. Nicotra, C. Spinella, G. Spinelli, S. Riela, *J. Colloid Interface Sci.* 552 (2019) 236–246, <https://doi.org/10.1016/j.jcis.2019.05.062>.
- [134] Y.-F. Shi, Z. Tian, Y. Zhang, H.-B. Shen, N.-Q. Jia, *Nanoscale Res. Lett.* 6 (2011) 608, <https://doi.org/10.1186/1556-276X-6-608>.
- [135] J. Liu, Y. Zhang, Q. Zeng, H. Zeng, X. Liu, P. Wu, H. Xie, L. He, Z. Long, X. Lu, *Sci. Adv.* 5 (2019) eaaw6499, <https://doi.org/10.1126/sciadv.aaw6499>.
- [136] F.-H. Lin, C.-H. Chen, W.T. Cheng, T.-F. Kuo, *Biomaterials* 27 (2006) 3333–3338, <https://doi.org/10.1016/j.biomaterials.2005.12.029>.
- [137] T.A. Sironmani, *Appl. Clay Sci.* 103 (2015) 55–61, <https://doi.org/10.1016/j.clay.2014.11.004>.
- [138] M.T. Huggett, M. Jermyn, A. Gillams, R. Illing, S. Mosse, M. Novelli, E. Kent, S. Bown, T. Hasan, B. Pogue, *Br. J. Cancer* 110 (2014) 1698–1704, <https://doi.org/10.1038/bjc.2014.95>.
- [139] S.S. Lucky, K.C. Soo, Y. Zhang, *Chem. Rev.* 115 (2015) 1990–2042, <https://doi.org/10.1021/cr5004198>.
- [140] L. Cheng, C. Wang, L. Feng, K. Yang, Z. Liu, *Chem. Rev.* 114 (2014) 10869–10939, <https://doi.org/10.1021/cr400532z>.
- [141] L.Y. Li, Y.M. Zhou, R.Y. Gao, X.C. Liu, H.H. Du, J.L. Zhang, X.C. Ai, J.P. Zhang, L.M. Fu, L.H. Skibsted, *Biomaterials* 190–191 (2019) 86–96, <https://doi.org/10.1016/j.biomaterials.2018.10.046>.
- [142] T.S. Anirudhan, S. Sandeep, *J. Mater. Chem.* 22 (2012) 12888, <https://doi.org/10.1039/c2jm31794j>.
- [143] A.Y. Rwei, W. Wang, D.S. Kohane, *Nano Today* 10 (2015) 451–467, <https://doi.org/10.1016/j.nantod.2015.06.004>.
- [144] D. Jaque, L.M. Maestro, B. Del Rosal, P. Haro-Gonzalez, A. Benayas, J. Plaza, E. M. Rodriguez, J.G. Sole, *Nanoscale* 6 (2014) 9494–9530, <https://doi.org/10.1039/C4NR00708E>.
- [145] X. Song, Q. Chen, Z. Liu, *Nano Res.* 8 (2015) 340–354, <https://doi.org/10.1007/s12274-014-0620-y>.
- [146] P. Wu, D. Deng, J. Gao, C. Cai, *ACS Appl. Mater. Interfaces* 8 (2016) 10243–10252, <https://doi.org/10.1021/acsami.6b02270>.
- [147] X.-F. Zhao, Z.-L. Liu, X.-D. Li, S.-P. Li, F.-G. Song, *J. Phys. Chem. Solids* 124 (2019) 73–80, <https://doi.org/10.1016/j.jpcs.2018.06.017>.
- [148] J. Zhang, X. Luo, Y.P. Wu, F. Wu, Y.F. Li, R.R. He, M. Liu, *ACS Appl. Mater. Interfaces* 11 (2019) 3690–3703, <https://doi.org/10.1021/acsami.8b17533>.
- [149] M. Massaro, S. Piana, C.G. Colletti, R. Noto, S. Riela, C. Baiamonte, C. Giordano, G. Pizzolanti, G. Cavallaro, S. Milioto, G. Lazzara, *J. Mater. Chem. B* 3 (2015) 4074–4081, <https://doi.org/10.1039/C5TB00564G>.
- [150] M. Massaro, S. Riela, C. Baiamonte, J.L. Blanco, C. Giordano, P. Lo Meo, S. Milioto, R. Noto, F. Parisi, G. Pizzolanti, G. Lazzara, *RSC Adv.* 6 (2016) 87935–87944, <https://doi.org/10.1039/C6RA14657K>.
- [151] R. Salehi, E. Alizadeh, H.S. Kafil, A.M. Hassanzadeh, M. Mahkam, *RSC Adv.* 5 (2015) 105678–105691, <https://doi.org/10.1039/C5RA22784D>.
- [152] J. Forsgren, E. Jämstorp, S. Bredenberg, H. Engqvist, M. Strømme, *J. Pharm. Sci.* 99 (2010) 219–226, <https://doi.org/10.1002/jps.21814>.
- [153] M.G. Bekaroğlu, F. Nurili, S. İşiçi, *Appl. Clay Sci.* 162 (2018) 469–477, <https://doi.org/10.1016/j.clay.2018.06.039>.
- [154] S. Han, F. Liu, J. Wu, Y. Zhang, Y. Xie, W. Wu, W. Liu, Q. Wang, Y. Tang, *Appl. Clay Sci.* 101 (2014) 567–573, <https://doi.org/10.1016/j.clay.2014.09.020>.
- [155] Y. Zhang, P. Huang, M. Long, S. Liu, H. Yang, S. Yuan, S. Chang, *Sci. China Chem.* 62 (2018) 58–61, <https://doi.org/10.1007/s11426-018-9364-8>.
- [156] E. Rozhina, S. Batasheva, A. Danilushkina, M. Kryuchkova, M. Gomzikova, Y. Cherednichenko, L. Nigamatyanova, F. Akhatova, R. Fakhruullin, *Med. Chem. Commun.* 10 (2019) 1457–1464, <https://doi.org/10.1039/C8MD00633D>.
- [157] Z. Long, Y.-P. Wu, H.-Y. Gao, J. Zhang, X. Ou, R.-R. He, M. Liu, *J. Mater. Chem. B* 6 (2018) 7204–7216, <https://doi.org/10.1039/C8TB01382A>.
- [158] R. Abhinayaa, G. Jeevitha, D. Mangalaraj, N. Ponpandian, K. Vidhya, J. Angayarkanni, *Colloids Surf. B Biointerfaces* 169 (2018) 395–403, <https://doi.org/10.1016/j.colsurfb.2018.05.040>.
- [159] P.-R. Li, J.-C. Wei, Y.-F. Chiu, H.-L. Su, F.-C. Peng, J.-J. Lin, *ACS Appl. Mater. Interfaces* 2 (2010) 1608–1613, <https://doi.org/10.1021/am1001162>.
- [160] M. Baek, J.-A. Lee, S.-J. Choi, *Mol. Cell Toxicol.* 8 (2012) 95–101, <https://doi.org/10.1007/s13273-012-0012-x>.
- [161] Q. Liu, Y. Liu, S. Xiang, X. Mo, S. Su, J. Zhang, *Appl. Clay Sci.* 51 (2011) 214–219, <https://doi.org/10.1016/j.clay.2010.11.019>.
- [162] K. Rawat, S. Agarwal, A. Tyagi, A.K. Verma, H. Bohidar, *Appl. Biochem. Biotechnol.* 174 (2014) 936–944, <https://doi.org/10.1007/s12010-014-0983-2>.
- [163] A.K. Gaharwar, S.M. Mihaila, A. Swami, A. Patel, S. Sant, R.L. Reis, A.P. Marques, M.E. Gomes, A. Khademhosseini, *Adv. Mater.* 25 (2013) 3329–3336, <https://doi.org/10.1002/adma.201300584>.
- [164] S.M. Mihaila, A.K. Gaharwar, R.L. Reis, A. Khademhosseini, A.P. Marques, M.E. Gomes, *Biomaterials* 35 (2014) 9087–9099, <https://doi.org/10.1016/j.biomaterials.2014.07.052>.
- [165] A.K. Gaharwar, P.J. Schexnaider, B.P. Kline, G. Schmidt, *Acta Biomater.* 7 (2011) 568–577, <https://doi.org/10.1016/j.actbio.2010.09.015>.
- [166] A.K. Gaharwar, L.M. Cross, C.W. Peak, K. Gold, J.K. Carrow, A. Brokesh, K.A. Singh, *Adv. Mater.* 31 (2019) 1900332, <https://doi.org/10.1002/adma.201900332>.
- [167] F.R. Ahmed, M.H. Shoaib, M. Azhar, S.H. Um, R.I. Yousuf, S. Hashmi, A. Dar, *Colloids Surf. B Biointerfaces* 135 (2015) 50–55, <https://doi.org/10.1016/j.colsurfb.2015.07.021>.
- [168] E. Tarasova, E. Naumenko, E. Rozhina, F. Akhatova, R. Fakhruullin, *Appl. Clay Sci.* 169 (2019) 21–30, <https://doi.org/10.1016/j.clay.2018.12.016>.
- [169] M. Di Paola, P. Pisani, F. Conversano, E. Sbenaglia, S. Casciaro, S. Leporatti, in: 2015 1st Workshop on Nanotechnology in Instrumentation and Measurement (NANOFIM), IEEE, 2015, pp. 126–130. <https://doi.org/10.1109/NANOFIM.2015.8425325>.
- [170] M. Di Paola, A. Quarta, P. Pisani, F. Conversano, E.A. Sbenaglia, S. Leporatti, G. Gigli, S. Casciaro, *IEEE Trans. Nanotechnol.* 15 (2016) 770–774, <https://doi.org/10.1109/TNANO.2016.2546955>.
- [171] F. Chiriaco, F. Conversano, E.A. Sbenaglia, S. Casciaro, S. Leporatti, A. Lay-Ekuakille, in: 2014 IEEE International Symposium on Medical Measurements and Applications (MeMeA), IEEE, 2014, pp. 1–4. <https://doi.org/10.1109/MeMeA.2014.6860126>.
- [172] S. Ragu, E. Dardillac, D.A. Brooks, F.A. Castro-Smirnov, P. Aranda, E. Ruiz-Hitzky, B.S. Lopez, *Appl. Clay Sci.* 194 (2020), <https://doi.org/10.1016/j.clay.2020.105655> 105655.
- [173] J. Cervini-Silva, M.T. Ramírez-Apan, V. Gómez-Vidales, E. Palacios, A. Montoya, E.R. de Jesús, *Colloids Surf. B Biointerfaces* 129 (2015) 1–6, <https://doi.org/10.1016/j.colsurfb.2015.03.019>.
- [174] A. Wagner, A.P. White, T.A. Stueckle, D. Banerjee, K.A. Sierros, Y. Rojanasakul, S. Agarwal, R.K. Gupta, C.Z. Dinu, *ACS Appl. Mater. Interfaces* 9 (2017) 32323–32335, <https://doi.org/10.1021/acsami.7b06657>.
- [175] S. Jayrajshin, G. Shankar, Y.K. Agrawal, L. Bakre, *J. Drug Delivery Sci. Technol.* 39 (2017) 200–209, <https://doi.org/10.1016/j.jddst.2017.03.023>.
- [176] G.I. Fakhruullina, F.S. Akhatova, Y.M. Lvov, R.F. Fakhruullin, *Environ. Sci. Nano* 2 (2015) 54–59, <https://doi.org/10.1039/C4EN00135D>.
- [177] X. Wang, J. Gong, Z. Gui, T. Hu, X. Xu, *Environ. Toxicol.* 33 (2018) 623–630, <https://doi.org/10.1002/tox.22543>.
- [178] X. Wang, J. Gong, R. Rong, Z. Gui, T. Hu, X. Xu, *J. Agric. Food Chem.* 66 (2018) 2925–2933, <https://doi.org/10.1021/acs.jafc.7b04615>.
- [179] T. Hu, Z. Gui, J. Gong, R. Rong, X. Wang, W. Tan, Z. Wang, X. Xu, *Environ. Pollut.* 258 (2020), <https://doi.org/10.1016/j.envpol.2019.113758> 113758.
- [180] T. Hu, X. Wang, W. Tan, K. Nie, X. Xu, *Environ. Sci. Pollut. Res.* 27 (2020) 17730–17737, <https://doi.org/10.1007/s11356-020-08314-1>.
- [181] R. Rong, Y. Zhang, Y. Zhang, Y. Hu, W. Yang, X. Hu, L. Wen, Q. Zhang, *Nanotoxicology* 13 (2019) 354–368, <https://doi.org/10.1080/17435390.2018.1549688>.
- [182] K.K. Barford, K.M. Bendtsen, T. Berthing, A.J. Koivisto, S.S. Poulsen, E. Segal, E. Verleysen, J. Mast, A. Holländer, K.A. Jensen, K.S. Hougaard, U. Vogel, *Environ. Toxicol. Pharmacol.* 73 (2020), <https://doi.org/10.1016/j.etap.2019.103266> 103266.
- [183] A.J. Koivisto, A.B. Bluhme, K.I. Kling, A.S. Fonseca, E. Redant, F. Andrade, K.S. Hougaard, M. Krepker, O.S. Prinz, E. Segal, A. Holländer, K.A. Jensen, U. Vogel, I.K. Koponen, *Nanomedicine* 10 (2018) 153–160, <https://doi.org/10.1016/j.nano.2018.04.003>.
- [184] N. Khatoun, M.Q. Chu, C.H. Zhou, *J. Mater. Chem. B* 8 (2020) 7335–7351, <https://doi.org/10.1039/D0TB01031F>.
- [185] M.C. Wiles, H.J. Huebner, E. Afriyie-Gyawu, R.J. Taylor, G.R. Bratton, T.D. Phillips, *J. Toxicol. Environ. Health* 67 (2004) 863–874, <https://doi.org/10.1080/15287390490425777>.

- [186] A.K. Sharma, A. Mortensen, B. Schmidt, H. Frandsen, N. Hadrup, E.H. Larsen, M.L. Binderup, *Mutat. Res. Genet. Toxicol. Environ. Mutagen.* 770 (2014) 66–71, <https://doi.org/10.1016/j.mrgentox.2014.04.023>.
- [187] M.A. Abdel-Wahhab, S.A. Nada, F.A. Khalil, *Anim. Feed Sci. Technol.* 97 (2002) 209–219, [https://doi.org/10.1016/S0377-8401\(01\)00342-X](https://doi.org/10.1016/S0377-8401(01)00342-X).
- [188] E. Afriyie-Gyawu, J. Mackie, B. Dash, M. Wiles, J. Taylor, H. Huebner, L. Tang, H. Guan, J.-S. Wang, T. Phillips, *Food Addit. Contam.* 22 (2005) 259–269, <https://doi.org/10.1080/02652030500110758>.
- [189] M.D. Subramaniam, I.H. Kim, *J. Animal Sci. Biotechnol.* 6 (2015) 38, <https://doi.org/10.1186/s40104-015-0037-9>.
- [190] N.J. Mitchell, J. Kumi, M. Aleser, S.E. Elmore, K.A. Rychlik, K.E. Zychowski, A.A. Romoser, T.D. Phillips, N.A. Ankrah, *Am. J. Trop. Med. Hyg.* 91 (2014) 777–785, <https://doi.org/10.4269/ajtmh.14-0093>.
- [191] Y.-H. Lee, T.-F. Kuo, B.-Y. Chen, Y.-K. Feng, Y.-R. Wen, W.-C. Lin, F.H. Lin, *Biomed. Eng.* 17 (2005) 72–78, <https://doi.org/10.4015/S101623720500010X>.